2005-01-14

Study and characetrization of plastic encapsulated packages for MEMS

Anjali W. Deshpande
Worcester Polytechnic Institute

Study and characterization of plastic encapsulated packages for MEMS

A Thesis
submitted to the faculty of the

Worcester Polytechnic Institute

in partial fulfillment of the requirements for the
Degree of Master of Science
in
Mechanical Engineering

by

Anjali W. Deshpande

12 January 2005

Study and characterization of plastic encapsulated packages for MEMS

A Thesis
submitted to the faculty of the

Worcester Polytechnic Institute

in partial fulfillment of the requirements for the
Degree of Master of Science
in
Mechanical Engineering

by

Anjali W. Deshpande

12 January 2005

Approved:

Prof. Cosme Furlong, Member, Thesis Committee

Prof. Jianyu Liang, Member, Thesis Committee

Dr. Thomas F. Marinis, Draper Laboratory, Member, Thesis Committee

Prof. Ryszard J. Pryputniewicz, Major Advisor

Prof. John M. Sullivan, Jr., Graduate Committee Representative

by
Anjali W. Deshpande
NEST – NanoEngineering, Science, and Technology
CHSLT- Center for Holographic Studies and Laser micro-mechaTronics
Mechanical Engineering Department
Worcester Polytechnic Institute
Worcester, MA 01609-2280

SUMMARY

Technological advancement has thrust MEMS design and fabrication into the forefront of modern technologies. It has become sufficiently self-sustained to allow mass production. The limiting factor which is stalling commercialization of MEMS is the packaging and device reliability. The challenging issues with MEMS packaging are application specific.

The function of the package is to give the MEMS device mechanical support, protection from the environment, and electrical connection to other devices in the system. The current state of the art in MEMS packaging transcends the various packaging techniques available in the integrated circuit (IC) industry. At present the packaging of MEMS includes hermetic ceramic packaging and metal packaging with hermetic seals. For example the ADXL202 accelerometer from the Analog Devices. Study of the packaging methods and costs show that both of these methods of packaging are expensive and not needed for majority of MEMS applications. Due to this the cost of current MEMS packaging is relatively high, as much as 90% of the finished product. Reducing the cost is therefore of the prime concern.

This Thesis explores the possibility of an inexpensive plastic package for MEMS sensors like accelerometers, optical MEMS, blood pressure sensors etc. Due to their cost effective techniques, plastic packaging already dominates the IC industry. They cost less, weigh less, and their size is small. However, porous nature of molding materials allows penetration of moisture into the package. The Thesis includes an extensive study of the plastic packaging and characterization of three different plastic package samples.

Polymeric materials warp upon absorbing moisture, generating hygroscopic stresses. Hygroscopic stresses in the package add to the thermal stress due to high reflow temperature. Despite this, hygroscopic characteristics of the plastic package have been largely ignored. To facilitate understanding of the moisture absorption, an analytical model is presented in this Thesis. Also, an empirical model presents, in this Thesis, the parameters affecting moisture ingress. This information is important to determine the moisture content at a specific time, which would help in assessing reliability of the package. Moisture absorption is modeled using the single phase absorption theory, which assumes that moisture diffusion occurs freely without any bonding with the resin. This theory is based on the Fick's Law of diffusion, which considers that the driving force of diffusion is the water concentration gradient.

A finite difference simulation of one-dimensional moisture diffusion using the Crank-Nicolson implicit formula is presented. Moisture retention causes swelling of compounds which, in turn, leads to warpage. The warpage induces hygroscopic stresses. These stresses can further limit the performance of the MEMS sensors. This Thesis also presents a non invasive methodology to characterize a plastic package. The warpage deformations of the package are measured using Optoelectronic holography (OEH) methodology. The OEH methodology is noninvasive, remote, and provides results in full-field-of-view. Using the quantitative results of OEH measurements of deformations of a plastic package, pressure build up can be calculated and employed to assess the reliability of the package.

ACKNOWLEDGEMENTS

I would like to sincerely express my gratitude to Prof. R. J. Pryputniewicz for all his guidance and support during this Thesis. Personally, also he gave me a lot of encouragement during this course of the study. Thank you.

Very special thanks to Mr. Peter Hefti for his timely help and jovial conversations that lifted my spirits and inspired the drive to work harder.

I am very thankful to Mizar S. Pai, for his time and invaluable support during my experimental work.

Special thanks to Ryan T. Marinis for all the random questions I always had for him and his very helpful nature. Thanks, Ryan.

I have to extend my thanks to Adam Klempner, who helped me in the analysis of the data obtained from the experiment. Thanks, Adam.

I would also like to thank everyone else at CHSLT-NEST labs, Dr. Wei Han, Ronald Kok, Krzysztof A. Nowakowski, and Prof. Cosme Furlong. They have all helped me achieve this in their own special way. I am grateful to Adrian Hera too.

I have to mention the names of Barbara Edilberti, Barabara Furmann, Sia Najafi and Ben Higgins who made me feel at home, away from home, at WPI. Thank You.

Last, but not the least I am very grateful to my elder brother Sandeep Deshpande and my sister-in-law Rashmi Deshpande, for making my aspirations possible. Thank you, Sandeep and Rashmi.

This thesis is the result of the hopes and trust my parents have in me. This is to you Aai and Baba. Thanks for believing.

TABLE OF CONTENTS

LIST OF FIGURES

LIST OF TABLES

NOMENCLATURE

C	concentration of the diffusing moisture
D	diffusing coefficient
C_o	initial uniform concentration
C_l	constant surface concentration
M_t	total amount of diffusing moisture at time t
M_∞	total amount of diffusing moisture at infinite time
$M_\infty\%$	percentage weight gain at saturation
$M\%$	percentage weight gain as function of time
N	absorbed moisture content per unit time
D_o	diffusivity constant
E_a	activation energy
T_a	ambient temperature
RH	relative humidity
P_{sat}	saturation vapor pressure at the ambient temperature
S_{sol}	moisture solubility
T_m	mold compound temperature
S_o	solubility constant
V	volume of the deformed package
R	universal gas constant
A	area of the package
P_r	pressure developed in the package
P_h	hydrostatic pressure
E	Young's modulus of elasticity
X	function of space coordinate x
T	function of time coordinate t
A	constant of integration
B	constant of integration
K	plate stiffness
E	modulus of elasticity
A_m, B_m, λ_m	constants determined by boundary conditions
$I(u,v)$	speckle intensity patterns before event effect
$I'(u,v)$	speckle intensity pattern after event effect
$I_B(u,v)$	background irradiance
$I_M(u,v)$	modulation irradiance
$I_o(u,v)$	object beam
$I_r(u,v)$	reference beam
h	thickness of the package till mid-plane
$2h$	thickness of the package
x,y,z	Cartesian coordinates
t	time
k	Boltzmann constant

m	accumulated moisture
l	length of the package
wi	width of the package
p	load on the plate
q_y, $q_{z,y}$	shear forces at infinitesimal element
m_y, m_{yz}	moments at infinitesimal element
(u,v)	Cartesian coordinates of the image space
r	beam ratio
λ	constant
α	probability of a molecule of water passing from a combined state to free phase
β	probability of a molecule of water passing from the free to the combined phase, hygroscopic swelling coefficient
δ	deformation obtained from the experiment
κ_x κ_y κ_z	curvatures causing deformations
κ_c	curvature due to concentration
ν	Poisson's ratio
$\Delta\Omega$	change in optical phase
θ_n	applied n-th phase step
σ_l	surface energy of the liquid
σ_s	surface energy of the solid
σ_{sl}	surface energy of the solid liquid interface
θ	contact angle in the Young's equation, parameter for half point average
CERDIP	ceramic dual in-line package
CMOS	complementary metal oxide semiconductor
CTE	coefficient of thermal expansion
DIP	dual in-line package
ICs	integrated ciruits
MEMS	microelectromechanical systems
MOSFET	metal-oxide semiconductor field-**e**ffect transistor
NDT	non-destructive testing
PDIP	plastic dual in-line package
PEPs	plastic encapsulated packages
PEMs	plastic encapsulated microcircuits
PLCC	plastic leaded chip carrier
PPGA	plastic pin grid array
PQFP	plastic quad flatpack package
SIP	single in-line package
SOP	small-outline package
TSOP	thin small outline package

1. INTRODUCTION

1.1. What is MEMS ?

MicroElectroMechanical Systems is popularly known as MEMS. MEMS is a diverse technology which is an amalgamation of all the faculties of engineering and science. A few years ago it was a nascent technology stressing on the physics and chemistry of the silicon wafer and microfabrication. Now is the actual boom time for this field which promises to make fully assembled systems that can do what large scale systems cannot do as affordably as MEMS. Things behave substantially different in micro domain. Forces related to volume, like weight and inertia, tend to decrease in significance. Forces related to the surface area, such as friction and electrostatics tend to be large. Forces like surface tension that depend upon an edge become enormous (Madou, 1997). MEMS devices are currently fabricated, integrated with controlling microelectronics on a single chip Fig. 1.1 (Baltes et al., 2002; Pryputniewicz, 2003a).

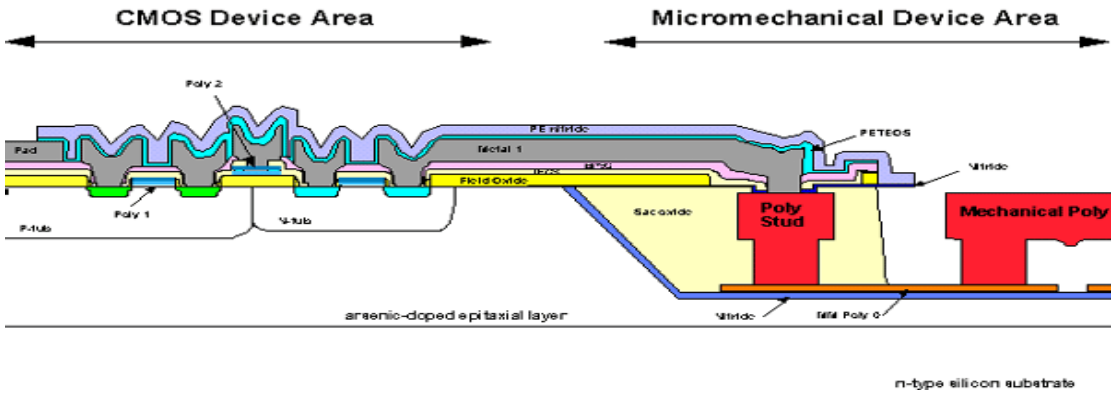

Fig. 1.1. CMOS and MEMS integration (Courtesy: Sandia National Laboratories).

MEMS consist of sensors, actuators, passive components, power management circuits, analog and digital integrated circuits. These smart devices transduce physical parameters of the process environment to electrical signals and vice versa.

MEMS design methodology can be summarizes with flow chart, Fig. 1.2.

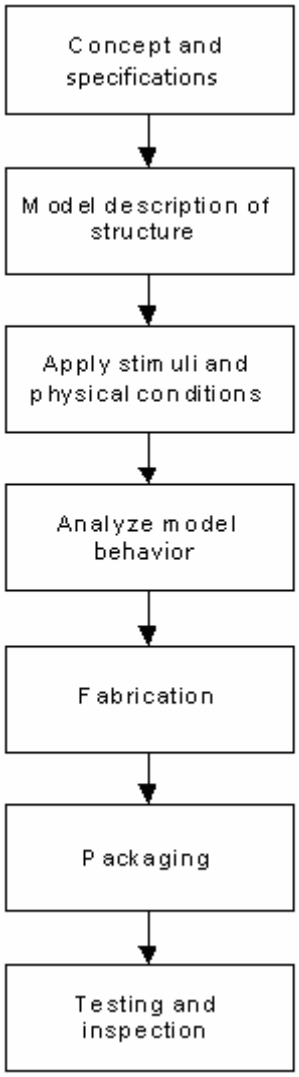

Fig. 1.2. MEMS design methodology.

Using the fabrication techniques and materials of microelectronics as bases, MEMS processes construct both mechanical and electrical components. MEMS are not about any one single fabrication or limited to a few materials. It is a fabrication approach that conveys the advantage of miniaturization, multiple components, and microelectronics to the design and construction of integrated electromechanical systems. Regardless of what type of micromachining processes are used all MEMS fabrication share the following key characteristics:

1) miniaturization: structures that are relatively small and light in weight lead to devices that have relatively high resonating frequencies. These high resonant frequencies, in turn, mean higher operating frequencies and bandwidth for sensors and actuators. Thermal time constants-the rates at which structures absorb and release heat are short for smaller, less massive structures. But miniaturization is not the principal driving force for MEMS that it is for microelectronic devices such as IC's. Because MEMS devices are by definition interacting with some aspect of the physical world such as pressure, inertia, fluid flow, light etc. There is a size below which further smallness is detrimental to the device and system operation. The minimum size usually varies between one to two orders of magnitude larger than the smallest microelectronic device (Madou, 1997),
2) multiplicity: it makes it possible to fabricate a million components easily and quickly in one fabrication process. Such economics of costs and scale are critical for reducing unit costs. Equally important advantage of multiplicity is the

additional flexibility in the design of massively parallel and interconnected systems.

3) microelectronics: these integrated into the MEMS devices provide the latter with greater intelligence and allow closed loop feedback systems, localized signal conditioning, and control, for example control of parallel actuator arrays becomes possible with integrated circuitry,
4) active surfaces: devices are attached to a surface so that there is a fixed topology. The devices are coupled primarily to the dynamics of the medium they are manipulating, leading to a movement in the degree of global as well as local coordinate systems.

1.2. Applications of MEMS

MEMS devices can be used as miniature sensors, controllers or actuators. They have become increasingly dominant in every aspect of commercial marketplace as the technologies for microfabrication continue to be developed. World market projection for MEMS sensors is shown in Table 1.1 (Madou, 1997). MEMS find applications in various fields. But so far, very few commercial applications exist. Some that are present in the commercial market are inertial sensors like accelerometers, gyroscopes, inkjet printers, video projection systems, gas and chemical sensors, and biomedical devices like muscle stimulation, blood monitors, etc (Camporesi, 2003). Vast amount of research can help MEMS find place in the following field Table 1.2 (Madou, 1997).

Table 1.1. World market projection for MEMS and sensors (in million of dollars).

	1995	1997	1999	2000
Si sensors in all applications	1316	1858	2549	Not available
Si sensors in automobiles specifically	414	621	884	Not available
Si sensors and Si Microsystems	Not available	Not available	Not available	3665
Si bases MEMS	2700	Not available	Not available	11900
All sensors	8500	Not available	Not available	13100
All industries and scientific instruments	5900	Not available	Not available	82000

Table 1.2. Applications of MEMS sensors.

Area	Application
Automotive	pressure sensors, flow sensor, accelerometer gyroscopes
Aerospace industry	tempertature sensors, chemical sensors, active flight control surfaces, microsatellites
Healthcare and biomedical	disposable blood pressure transducer (DPT), intrauterine pressure sensor, angioplasty pressure sensor, micronozzle injection systems microfluidic systems, hearing aids, DNA testing (gene probes)
Information technology	data storage (millipede), displays, video projectors, ink jet print heads
Telecommunications	RF switches, variable optical amplifier, tunable lasers, inductors
Consumers products	Bicycle computers, fitness gear using hydraulics, washers with water level controls in washing machines, smart toys

1.3. Fabrication of MEMS

MEMS are incredibly small devices that are fabricated using state of the art integrated circuit (IC) batch processing technology (Pryputniewicz, 2003a). Microfabrication of MEMS can be divided into three types, surface micromachining and bulk micromachining and LIGA.

1.3.1. Surface micromachining

This technique deposits layers of sacrificial and structural material on the surface of a silicon wafer. As each layer is deposited it is patterned and some of the material is removed by etching, leaving material only where the designer wishes. When the sacrificial material is removed, completely formed and assembled mechanical devices are obtained (Trimmer, 1997).

SUMMiT V^{TM} known as Sandia Ultra Planar, MEMS Technology using 5 structural layers, is a state of the art fabrication technique (Pryputniewicz, 2002). The fabrication process is a five-layer polycrystalline silicon surface micromachining process (one ground plane/electrical interconnect layer and four mechanical layers). With this more advanced systems can be created on moveable platforms, Fig. 1.3a. Much taller devices can be made (up to 12 microns high), making possible greater stiffness and mechanical robustness in the devices, Fig. 1.3b. The additional height can also be used to increase the force produced by actuators, Fig. 1.3c. The design flexibility in a five-layer

technology is truly enormous - devices for applications that have not yet been imagined are now a possibility.

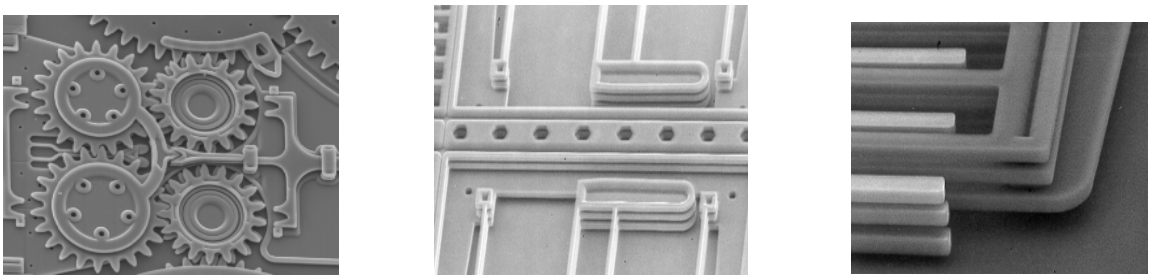

(a) (b) (c)

Fig 1.3. Advanced MEMS systems (a) meshing gears on a movable platform, (b) laminated support springs, (c) a laminated comb (Courtesy: Sandia National Laboratories).

The SUMMIT^{TM}-V is a batch fabrication process using conventional IC processing tools (Shepherd, 2002; Pryputniewicz et al., 2003d). Using this technology, high volume, low-cost production can be achieved. The processing challenges, including topography and film stress, are overcome using methods similar to those used in the SUMMiT^{TM} Process: topography issues are mitigated by using Chemical-Mechanical Polishing (CMP) to achieve planarization, and stress is maintained at low levels using a proprietary process.

MEMS are also produced in the SUMMiT^{TM}-V Fabrication Process by alternately depositing a film, photo lithographically patterning the film, and then performing chemical etching. By repeating this process with layers of silicon dioxide and polycrystalline silicon, extremely complex, inter-connected three-dimensional shapes can be formed (Pryputniewicz et al., 2003d). The photolithographic patterning is achieved

with a series of two-dimensional "masks" that define the patterns to be etched. The SUMMiT^{TM}-V process uses 14 individual masks in the process, approximately the same quantity as in many CMOS, IC processes.

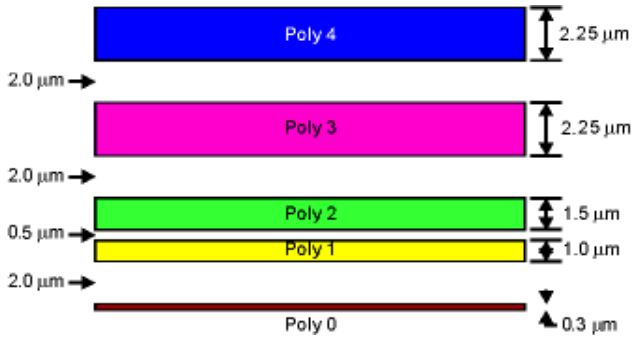

Fig. 1.4. Five fabrication layers (Courtesy: Sandia National Laboratories).

1.3.2. Bulk micromachining

Silicon bulk micromachining means that three-dimensional features are etched into the bulk of crystalline and non-crystalline materials. Dry etching defines the surface features in the *x-y* plane and wet etching releases them from the plane by undercutting. These sculpted-out cavities can then become the building blocks for cantilevers, diaphragms, or other structural elements needed to make devices such as pressure, or acceleration, sensors. This technique has come to be known as bulk micromachining because the chemicals that pit deeply into the silicon produce structures that use the entire mass of the chip (Tao and Bin, 2002). This process has the disadvantage that it uses alkaline chemicals to conventional chip processing (Camporesi, 2003).

A surprising number of structures can be made using the etch stop planes in crystalline silicon, Fig. 1.5.

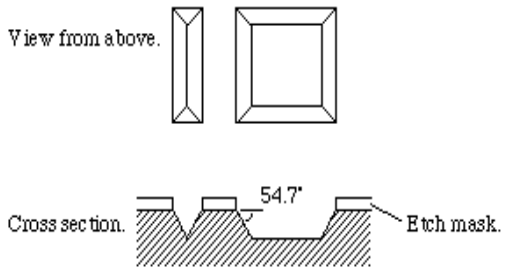

Fig. 1.5. Wet etching (Trimmer, 1997).

1.3.3. LIGA

The acronym LIGA comes from the German name for the process (Lithographie, Galvanoformung, Abformung). LIGA uses lithography, electroplating, and moulding processes to produce microstructures. It is capable of creating very finely defined microstructures of up to 1000μm high. In the process as originally developed, a special kind of photolithography using X-rays (X-ray lithography) is used to produce patterns in very thick layers of photoresist (Banks, 2002). The X-rays from a synchrotron source are shone through a special mask onto a thick photoresist layer (sensitive to X-rays) which covers a conductive substrate, Fig. 1.6a. This resist is then developed, Fig. 1.6b. The pattern formed is then electroplated with metal, Fig. 1.6c. The metal structures produced can be the final product, however it is common to produce a metal mould, Fig. 1.6d. This

mould can then be filled with a suitable material, such as a plastic, Fig. 1.6e, to produce the finished product in that material, Fig. 1.6f.

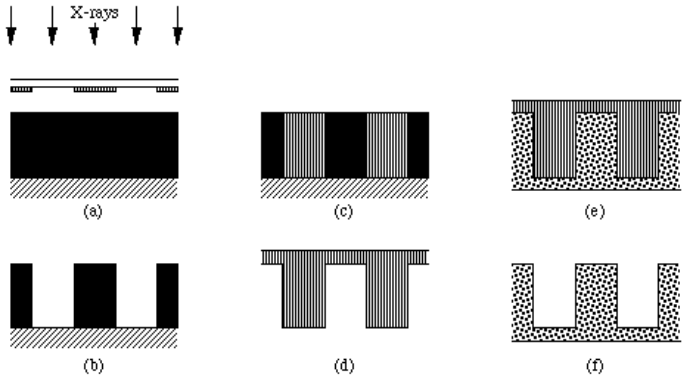

Fig. 1.6. LIGA fabrication (Banks, 2002).

2. PACKAGING OF MEMS

With an in depth research and a multi-million dollar industrial growth, fabrication and testing of MEMS has been well established. Most of the early packaging technologies of semiconductor microelectronics influence the choice of packaging of MEMS devices. The Webster dictionary defines package as "a group or a number of things, boxed and offered as a unit" (Gerke, 2003). The art of packaging manifests itself in novel and unique creations that ingeniously reconcile and satisfy what seems like mutually exclusive application requirements and constraints posed by the laws of nature and the properties of materials and processes. All application requirements can be summed up in three words: cost, performance, and reliability (Tummala, 1989).

Packaging, as summarized in Table 2.1, involves many disciplines. Skillful applications of these and other disciplines provide successful solutions to the driving forces of packaging applications. The evolution of packaging is a response to the need to optimize for cost, performance and reliability, with the emphasis shifting according to application priorities.

2.1. Overview of packaging for microelectronics

In the state of the art, MEMS are fabricated using manufacturing processes and tools similar to those used in the microelectronics industry. Many of these tools are directly used, while others are modified to meet the specific needs of MEMS (O'Neal et al., 1999).

Table 2.1. Packaging disciplines (Tummala, 1989).

Discipline	To address
Applied physics	Stress analysis
Ceramic engineering	Ceramic materials and processes
Chemical engineering	Chemical process systems
Chemistry	Package process
Electrical engineering	Electrical design
Industrial engineering	Cost and production analysis
Mechanical engineering	Mechanical design tools
Metallurgical engineering	Metallization process, solder and braze connections
Physics	Electrical, thermal and mechanical characteristics
Polymer chemistry	Polymers and plastic materials and processes
Thermal engineering	Heat transfer

It is necessary for this Thesis to study the packaging of microelectronics because MEMS packaging transcends and works on the rules of the IC industry. There are generally four levels in the hierarchy of the microelectronics packaging structure (Tummala, 1989).

Packaging has evolved as a physical hierarchy of interconnect structures that are delineated according to specific levels, Fig 2.1. Although there are actually 4 levels, the number expands to 5 if integrated circuits are included. The IC can be represented as level 0 because it involves the interconnection of numerous transistors, gates, or cells within the chip itself (Johnson, 1989). Level 1 occurs when the individual circuit or chip is extracted from the wafer and placed into an individual carrier or container. Several carriers are then mounted and interconnected on a printed circuit board (PCB),

representing level 2. An array of boards, interconnected by means of a mother board and configured into a sub system, represent level 3, and the complete system, level 4.

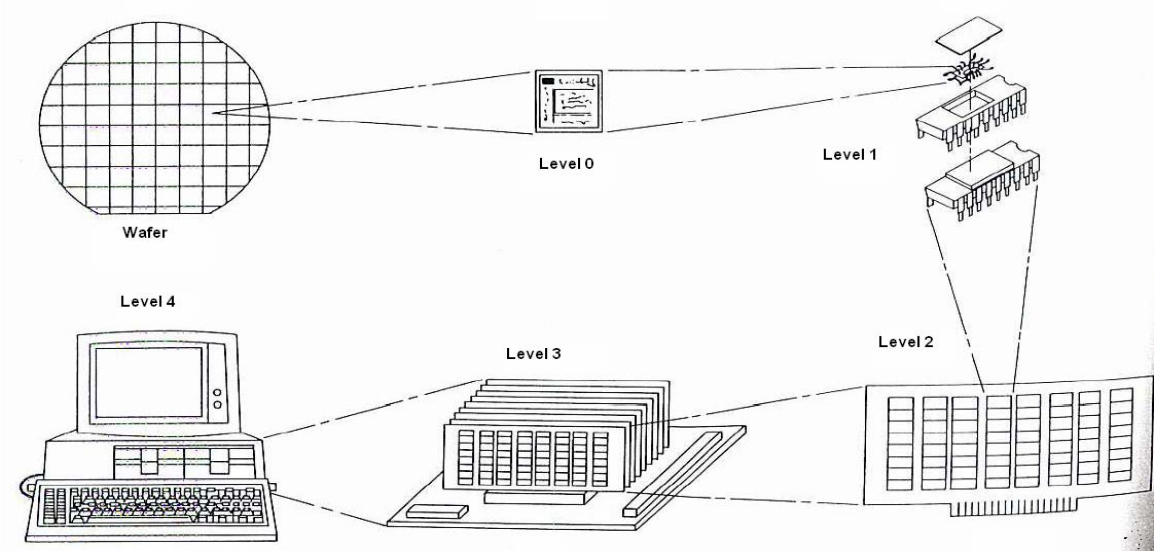

Fig. 2.1. Hierarchy of IC packaging (Johnson, 1989).

In such a coordinated system, every level of packaging, must perform certain functions. First the package must provide electrical connection for the transfer of power and information bearing signals between the semiconductor chip and the outside world. Second, the package must mechanically support the small, fragile chip for subsequent processing, handling, and performance. Third, it must protect the sensitive chip from atmospheric variables such as moisture, dust, and gases that may adversely influence its performance. Fourth, because the chip converts most of the electrical power it consumes into heat, the package must dissipate the heat in order to prevent degradation in performance and a concomitant reduction in operational lifetime (Harper, 1969). In fulfilling these functions the package imposes constraints on the chip. It typically degrades the electrical performance of the device, substantially increases the effective

size and weight of the chip, encumbers testing, and introduces reliability problems. The package also adds to the cost, that often exceeds that of the chip itself. Hence packaging is a complex balance between the provision of desired functions and reduction of associated constraints, all at an affordable price (Johnson, 1989).

2.1.1. MEMS packaging vs IC packaging

But MEMS packaging differs from IC packaging techniques. Unlike the IC die packaging, MEMS dice need to interface with the environment for sensing, interconnections and actuation (Hsieh et al., 2002). MEMS packaging is application specific and the package allows the physical interface of the MEMS device to the environment. In the case of fluid mass flow control sensor, the medium flows into and out of the package. This type of packaging is referred to as media compatible packaging. Harsh environments may create different challenges for the packaging of MEMS. Table 2.2 shows the comparison of MEMS packaging and IC packaging with reference to some processes (Hsieh et al., 2002).

Packaging of MEMS is considerably more complex as they serve to protect from the environment, while somewhat in contradiction, enabling interaction with that environment in order to measure or affect the desired physical or chemical parameters (Ramesham, 2000). The difference can be apparent as shown in Figs 2.2 and 2.3.

Table 2.2. Comparison of MEMS packaging and IC packaging.

	Item	IC packaging	MEMS packaging
1	Capping		✓
2	Dicing	✓	✓
3	Die Bonding	✓	✓
4	Wire bonding	✓	✓
5	Pre-molding		✓
6	Post molding	✓	
7	Hermetic	✓	✓
8	Wafer Bonding		✓
9	Testing	✓	✓
10	Stiction	✓	✓
11	Reliability	✓	✓
12	Standard	✓	✓
13	Cost	✓	✓

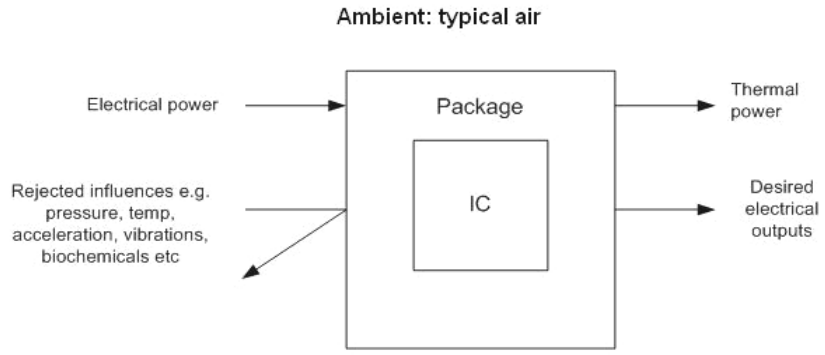

Fig. 2.2. Functionality of IC package.

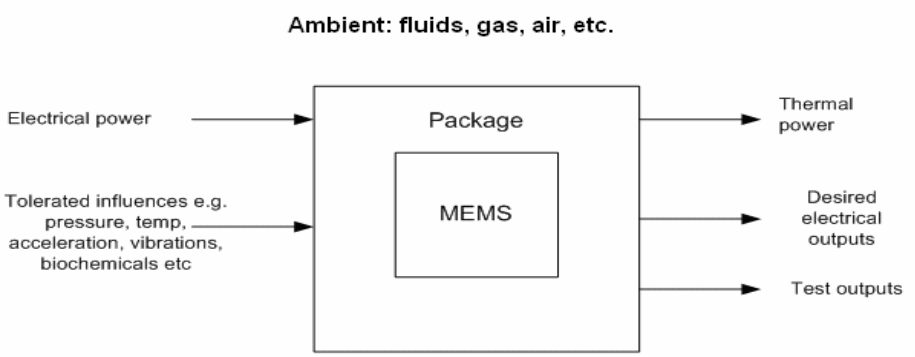

Fig. 2.3. Functionality of MEMS package.

The goal of IC packaging is to provide physical support and an electrical interface to the chip and to isolate it physically from adverse effects of its environment. MEMS devices, on the other hand, often are interfaced intimately with their environment and are less generic in nature. Consequently, MEMS packaging must address different and more diverse needs than IC packaging (Baert et al., 2004):

1) MEMS do not obey scaling laws like IC's do,

2) they consist of a larger variety of basic building blocks; sensors and actuators and are comprised of acoustic, chemical, magnetic, optical and pyroelectric, resistive and thermoelectric elements,
3) MEMS packaging functionalities are inherently broader. IC packages must accommodate ever-denser electrical I/Os and increasing levels of electrical power and thermal dissipation. Ambient parameters such as moisture or pressure are treated as undesirable noise signals to be isolated from the IC by the package. In MEMS packaging, the electrical I/O typically is unidirectional and less dense. The electrical and thermal power handling is less demanding, but at least one of the non-electrical influences becomes a desired input.

Due to additional packaging requirements for MEMS, the classification of traditional IC packaging into at least four hierarchical levels of packaging is less applicable to MEMS. While wafer-level packaging (also known as 0-level packaging) for ICs comprises the interconnection of numerous transistors, gates or cells within the chip itself, wafer-level packaging of MEMS encompasses all wafer-level operations. First-level packaging is performed after individual MEMS devices have been extracted from the wafer (Baert et al., 2004).

2.2. Requirements and functions of MEMS packages

MEMS package requirements are different from those of the IC industry and extrapolating the philosophies of IC packaging to MEMS seems arguable. All MEMS devices move, but the mode and the purpose of motion determine the packaging requirements. The following list indicates some of the basic modes of motion (Gilleo, 2002):

1) deformation: no moving parts that touch, can be considered to be just bending or twisting,
2) moving parts, but with no rubbing.
3) moving parts with rubbing, no impact.
4) motion with impact.
5) moving parts with rubbing and impact.

The package serves to integrate all of the components required for a system application in a manner that minimizes size, cost, mass, and complexity (Persson et al., 2002). The package provides the interface between the components and the overall system. On basis of this the various functions of a MEMS package can be enumerated as follows (Gerke, 2003):

1) mechanical support: due to the presence of moving parts the very nature of MEMS is mechanical. Hence there is a need to support and protect the device from thermal and mechanical shock, vibration, etc. The mechanical stress endured depends on the final output of a specific application. With respect to this understanding one consideration is that the coefficient of thermal expansion

(CTE) of the package should be equal to or slightly greater than the CTE of silicon for reliability, since thermal shock or thermal cycling may cause die cracking and de-lamination if the materials are unmatched.

2) protection from environment: MEMS devices are used to measure something in the intermediate surrounding environment. Hence the hermeticity may not apply to all MEMS devices. These devices might be just encapsulated or housed to prevent damage. Many elements in the environment can cause corrosion or physical damage to the metal lines of MEMS as well as other components. Hence moisture is a major concern. The susceptibility of the MEMS to moisture damage is dependent on the materials used in manufacture. Moisture is readily absorbed by some materials used in the MEMS fabrication, die attachment, or within the package, this absorption causes swelling, stress, and possibly delamination,
3) electrical connection to other system components: the package is the primary interface between the MEMS and the system, it must be capable of transferring DC power and in some designs, RF signals (Persson et al., 2002).
4) thermal considerations: with the push to increase the integration of MEMS with power from other circuits such as amplifiers perhaps even within a single package, the temperature rise in the device junctions is substantial and may cause the circuits to operate in unsafe region.

2.3. Packaging issues and challenges

Packaging of MEMS has been and continues to be a major challenge. It costs about 50% to 90% of the total cost of the MEMS product (Deshpande and Pryputniewicz, 2004a). MEMS packaging encompasses three major tasks: assembly, packaging and testing.

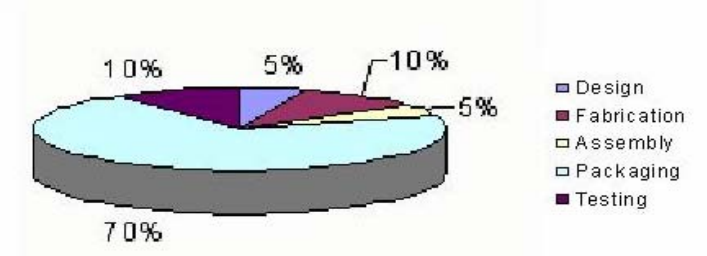

Fig. 2.4. Percentage costs incurred in MEMS production.

The challenges faced during the packaging of the MEMS are:

1) media compatibility: MEMS devices need to operate in diverse environments such as under automobile hoods, intense vibrations, in salt water, strong acids or other chemicals, alkaline or organic solutions. The package while performing detection or actuation must be able to withstand the environments (Ulvensoen, 1999),
2) the effect on reliability of the MEMS die, that packaging parameters induce: the package is a part of the complete system and should be designed as the MEMS chip is designed, with specific and many times custom package. It is necessary for the chip, package and environment to function together and must be

compatible with each other (Senturia et al., 1988). This determines which materials and what design considerations and limitations become important. One of the major challenges is the issue of material properties. The properties of materials depend on how they are used, processed, the heat treatments to which the materials are subjected. One positive point is that the defect density decreases with the size for materials and MEMS devices are so small that the chance of a killer defect occurring in a device is reduced,

3) packaging of MEMS dice is application specific and hence desired process steps vary significantly. It is important to classify MEMS dice from the packaging requirements and develop the packaging standards and related knowledge base (Pryputniewicz, 2003b).
4) release and stiction: typically the polysilicon features are supported by silicon dioxide, which is used as a sacrificial layer (Gilleo, 2001). The challenge in this is when the etching should be done to release the features. Complementary to this is the issue of stiction. The risk of stiction occurs during the release and after the release. Stiction occurs from the capillary action of the evaporating rinse solution in the crevices between structural elements like cantilevers and the substrate.
5) dicing: the challenge is in dicing of the wafer into the individual dice. It is typically done with a diamond saw a few mils thick. This requires the coolant to flow over the surface of the very sensitive dice along with silicon and diamond particles. These particles combined with the coolant can contaminate the devices

and get into the crevices of the features causing the device to fail (Persson et al., 2002).

6) die handling: in order to handle MEMS chips, die handling fixtures and methods that hold the chips by the edges are required. These could be fingers or clamps that delicately handle these MEMS dice by their edges (Hsieh et al., 2002).
7) stress: when polysilicon is deposited a great deal of stress is produced in the films. This stress can be annealed out at a temperature of around 1000°C.
8) another source of stress results from the die attach materials at the interface between the MEMS die and the package substrate.
9) outgassing: when epoxies are used as in the case of plastic encapsulation, the die attach compounds outgas as they cure. These water and organic vapors redeposit on the features, in crevices and on bond pads (Hsieh et al., 2002).
10) moisture penetration: many MEMS chips are hermetically sealed to exclude oxygen and moisture that can cause wear, stiction, and friction problems. Oxygen can degrade lasers and water can damage optics. Hence the issue is to find a solution to eliminate the moisture penetration problem and answer the question whether the package needs to be a hermetic one or just dry (Gilleo, 2002),

2.4. Types of packaging

Each MEMS application usually requires a specific package design to optimize its performance or to meet the needs of the system for the given application. It is possible to

loosely group packages into the following several categories (Gerke, 2003). These various types have been adpated from the ones available in the IC industry (Tummala, 1989).

2.4.1. Metal packages

These are often used for microwave multichip modules and hybrid circuits because they provide excellent thermal dissipation and excellent electromagnetic shielding. Usually the metal packages is the outer most layer of the packaging process (3rd level packaging), the ceramic substrate and the device holder are all included in the packaged device. The selection of proper metal can be critical. Metal packages satisfy the pin count requirements and they can be prototyped in small volumes with rather short turnaround periods. Also they are hermetic when sealed (Tummala, 2001). They are more expensive than plastic package (Ramesham and Ghaffarian, 2000).

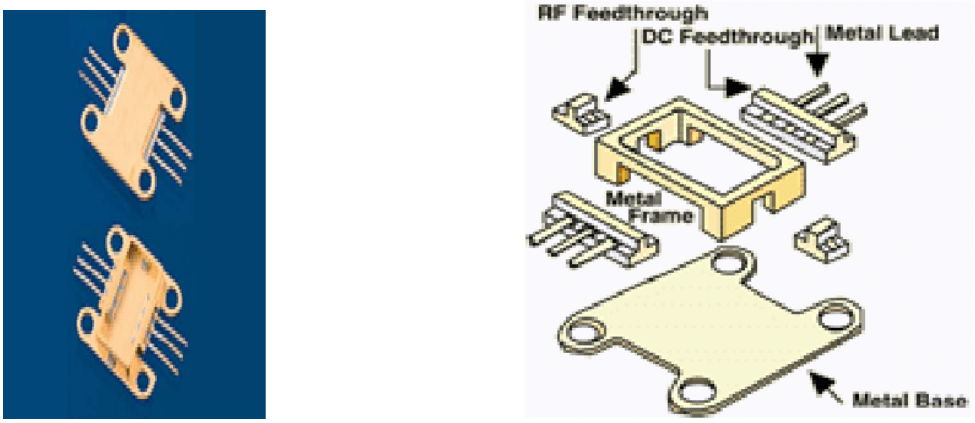

Fig. 2.5. Metal wall packages (Courtesy: Kyocera).

2.4.2. Ceramic packages

These packages have several features that make them suitable for MEMS. They provide low weight, are easily mass produced and can be low in cost. They can be made hermetic and can more easily integrate signal distribution lines and feed-through. The multilayer ceramic packages could reduce the size and the cost of the device. These types of packages are generally referred to as co-fired multiplayer ceramic packages (Gerke, 2003). Ceramics have dielectric constants from 4 to 10000, thermal expansion coefficients matching silicon 30×10^{-7}/ºC or copper 170×10^{-7}/ºC and thermal conductivities from one of the best insulators to better than aluminium metal 220 W/m-°K (Holmes, 2000). Dimensional stability as measured by shrinkage control has been achieved at better than ±0.1% of nominal shrinkage, allowing as many as 30 to 50 layers of ceramic to be metallized (Holmes, 2000). Ceramic packages can be found in a variety of forms, such as DIP's, chip carriers, flat packs, and pin grid arrays. A ceramic dual in line package will cost approximately $0.82 and a 14 pin plastic package costs $0.063 (Maluf, 2000).

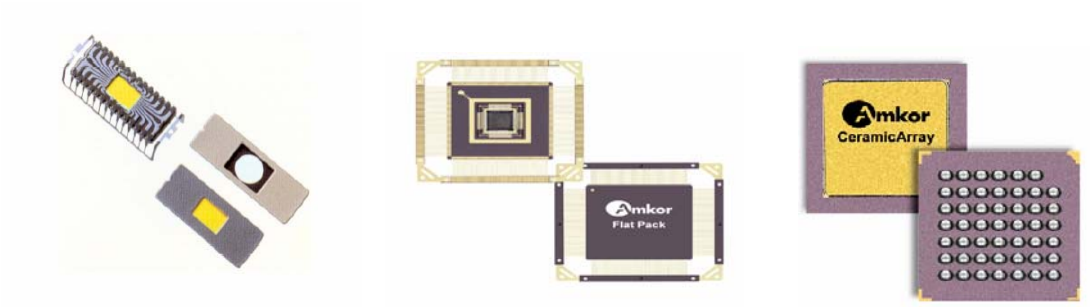

(a) (b) (c)

Fig. 2.5. Ceramic packages a) dual-inline package CerDIP, b) flat pack package, c) ball grid array (Courtesy: Amkor).

2.4.3. Thin film multilayer packages

Within the broad subject of thin-film multilayer packages, Fig 2.6a, two general technologies are used. One method is using sheets of polyimide laminated together in a way similar to that used for the low-temperature co-fired ceramic (LTCC) packages. Its a three-dimensional (3D) ceramic technology. It utilizes the z-dimension for interconnect layers, embedded circuit elements, and integral features like shelves and cavities, Fig. 2.6b. Each individual sheet is typically 25µm and is processed separately using thin-film metal processing. In another such technique polymer material is used (Harper, 1969).

(a) (b)

Fig. 2.6. Multilayer packages a) multilayer packages, b) LTCC package (Lawson, 2003) (Courtesy: Kyocera).

2.4.4. Plastic packages

Plastic packages have been widely accepted by the electronics industry due to their attractive low prices and low manufacturing costs (Tummala, 1989). This kind of packaging can be very attractive to the MEMS because they cost less, weigh less, and can be small. Unfortunately they suffer from moisture absorption which decreases reliability

(Tummala, 1989). Molded packages are not hermetic, unlike the metal and ceramic packages (Ramesham and Ghaffarian, 2000). Polymer and metal are flesh and bones of a plastic package. There are two main approaches to plastic packaging such as post-molding and pre-molding. The pre-molding packages separate into injection molding and transfer molding (Hsieh et al., 2002). The molding process is a harsh process which involves melting the thermosetting plastic at 175ºC, then flowing it under relatively high pressure of about 6 MPa, into the mold cavity before it is allowed to cool. The temperature cycle gives rise to sever thermal stresses, due to mismatch in coefficients of thermal expansion between plastic, lead frame, and die (Ramesham and Ghaffarian, 2000).

3. MATERIALS FOR MEMS AND PACKAGES

3.1. Materials used in making the micromechanical system

The integrated MEMS comprise of the IC and the micromechanical device on the same die. The IC side generally comprises of the CMOS, MOSFET, etc. Design of microsystems and their packaging however is different from that of microelectronics. A checklist of factors that help the MEMS designer in selecting substrate materials for microsystems is summarized in Table 3.1 (Madou, 1997).

Table 3.1. Typical electrical resistivity of insulators, semiconductors and conductors.

Materials	Approximate electrical resistivity ρ, Ω-cm	Classification
Silver	10^{-6}	Conductors
Copper	$10^{-5.8}$	
Aluminium	$10^{-5.5}$	
Platinum	10^{-5}	
Germanium	10^{-3}-$10^{1.5}$	Semiconductors
Silicon	10^{-3}-$10^{4.5}$	
Gallium arsenide	10^{-3}-10^{8}	
Gallium phosphide	10^{-2}-$10^{6.5}$	
Oxide	10^{9}	thermal insulators
Glass	$10^{10.5}$	
Nickel	10^{13}	
Diamond	10^{14}	
Quartz	10^{18}	

3.1.1. Silicon as a substrate material for MEMS

Silicon is the most abundant materials of earth. Mostly it occurs in compounds with other elements. Silicon is an extremely good mechanical material (Pryputniewicz, 2003a). The basis of micromechanics is that silicon in conjunction with its conventional

role as an electronic material that can take advantage of an advanced microfabrication technology, can be exploited as a high precision, high strength, high reliability mechanical material (Madou, 1997).

The four factors that have made silicon important as a mechanical material are:

1) available in abundance, inexpensive, can be produced and processed controllably to unparalleled standards of purity and perfection,
2) silicon processing is based on very thin deposited films which are highly amenable to miniaturization,
3) definition and reproduction of the device shapes and patterns are performed using lithographic techniques,
4) it can be batch fabricated.

Polysilicon is a polycrystalline compound of silicon which is popularly used. Polysilicon can be deposited onto silicon substrates by chemical vapor deposition as illustrated in Fig. 3.1.

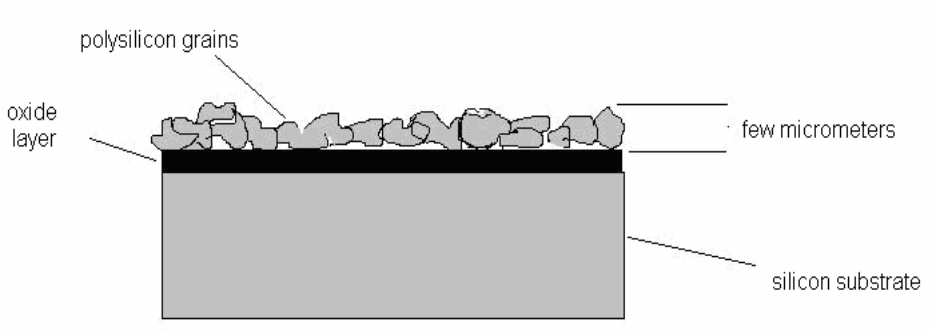

Fig. 3.1. Polysilicon deposition on a silicon substrate.

A comparison of some key properties of polysilicon and other materials is presented in Table 3.2 (Madou, 1997; Pryputniewicz, 2003a).

Table 3.2. Comparison of mechanical properties of polysilicon and other materials.

Materials	Modulus of elasticity GPa	Poisson's ratio	Coefficient of thermal expansion ppm/°C
As substrates			
Silicon	190	0.23	2.6
Alumina	415		8.7
Silica	73	0.17	0.4
As thin films			
Polysilicon	160	0.23	2.8
Thermal SiO_2	70	0.2	0.35
LPCVD SiO_2	270	0.27	1.6
PECVD SiO_2	-	-	2.3
Aluminium	70	0.35	25
Tungsten	410	0.28	4.3
Polymide	3.2	0.42	20-70

3.2. Material requirements for MEMS packaging

3.2.1. Die attach materials

MEMS devices are diced from a wafer and mounted on a substrate which may be ceramic, metal, or plastic (Pryputniewicz, 2003a). Some of the properties for choosing the die attach materials are:

1) tensile strength,
2) fatigue strength,
3) coeffcient of thermal expansion (CTE),
4) thermal conductivity,

5) outgassing,

6) shear strength,

7) fracture toughness,

8) moisture absorption rate,

9) cost.

The die attach material should strongly adhere to the substrate so that the die does not move with respect to the substrate. This kind of die movement can cause serious problems in all MEMS which require alignment. Fracture toughness for materials such as glass, is very important because it determines the material resistance to failure (Dressendorfer et al., 2000). The CTE mismatch between the die attach, silicon and substrate may result in undesirable stresses causing cracks in the bond. Most of the times the attachment material must conduct heat from die to the substrate, thermal conductivity then becomes important. Various die attach materials are enumerated below (Tummala, 2001).

1) soft materials:

    a) lead based solders,

    b) organics (epoxies and polyimides).

Thermal mismatch between the die and the heat sink, or board, is absorbed primarily by the bond itself, making it susceptible to fatigue fracture or disbanding, but transmitting little damage due to stress (Olsen and Berg, 1997).

2) hard materials:

    a) gold based eutectics (AuSi, AuSn, AuGe),

b) glass.

Bonds of these materials are highly resistant to fatigue, but transfer high mismatch stress to the device, which may lead to die cracking (Moghadam, 1983).

One way to reduce the stress induced to the die is to use organic rather than inorganic materials for the die attach (Dressendorfer et al., 2000). Also organic adhesives are widely used due to their low cost and ease of rework. Organic die attach materials are typically not used for ceramic packages because, the higher temperature needed to produce frit seal after the die attach process, may degrade the properties of the adhesive. Common organic die attach materials are epoxies, silicones, and polyimides, Table 3.3.

Table 3.3. Mechanical properties of die attach materials (Pecht et al., 1999).

Material	Tensile strength (MPa)	Shear strength (MPa)	Modulus of elasticity (GPa)
Silicone	10.3	-	2.21
Urethane	5.5-55	15.5	-
Acrylic	12.4-13.8	-	0.69-10.3
Epoxy silicone	-	11.7	-
Epoxy novolak	55-82.7	26.2	2.76-3.45
Polyimide	-	16.5	3.0
Epoxy polyimide	-	41	-
Modified polyimide	-	-	0.275
Epoxy bisphenol	43-85	-	2.7-3.3

Epoxies and polyimides are sometimes filled with precious metals such a silver (70% to 80%) which enhances electrical and thermal conductivity (Pecht et al., 1995). Example of a new epoxy used frequently in MEMS packaging is Ablefilm 5025 which is a silver filled epoxy adhesive film designed to provide good thermal and electrical conductivity when MEMS and ICs are integrated on a single die, Table 3.4.

Table 3.4. Properties of Ablefilm 502E (Pecht et al., 1999).

Property	Unit
Shear strength	17237 KPa-20684.4 KPa
Glass transition temperature	90°C
CTE below T_g	65 ppm/°C
CTE below T_g	1.5 ppm/°C
Thermal conductivity	3.462 W/m°C

3.2.2. Substrate materials

The following factors determine the selection of a substrate material for MEMS packages:

1) dielectric constant,
2) loss tangent,
3) CTE,
4) elastic modulus,
5) thermal conductivity,
6) resistance to chemical.,
7) porosity and purity,
8) cost.

High dielectric constant causes cross talk between "wires" or traces, because it is directly proportional to the capacitance. High loss tangent (means a lot of dielectric absorption) causes the signals to lose their amplitude and frequency as they propagate through wires. If the substrate has loss, the performance of MEMS devices are reduced significantly since many MEMS devices are sensitive to the frequency of the applied

signals (Feng et al., 2000). An appropriate CTE is also required for substrates. The CTE of the substrate must match the CTE of the die and die attach materials in order to minimize the thermal-mechanical stresses in package (Dressendrofer, 2000; Pryputniewicz, 2003b). The commonly used substrates and some of their properties are summarized in Tables 3.5 and 3.6, while Table 3.7 lists common materials with respect to the various components of packaging.

Table 3.5. Mechanical properties of some common substrates (Pecht et al., 1999).

Material	Tensile strength (MPa)	Modulus of elasticity (GPa)	Flexural strength (MPa)
BeO	230	345	250
AIN	-	310-343	360
Si	-	190	580
Alumina (96%)	17.4	310.3	317
Alumina (99%)	206.9	345	345
Steatite	55.2-69	90-103	110
Fosterite	55.2-69	90-103	124
Quartz	48.5	71.7	-

Table 3.6. Thermal properties of some common substrates (Pecht et al., 1999).

Material	Thermal conductivity (W/m°C)	CTE (ppm/°C)
BeO	150-300	6.3-7.5
AIN	82-320	4.3-4.7
Si	125-148	2.33
Alumina (96%)	15-33	4.3-7.4
Alumina (99%)	15-33	4.3-7.4
Steatite	2.1-2.5	8.6-10.5
Fosterite	2.1-4.2	11
Quartz	43	1.0-5.5

Table 3.7. Common materials used in packaging, (Hsu, 2002).

Components	Available materials
Die	Silicon, polysilicon, GaAs, ceramics, quartz, polymers
Insulators	SiO_2, Si_3N_4, quartz, polymers
Constraint base	Glass, quartz, alumina, silicon carbide
Die bonding	Solder alloys, epoxy resins, silicone rubber
Wire bonds	Gold, silver, copper, aluminium, tungsten
Interconnect pins	Copper, aluminium
Headers and casings	Plastic, aluminium, and stainless steel

4. Packaging methods and processes

Packaging of MEMS, similar to IC technologies, need environmental protection, electrical signal conduit, mechanical support, and thermal management paths. Packaging of MEMS is considerably complex as they serve to protect from the environment, while somewhat in contradiction, enabling interaction with that environment in order to measure or affect the desired physical or chemical parameters (Ramesham and Ghaffarian et al., 2000; Pryputniewicz, 2003b).

4.1. Basic elements of a package

Four basic elements can be defined in a functional package, Fig 4.1 (Gilleo, 2001).

1) device: the device can be a surface micromachined cantilever beam, or a diaphragm. It can also be a microchannel die. Device is the die that is diced from a silicon wafer.
2) wiring or routing: the next part of the system is some form of wiring structure that creates the pathway between the device and the bottom of the package that will ultimately connect to the printed wiring board (PWB).
3) packaging enclosure: the package must have some form of enclosure to protect the device, wiring structure, and chip level interconnects. The enclosure also has other applications of handling, board level assemblies and heat management.

4) board level joining system: metal leads, ball grid array, flip chip, etc., are some methods utilized for the board level joining system.

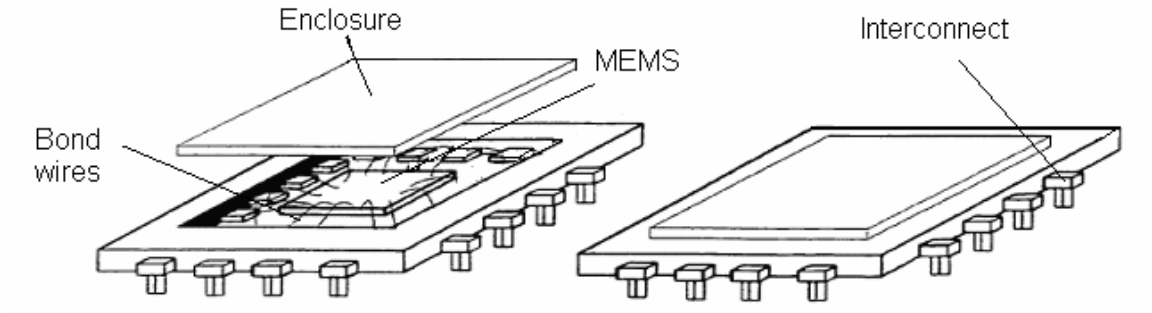

Fig. 4.1. Elements of the package (Liu, 2002).

4.2. Packaging hierarchy

The MEMS packaging can be categorized into three levels, unlike the electronic packaging with a hierarchy of four levels (Hsu, 2002), Fig 4.2.

1) Level 1: die level
2) Level 2: device level
3) Level 3: system level

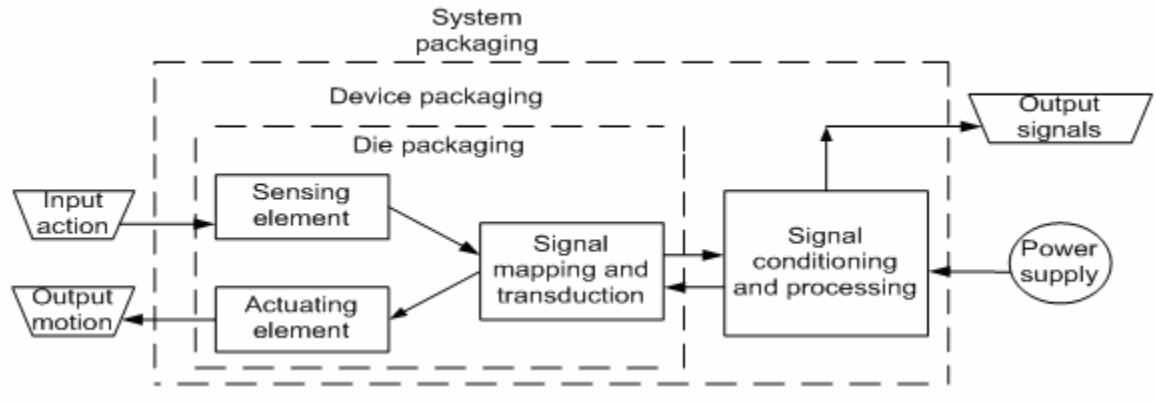

Fig. 4.2. Three levels of packaging (Hsu, 2002).

4.2.1. Die-level packaging

This level of packaging involves the assembly and protection of many delicate components formed on the silicon wafer. These delicate structures are, e.g., diaphragm, cantilever, microvalves, micropumps, etc. The primary objectives of this level packaging are (Hsu, 2002):

1) to protect the die or other core elements from plastic deformation and cracking,
2) to provide necessary electrical and mechanical isolation of these elements,
3) to ensure that the system functions at both normal operating and overload conditions.

4.2.2. Device level packaging

This level of packaging requires the inclusion of proper signal conditioning and processing, which in most cases involves electric bridges and signal conditioning circuitry for sensors and actuators (Hsu, 2002).

4.2.3. System-level packaging

System level packaging involves the packaging of primary signal circuitry with the die, or core element unit. System packaging requires proper mechanical and thermal isolation as well as electromagnetic shielding of the circuitry (Hsu, 2002).

4.3. Basic packaging operations

The basic packaging operations can be enumerated as follows:

1) die preparation: is the process by which the wafer is singulated into individual dice in preparation for assembly. Die preparation consists of two major steps, namely, wafer mounting and wafer sawing. Wafer mounting is the process of providing support for the wafer, to facilitate the processing of the wafer from Wafer Saw through Die Attach. During wafer mounting, the wafer and a wafer frame are simultaneously attached on a wafer, or dicing tape. The wafer frame may be made of plastic or metal., but it should be resistant to warping, bending, corrosion, and heat. The dicing tape (also referred to as a wafer film) is just a PVC sheet with synthetic adhesive on one side to hold both the wafer frame and the wafer. Typically measuring 3 mils thick, it should be flexible yet tough and strong, and with low impurity levels as well. Wafer saw follows wafer mounting and is the step that actually cuts the wafer into individual dice for assembly in MEMS/IC packages.

(a) (b)

Fig. 4.3. a) Wafer mounts (Courtesy: Semicon) b) Dicing saws (Courtesy: Semicon).

2) die attach: is the process of attaching the silicon chip to the die pad or die cavity of the support structure (e.g., the leadframe) of the package, Fig. 4. 4. There are two common die attach processes, i.e., adhesive die attach and eutectic die attach. Adhesive die attach uses adhesives such as polyimide, epoxy and silver-filled glass to mount the die on the die pad or cavity. The adhesive is first dispensed in controlled amounts on the die pad or cavity. The die for mounting is then ejected from the wafer by one or more ejector needles. While being ejected, a pick-and-place tool commonly known as a 'collet' then retrieves the die from the wafer tape and positions it on the adhesive. Eutectic die attach, which is commonly employed in hermetic packages, uses a eutectic alloy to attach the die to the cavity. A eutectic alloy is an alloy with the lowest melting point possible for the metals combined in the alloy. The Au-Sn eutectic alloy is the most commonly used die attach alloy in semiconductor packaging.

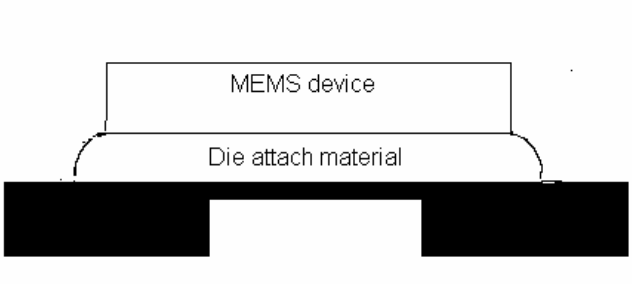

Fig. 4.4. Die attachment on substrate.

3) wirebonding: it is the most widely used method of chip interconnection in the microelectronics industry. The wirebonding begins by firmly attaching back side

of a chip to the appropriate substrate location, or package bottom, Fig 4.5. The wires are then bonded or welded, one at a time, using a special tool, wedge or capillary and a combination of heat, pressure and/or ultrasonic energy. Types of wirebonding are (Charles, 1989):

a) thermocompression bonding: results when two metal surfaces are brought in intimate contact during a controlled time, temperature, and pressure cycle. During this cycle, the wire and, to some extent, the underlying metallization, undergo plastic deformation and atomic interdiffusion between the wire and bonding pad.

b) ultrasonic bonding: is a low temperature process in which the source of energy for the metal welding is a transducer vibrating the bonding tool in a frequency range from 20 kHz to 60 kHz.

c) thermosonic bonding: combines ultrasonic energy with the ball bonding capillary technique of thermocompression bonding.

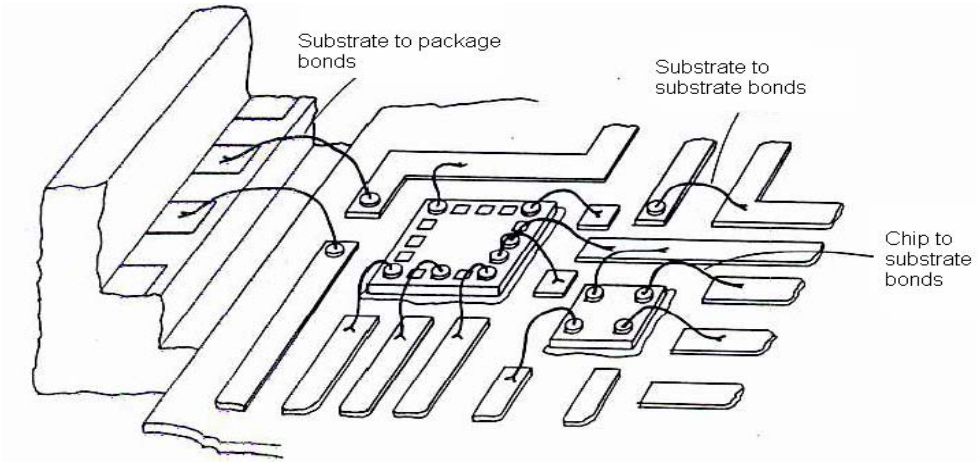

Fig. 4.5. Circuit with its wire bonds (Charles, 1989).

4) testing: testing is performed to allow any necessary rework to be accomplished judiciously and at the same quality level as the initial manufacturing process (Grzelak, 2000). Testing can be classified into three parts:

    a) wafer level testing: the internal microstructure of materials exerts a greater influence on properties of materials. Requirements for low level contaminant identification, and control becomes more stringent with decreasing dimensions. Hence, wafer level testing deals with mostly material analysis (Davies, 1989). This can be done by scanning electron microscopy (SEM), X-Ray microprobe spectroscopy, transmission electron spectroscopy (TEM), Auger electron spectroscopy, or Optoelectronic Holography (OEH).

    b) package level testing: electronic components are contained in a hermetic, or plastic, enclosures for protection from physical damage and/or the adverse effects of gaseous ambient products. Consequently, package level tests have been developed as a means of ensuring reliable package performance. These tests are useful in assessing the quality of package design and assembly, and they provide an estimate of package reliability in field use (Moore et al., 1989).

    c) component and board level physical tests: physical tests to qualify a component or printed circuit board (PCB) are often considered to be back end hurdles that can bring into focus some non-functionality. Complete physical and mechanical verification is impossible, but the maturing

automation of inspection has greatly improved quality and reliability. These include automatic optical testing, solder joint inspection, plating thickness, and environmental testing (Palmer, 1989).

5) sealing: sealing is a process that contains the electronic packages within an inert environment. This is the known as hermetic packaging. The process consists of following "steps" (Tummala, 2001):
    a) fused metal sealing,
    b) soldering,
    c) brazing,
    d) welding,
    e) glass sealing.

    Non hermetic pakcages are also gaining importance. These feature epoxy molding and a blob top.
6) marking: is the process of putting identification, traceability, and distinguishing marks on the package. The device name, company logo, date code, and lot ID are examples of information commonly marked on the packages. Some marks are put on the package during assembly and some marks are put on the package during test. There are two common marking processes, namely, ink marking and laser marking. The most common ink marking process for semiconductor products is pad printing. Pad printing consists of transferring an ink pattern from the plate, which is a flat block with pattern depressions that are filled with ink, to the package, using a silicone rubber stamp pad. Silicone rubber repels ink, making

the transfer of the ink pattern clean and efficient. It is also resilient and elastic, making it possible to print even on uneven surfaces.

4.4. State of the art packaging of MEMS

State of the art packaging of MEMS can be divided into three main areas (Bossche et al., 1998):

1) single chip packaging,
2) wafer level packaging,
3) multi-chip modules.

4.4.1. Single chip packaging

This packaging method is defined for typical IC standard packages. For example T0-packages, ceramic packages, or pre-formed injected molded packages, are used for single MEMS chips. The single chips are provided with protective layers to shield the vulnerable structures and circuits from environmental influences (Gessner et al., 2004). MEMS are diced then released to protect them from the sawing process. Die are then packaged in ceramic cavity, metal can, glass and pre-molded plastic, Fig 4.6.

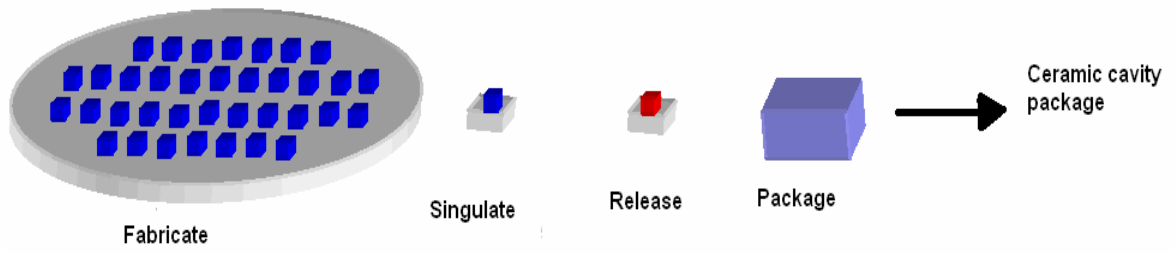

Fig. 4.6. Single chip packaging (Rao, 2002).

4.4.2. Wafer level packaging

A relatively new field of packaging is the wafer level packaging (WLP). Wafer bonding techniques have gained a lot of importance during the past 10 years (Bossche et al., 1998). In this process the MEMS are released at the wafer level with protection by another wafer cap, Fig. 4.7.

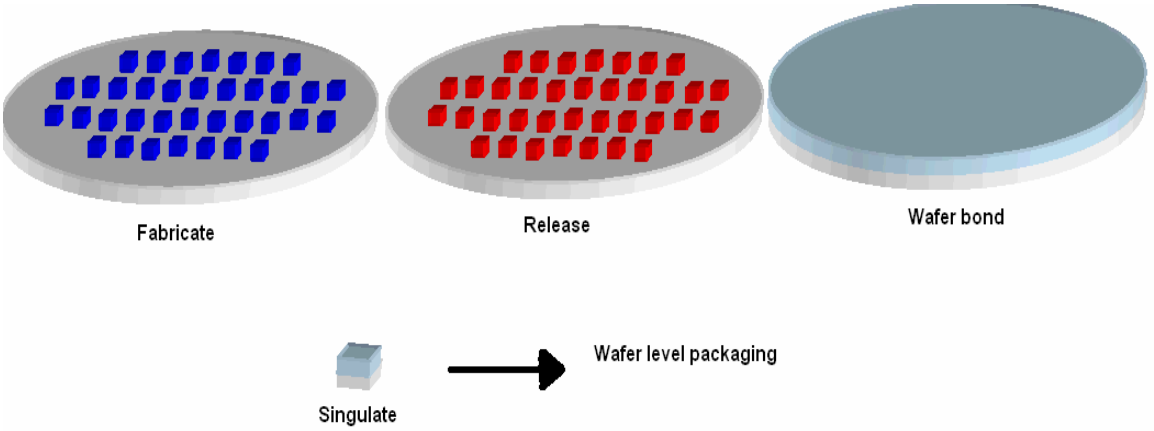

Fig. 4.7. Wafer level packaging (Rao, 2002).

A number of methods exist to bond silicon wafers to other silicon, or glass, wafers. These include anodic bonding, glass frit bonding, silicon direct wafer bonding (DWB), eutectic bonding, epoxy bonding, thermo-compression bonding, and glass to glass bonding (Mirza, 2000). This method is beneficial to pursue the plastic packaging of MEMS on a more reliable basis. Researchers at IC Mechanics (Guillou, 2003) have developed a thin film cap deposited during wafer manufacturing, Fig 4.8.

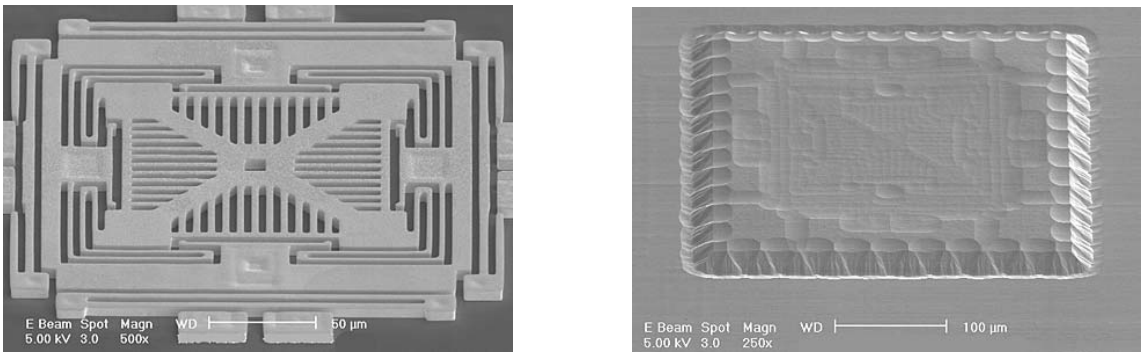

(a) (b)

Fig. 4.8. 3-axis MEMS accelerometer: (a) without wafer cap, (b)with wafer cap (Courtesy: SensorMag).

4.4.3. Multi chip modules

This type of packaging involves the packaging of different devices, such as sensors, actuators, and electronics, in a single compact module to make smart miniaturized systems (Bossche et al., 1998). The economic aspect has caused the effect that the use of microsystems could be established in all those areas where large quantities are needed.

5. PLASTIC ENCAPSULATED PACKAGES

Plastic encapsulated packages consist of the IC or the MEMS die, physically attached to the leadframe, electrically interconnected to input-output leads, and molded in plastic. Plastic encapsulated packages are made in either surface-mount, or through-hole, configurations. The common families of surface mounted are the small-outline package (SOP), the plastic-leaded chip carrier (PLCC), and the plastic quad flatpack package (PQFP). The common families of through-hole mounted devices are the plastic dual in-line package (PDIP), single in-line package (SIP), and the plastic pin grid array (PPGA).

5.1. Why plastic encapsulated packages ?

Advantages of plastic encapsulated packages (PEPs) over hermetic packages:

1) size and weight: weight of plastic packages is about half as much as ceramic packages. The available plastic encapsulated microcircuits (PEMs) can give a general idea of the size and weight. A fourteen lead plastic dual in-line package (DIP) weighs about one gram, versus two grams for a fourteen-lead ceramic DIP. Smaller configurations such as SOPs and thinner configurations such as thin small outline package (TSOP) are available only in plastic.
2) performance: plastics have better dielectric properties than ceramics. For typical applications encountered commercially, in which frequencies do not exceed 2 to 3 GHz, plastic packages perform better than their ceramic counterparts, in the same form factor (Pecht et al., 1995). The dielectric constant of typical ceramics stays

the same over a wide frequency range whereas the dielectric constant changes for plastic molding compounds. This is because the dielectric constant is dependent on the amount of moisture absorption.

3) cost: hermetically packaged ICs may cost up to ten times more than a plastic-packaged IC because of the rigorous testing and screening required for low volume hermetic parts (Pecht et al., 1995). Hermetic packages usually have a higher material cost and are fabricated with more labor intensive manual processes. The cost of a packaged device in the microelectronics industry is determined by several factors. Figure 5.1, shows an example of items that affect the total cost of a package. Figure 5.2, presents the relative cost for various microcircuits packaging options.

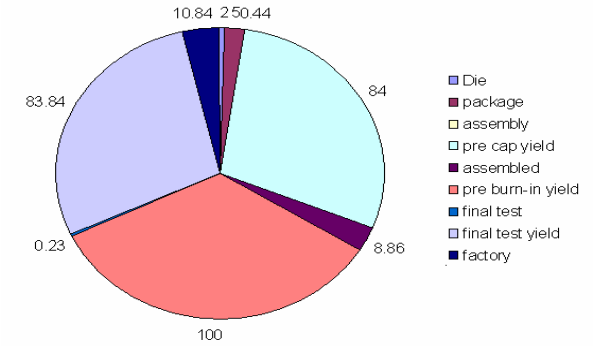

Fig. 5.1. Cost drivers in packaging (Pecht et al., 1995).

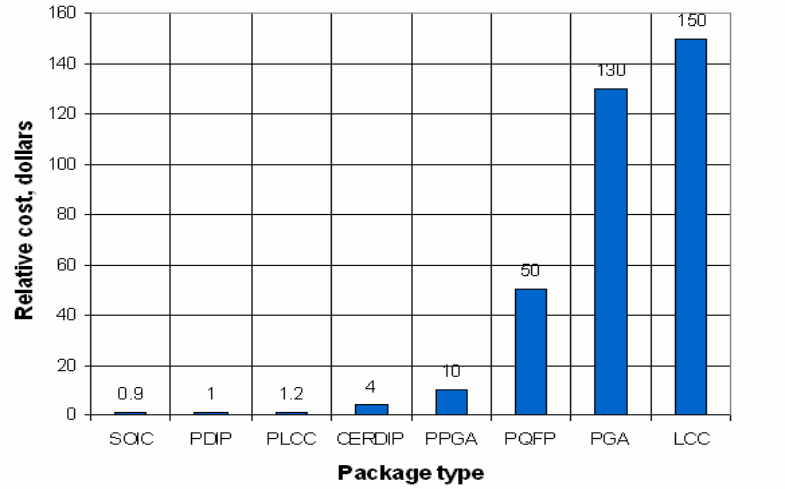

Fig. 5.2. Relative costs for various microcircuits packaging options (Pecht et al., 1995).

The cost benefits of PEMs decrease with higher integration levels and pin counts, because of the high price of the die, in relation to the total cost of the packaged device. The trend towards future multichip modules in laminated packaged in form factors such as PQFPs or ball grid arrays make the plastic package an innovative packaging option (Pecht et al., 1993). Table 5.1, compares ceramic to plastic cost for dual in-line packages (Pecht et al., 1995).

Table 5.1. Ratio of ceramic to plastic cost for dual in-line package.

Lead count	Cost of ceramic package/plastic package Dual-in-line package
8	4.0
16	6.7
18	6.3
20	6.0
24	8.3
28	7.5
40	6.9

4) availability: plastic devices are assembled and packaged on continuous production lines, as opposed to the on-demand production of hermetic parts. Hermetic packages are developed only when there are perceived high performance requirements and sufficient market interest. Thus acquisition lead times for plastic packages are significantly shorter.

5) reliability: due to the contributions improved encapsulant materials, die passivation, and manufacturing processes reliability of plastic encapsulated packages have increases tremendously (Pecht et al., 1993). Figure 5.3, presents the observed comparative failure-rate data for hermetic and non-hermetic devices from first year warranty information on commercial equipment operating primarily in ground base applications from 1978 to 1988 (Pecht et al., 1993).

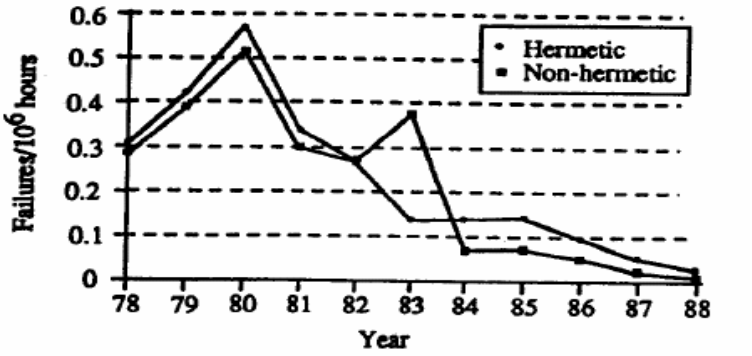

Fig. 5.3. IC failure rate as a function of year (Pecht et al., 1993).

5.2. Plastic packaging materials

This section presents the research work on the plastic encapsulated materials and their characteristics. The chapter has been organized in the same sequence as the materials used for various parts of the plastic package in the IC industry. Fig 5.4 shows that cross-sectional sketch of a typical plastic encapsulated package.

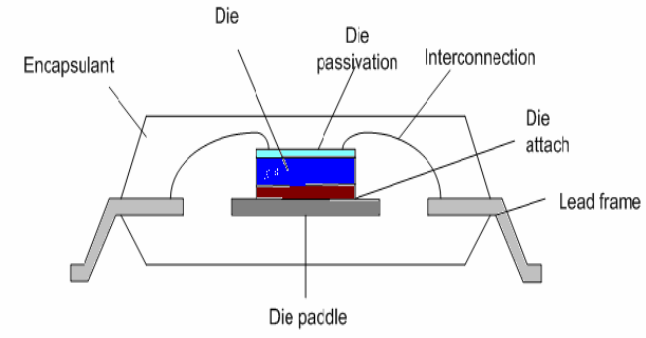

Fig. 5.4. Cross-section of a typical plastic encapsulated package.

5.2.1. Flow of materials and parts in plastic packaging

1) die: the silicon die to be packaged is diced from a fully processed wafer.
2) die passivation: the purpose of die passivation is to seal the active circuit elements from ambient moisture, ionic contaminants, mechanical damage due to handling and in some cases radiation and electrostatic discharge.
3) leadframe: the leadframe consist of a die mounting paddle and lead-fingers. It primarily acts as a mechanical support to the die during package manufacture. The lead-fingers connect the die to the circuitry external to the package. Material selection criterion includes (Pecht et al., 1995):

a. coefficient of thermal expansion,
b. thermal conductivity,
c. mechanical strength,
d. adhesion to encapsulant and die-attach material.,
e. oxidation and corrosion resistance,
f. stampability, formability, etchability,
g. solderability,
h. design configuration.

4) die attach: the silicon die is attached to the die paddle of the lead frame with a die attach. The die attach material include heat transfer from the dies to the leadframe and if needed die backside electrical contact. Material property considerations in choosing die attach materials include the shear strength, void density on application, impurity content, volume resistivity, thermal conductivity, manufacturability and cost effectiveness.
5) interconnections: of all the interconnection technologies used in packaging wirebonding is overwhelmingly dominant. The criterion are: ultimate tensile strength, flexural strength, bond pull strength, maximum die pad bonding temperature, resistance to intermetallic formation, surface contamination.
6) encapsulating compound: an encapsulant is generally an electrically insulating plastic material formulation that protects the die and leadframe assembly from the adverse effects of handling, operation, and storage. The selection criterion are:

a. moldability, cure speed, melt viscosity, flash,

b. hot hardness,

c. mold strain resistance,

d. ionic impurity level,

e. molding defects,

f. moisture resistance,

g. adhesion to all package elements,

h. curing stress,

i. coefficient of thermal expansion match with leadframe,

j. mechanical strength,

k. glass transition temperature,

l. thermal conductivity,

m. thermal stability.

The available materials for the various plastic package parts are summarized in Table 5.2.

Table 5.2. Materials for various parts (Pecht et al., 1995).

Die passivation	Lead frame	Die attach	Interconnection	Encapsulating compound
Phosphorus-doped silicon dioxide, Silion nitride,	Cu-Zr Cu-Fe Cu-Mg Fe-Ni	Polymer: resin based epoxies or polymides Solder die attach Gold eutectic die attach	Gold Aluminium Silver Copper	Epoxies Cyanate esters Urethanes Silicones

5.3. Plastic package types

Plastic packages for the ICs are available in a wide assortment of package styles and lead configurations. They can be classified as surface-mount or through-hole configurations.

5.3.1. Surface-mount configuration

Surface mount packages are designed for low-profile mounting on printed wiring boards for smaller products. The various package configurations are:

1) Plastic quad flat pack (PQFP): they are square or rectangular plastic packages with leads on all four sides. The package consists of a metal lead frame with a center paddle for chip attachment. The lead count varies from 40 to 240 pins (Pecht et al., 1995). The major advantage of these low-profile packages is density mounting.
2) Plastic leaded chip carrier (PLCC): they are molded plastic packages with leads on all four sides. The leads are formed in the J-bend configuration, with lead counts 18-124 (Pecht et al., 1995). This also offers the advantage of dense mounting.
3) Small outline package (SOP): they have leads only on two sides of the package body. Pin counts vary from 8-28. Body widths are typically narrow, 3.675 mm to 7.35mm (Pecht et al., 1995). The small body size and low profile occupies lesser space. The gull wing lead form allows ease of inspection of the solder joints.

The common families are as shown in Fig. 5.4.

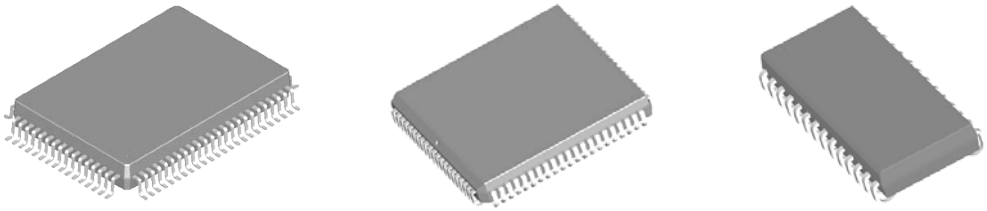

(a) (b) (c)

Fig. 5.5. Surface mount configurations: (a) Plastic quad flat pack, (b) Plastic leaded chip carrier, (c) small-outline package
(Courtesy: National Semiconductors).

5.3.2. Through-hole mounted configuration

The various types of through-hole mounted package designs are:

1) plastic dual-in-line package (PDIP): it is the most commonly used plastic package. It has rectangular body with two rows of leads on the long sides. Pin counts range from 4 to 64 leads (Pecht et al., 1995). These are a direct replacement of CERDIP packages at a much lower cost.
2) plastic pin grid array (PPGA): they are packages with pins in a grid array under a plastic body. It offers the highest density of through hole packages and the highest available pin counts for plastic packages (Pecht et al., 1995).
3) single in-line package (SIP): they are rectangular plastic packages with leads on one of the long sides. Not used much as it results in a high profile after mounting (Pecht et al., 1995).

The common families for the through-hole mounted configuration are as shown in Fig 5.5.

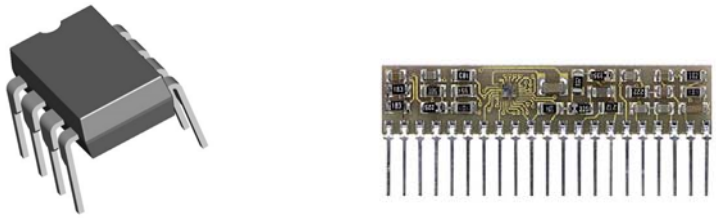

(a) (b)

Fig. 5.6. Through-hole mounted configurations: (a) Plastic dual-in-line package (b) single-in-line package (Courtesy: National Semiconductors).

Some MEMS that have used the plastic packaging approach are MEMS accelerometers and non-hermetic camera modules, which use the plastic molded packages (Amkor, 2003). Most of the MEMS devices can use the plastic encapsulation approach by protecting the MEMS die at the wafer level. It involves an extra fabrication process, where the micro-machine wafer is bonded to a second wafer which has appropriate cavities etched into it. Once bonded this creates a protective cavity over the micro-machine structure. This method leaves the micro-machine free to move within a vacuum or an inert gas atmosphere. Once protected in this way, the device can be assembled in a similar way to standard plastic packaging approach (Amkor, 2004). The method can be applied to any MEMS device that requires access to the environment, including chemical, pressure, or temperature-sensitive microsensors, CCD chips, photocells, laser diodes, VCSEL's, and UV-EPROMS (Peterson and Conely, 2002). MEMS used in the medical field like the blood pressure sensors and flush diaphragm sensors measure fluid pressure, that need to be disposed after one use can be packaged with the plastic packaging approach explained above (Swafford et al.,1997).

5.4. Manufacturing process

Plastic package manufacturing depends on the package style (Tummala, 1989). Functional requirements expected from the ideal plastic-packaging method are:

1) low resin viscosity: thermoplastic and thermosets exhibit high viscosities in the upper 100 Pa. In an ideal molding process, the reacting mixture should initially display a low viscosity. This would provide good wetting of the device topology.
2) good wetting of chip components: both resin and surface tension control the wetting of any chip component. Estimation of the wetting behavior of a given resin with a surface can be determined by the familiar Young's equation, Eq. 5.1.

$$\sigma_l \cos\theta = \sigma_s - \sigma_{sl} \quad . \tag{5.1}$$

relating the surface tensions of the solid and the liquid, and the interfacial tension between the two would apply for different cases (Wu, 1982).

3) good adhesion to chip components: adhesion is controlled by both resin chemistry and chip-surface pretreatment. The formation of good bonds between the reacting resin and the uppermost layer of the chip is a direct result of good wetting. Poor wetting leads to the formation of interfacial defects which act as potential sites for crack propagation (Mittal, 1976).
4) resin with inherently low CTE: the CTE of a polymeric encapsulant protecting a substrate dictates the magnitude of the residual stresses arising from the inherent thermal mismatch between the two materials. The differential expansion effects from a range of materials used in the device can cause small scale motions of several microns (Dale and Oldfield, 1977).

5.5. Encapsulation process technology

Molding techniques already established by the IC industry are transfer molding process, injection molding, and reaction-injection molding.

5.5.1. Transfer molding

Transfer molding is a process of forming components in a closed mold from a thermosetting material that is conveyed under pressure, in a hot, plastic state, from an auxiliary chamber, called the transfer pot, through runners and gates into the closed cavity or cavities (Pecht et al., 1995).

The various steps in transfer molding are:

1) leadframes are loaded in the bottom half of the mold,
2) moving platen and transfer plunger initially close rapidly, but the speed reduces as the close, progresses,.
3) after the mold is closed and clamping pressure is applied the molding material is placed in the pot, and the transfer plunger or ram is activated,
4) pre-heating of the molding compound is done by a high-frequency electronic method that works on a principle similar to microwave heating,
5) transfer plunger then applies the transfer pressure forcing the molding compound through the runners and gates into the cavities,
6) pressure is maintained for a certain optimum time, ensuring proper filling of the cavities,

7) then, the mold opens, and finally the component is ejected using the ejector system in the mold.

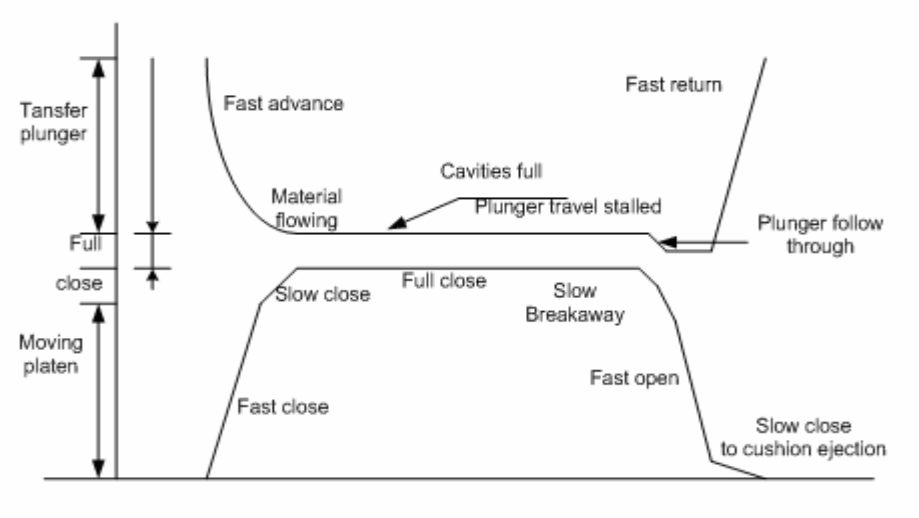

Fig. 5.7. Various stages of a typical transfer molding process (Courtesy: Pecht et al., 1995).

Fig. 5.8. Transfer molding press (Courtesy: Wabash MPI).

5.5.2. Injection molding

It is a technique that is used for making large volumes of molds at low costs. Injection molded parts are inexpensive because of the automated process and low cycle time. However the molds are extremely complex and withstand high pressures and hence costly. Injection molding was applied to semiconductor packaging in the 80s with thermoplastic materials (Tummala, 2001). Poor reliability hindered the usage of this technique. High viscosity of the thermoplastic material generates a lot of wire sweep due to the high injection pressure, which is typically an order of magnitude larger than the packing pressure of transfer molding. Injection molding was not considered optimum considering the cost of expensive capital investment (Pecht et al., 1995).

6. MOISTURE AS A FAILURE ACCELERATOR

The major accelerators of failure mechanisms in plastic-encapsulated packages are moisture, temperature, solvents, lubricants, contaminants, general environmental stresses, and residual stresses. It has been widely recognized that moisture plays a significant role in influencing the mechanical behavior, and therefore, the long term durability of the polymeric encapsulants (Roy et al., 2000). It has been established that the following factors and their unfavorable combinations play an important role, as far moisture induced failures are concerned:

1) high moisture content, which leads to high water vapor pressure. This might result in a considerable decrease in the ultimate, fatigue, and brittle strength of the molding compound,
2) low fracture toughness of the molding compound, which makes it unable to effectively resist the initiation and propagation of fatigue and brittle cracks,
3) low fracture toughness of the molding compound, which makes it unable to effectively resist the initiation and propagation of fatigue and brittle cracks,
4) high hygrothermal stresses, the swelling and warpage of the polymeric material induces hygroscopic stress in the package that adds to the thermal stresses at high reflow temperature, raisng the susceptibility of package to cracking, Fig. 6.1 (Wong et al., 2002).

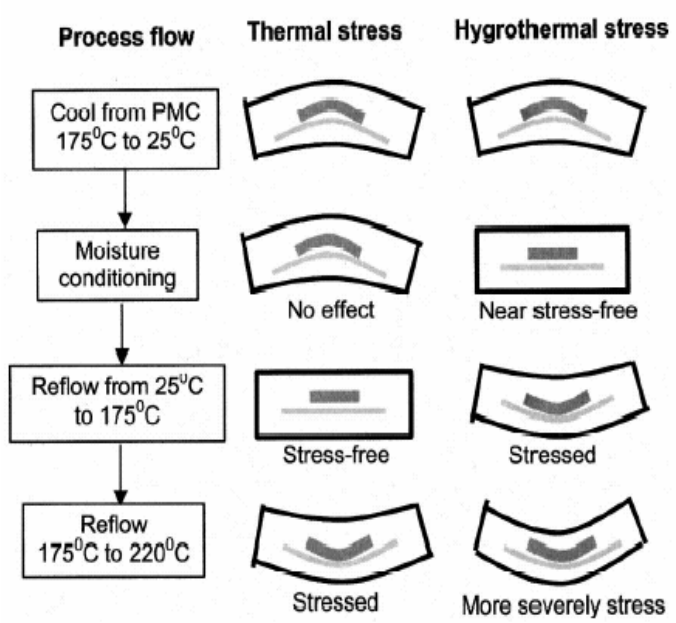

Fig. 6.1. Hygroscopic swelling raises package stress during solder reflow.

6.1. Moisture uptake in plastic encapsulants

A plastic encapsulant is generally an electrically insulating plastic material formulation that protects a micron size device from the adverse effects of handling, storage, and operation (Pecht et al., 1995). Encapsulant techniques include molding, potting, glob-topping, and conformal coating. The plastic molding compounds used in electronic packaging consist of resin, hardener, filler and other materials, Fig 6.2 (Ardebili et al., 2002).

In general., the majority of chip packages use epoxies and molding processes. Recent improvements in the properties of molding compounds, plastic package designs, and manufacturing technologies have resulted in substantial increase in the reliability of plastic packages (Suhir, 1995). A disadvantage of plastic molding compounds is that

they are hydrophilic and absorb moisture when exposed to a humid environment. Hence, use of plastic packaging for MEMS is hampered by moisture-induced failures. Plastic material is inevitable to moisture permeation. Moisture transport in polymer systems is related to the availability of molecular sized holes in the polymer structure and the polymer-water affinity. The availability of holes depends on the polymer microstructure, morphology, and crosslink density, which are functions of degree of cure, stoichiometry, molecular chain stiffness, and the cohesive energy density of the polymer.

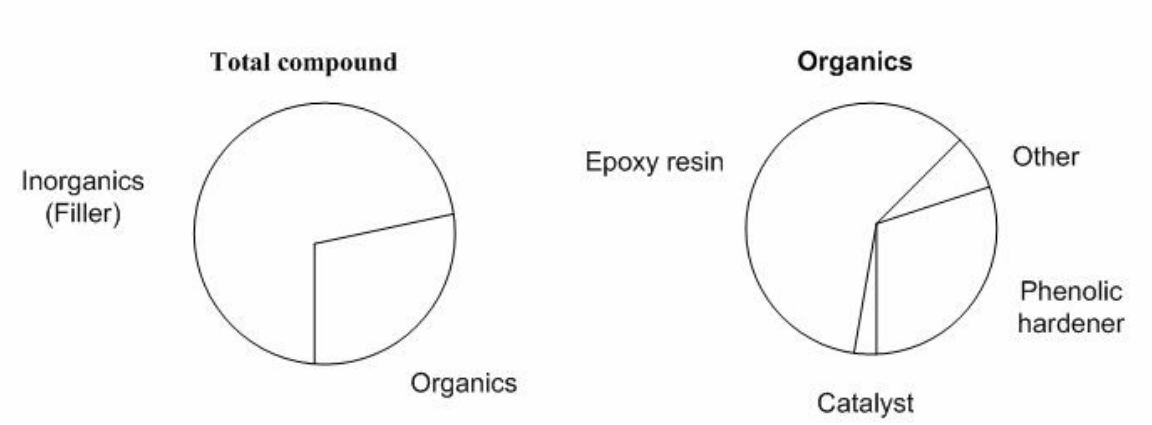

Fig. 6.2. Molding compound composition.

6.2. Moisture diffusion theory

Many researches have suggested that water molecules in a polymeric material can be present as free molecules in the voids or bound to the polymer chains via hydrogen bonding (Ardebili et al., 2003). Some issues related to the process of diffusion are:

1) the phase of the water molecules during absorption into the plastic package. In a typical environment to which plastic encapsulated packages are exposed, water molecules may be present in the forms of vapor, liquid, or both. Moisture absorption may involve phase transformation. Water vapor from the ambient may condense to the liquid phase at the exposed surfaces of the plastic package, or in the voids in the molding compounds. The condensed moisture can be either is the form of discrete droplets on the surface or in the form of uniform layers.
2) moisture absorption, is the path of diffusion. Moisture mainly diffuses through the molding compound, but a small portion can also diffuse through the interfaces between the molding compound and other materials like leads, if there is de-adhesion at their interfaces. Inside the molding compound, the moisture may diffuse through the polymeric resin, or through the filler-resin interface. The diffusion through polymeric resin can be referred to as bulk diffusion and the diffusion through interfaces between polymeric resin and other materials can be referred to as interfacial diffusion.
3) interaction between the water molecules and the polymer chains in the polymeric resin. Water molecules in the polymeric chains, can either diffuse freely through the free volume or form hydrogen bonding to the polymer chains. The free volume of the polymeric resin is defined as the volume of the resin without the volume of the polymer chains and the volume due to thermal vibrations of the polymer chains.

4) moisture absorption of molding compound samples is the thickness issue. For relatively thin samples, moisture sorption is considered one dimensional. In this research also the computational simulation is done considering it to be a one-dimensional diffusion.

The moisture diffusion phenomenon can be diagrammatically represented, Fig 6.3, (Ardebilli et al., 2003).

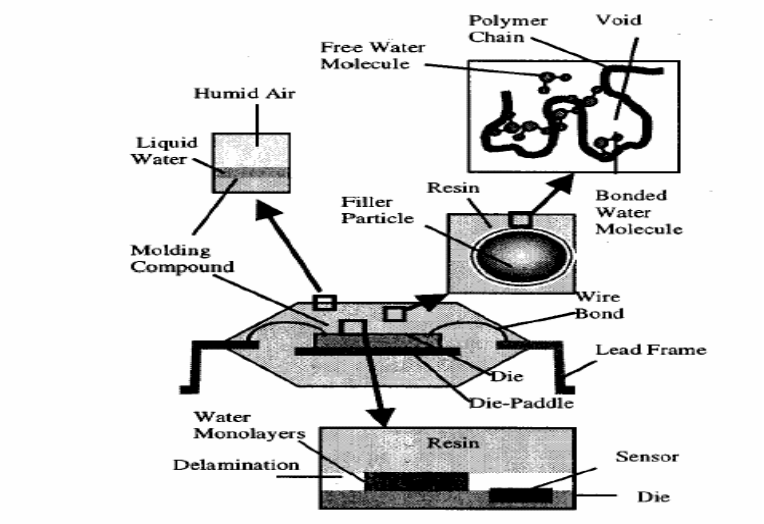

Fig. 6.3. Moisture diffusion in PEM.

6.3. Diffusion models

Two diffusion theories have been studied for the phenomenon of moisture diffusion in plastic encapsulants (Bonniau and Bunsell, 1981). The first is the classical single phase model of absorption in which the water molecules are not combined with the polymer matrix and the second, the Langmuir two phase model considers a free diffusion phase and a second combined phase which does not involve diffusion (Bonniau and

Bunsell, 1981). Both of these models are based on the Fick's law which considers that the driving force of diffusion is the water concentration gradient. The diffusion model is shown in Fig. 6.4 (Deshpande and Pryputniewicz, 2004a).

In order to simplify the analysis of the diffusion equations the following hypotheses have been made (Deshpande and Pryputniewicz, 2004a):

1) diffusion coefficient of the free phase is independent of the concentration,
2) consider a planar phase case so that diffusion occurs in one direction only, normal to the plane. The one dimensional diffusion of moisture is often considered valid, since the encapsulant layer adjacent to the die is relatively thin (Ardebili et al., 2002) for the size for the plastic encapsulant. In this Thesis the half model is considered, till the central plane. Hence further reduction in the thickness of the package. Thin packages can be off the range of about 0.2 to 0.02, thickness to length ratio (Pecht et al., 1995). This has also been discussed in Chapter 9. While a finite element modeling may provide a more accurate analysis of moisture diffusion as compared to 1-D analysis or use 3-D analytical solutions for simplified geometry, it has the major disadvantages in terms of cost and time,
3) non-steady state surface concentration is constant and initial distribution is uniform,

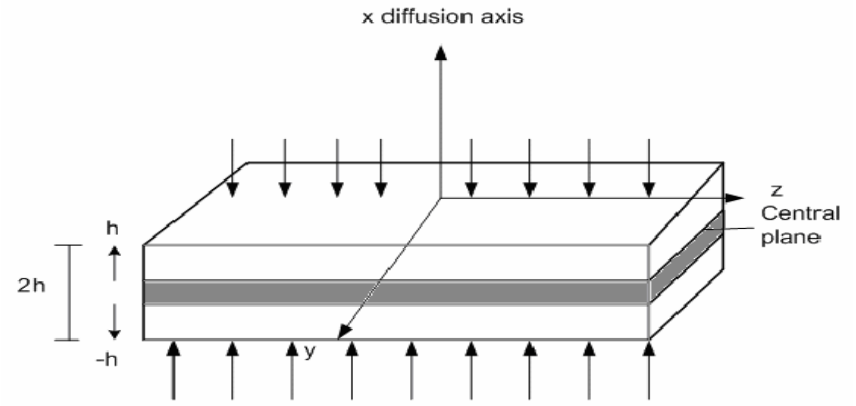

Fig. 6.4. Moisture diffusion model.

Fick's second law of diffusion for one-dimensional diffusion, i.e., if there is a gradient of concentration only along the *x*-axis is given by

$$\frac{\partial C}{\partial t} = D\frac{\partial^2 C}{\partial x^2} \quad , \tag{6.1}$$

where C is the concentration of the diffusing moisture, t is the time, and D is the diffusion coefficient. This equation can be solved assuming that the variables are separable. Thus we may attempt to find a solution by putting

$$C = X(x)T(t) \quad , \tag{6.2}$$

where X and T are functions of x and t respectively. Substitution of Eq. 6.2 into Eq. 6.1 yields

$$X\frac{dT}{dt} = DT\frac{d^2X}{dx^2} \quad , \tag{6.3}$$

which may be written as

$$\frac{1}{T}\frac{dT}{dt} = \frac{D}{X}\frac{d^2X}{dx^2} \quad , \tag{6.4}$$

The right hand side of Eq. 6.4 can be rewritten as

$$\frac{1}{T}\frac{dT}{dt} = -\lambda^2 D \quad , \tag{6.5}$$

where

$$\frac{1}{X}\frac{d^2X}{dx^2} = -\lambda^2 , \tag{6.6}$$

The solutions for Eq. 6.5 is

$$T = \exp^{-\lambda^2 Dt} \quad , \tag{6.7}$$

and the solution for Eq. 6.6 is

$$X = A\sin\lambda x + B\cos\lambda x \quad , \tag{6.8}$$

this leads to the solution for Eq. 6.1 using Eqs 6.7 and 6.8, of the form

$$C = (A\sin\lambda x + B\cos\lambda x)e^{-\lambda^2 Dt} \quad , \tag{6.9}$$

where A and B are constants of integration. Since Eq. 6.1 is a linear equation, the most general solution is obtained by summing solutions of the type of Eq. 6.9, so that we have

$$C = \sum_{m=1}^{\infty}(A_m \sin\lambda_m x + B_m \cos\lambda_m x)e^{-\lambda_m^2 Dt} \quad , \tag{6.10}$$

where A_m, B_m, and λ_m are determined by the initial and boundary conditions for the particular problem. Thus if we are interested in diffusion out of a plane sheet of thickness h, through which the diffusing substance is initially uniformly distributed and the surfaces of which are kept at zero concentration, the conditions are

$$C = C_o, \quad 0 < x < h \ , \quad t = 0 , \tag{6.11}$$

$$C = 0, \quad x = 0, \quad x = h, \quad t > 0. \tag{6.12}$$

the boundary conditions demand that

$$B_m = 0, \quad \lambda_m = m\pi / h, \tag{6.13}$$

and hence the Eq. 6.10 becomes

$$C_o = \sum_{1}^{\infty} A_m \sin(m\pi x / h), \quad 0 < x < h \quad . \tag{6.14}$$

By multiplying both sides of Eq. 6.14 by $sin(p\pi x/h)$ and integrating from 0 to h using the relationships

$$\int_0^h \sin\frac{p\pi x}{h} \sin\frac{m\pi x}{h} dx = \begin{cases} 0, & m \neq p, \\ \frac{1}{2}h, & m = p, \end{cases} \tag{6.15}$$

the terms for which m is even will be cancelled, and

$$A_m = 4C_o / m\pi, \quad m = 1, 3, 5, ...$$

The final solution is therefore

$$C = \frac{4C_o}{\pi} \sum_{n=0}^{\infty} \frac{1}{2n+1} \exp\left[-D(2n+1)^2 \pi^2 t / h^2\right] \sin\frac{(2n+1)\pi x}{h} \quad , \tag{6.16}$$

where $2n+1$ has been substituted for m for convenience so that n takes values 0,1,2…

The diffusion model considered is for the case of absorption by a plane sheet (Crank, 1975). If the region $-h < x < h$ is initially at an uniform concentration C_o, and the surfaces are kept at a constant concentration C_1, the solution in the form of trigonometric series becomes

$$\frac{C - C_o}{C_1 - C_o} = 1 - \frac{4}{\pi} \sum_{n=0}^{\infty} \frac{(-1)^n}{2n+1} \exp\left[-D(2n+1)^2 \pi^2 t / 4h^2\right] \cos\frac{(2n+1)\pi x}{2h} \quad . \tag{6.17}$$

If M_t denotes the total amount of diffusing substance which has entered the sheet at time t, and M_∞ the corresponding quantity after infinite time, then

$$\frac{M_t}{M_\infty} = 1 - \sum_{n=0}^{\infty} \frac{8}{(2n+1)^2 \pi^2} \exp\left[- D(2n+1)^2 \pi^2 t / 4h^2 \right] \quad . \tag{6.18}$$

The corresponding solutions useful for small times are

$$\frac{C - C_o}{C_1 - C_o} = \sum_{n=0}^{\infty} (-1)^n erfc \frac{(2n+1)h - x}{2\sqrt{Dt}} + \sum_{n=0}^{\infty} (-1)^n erfc \frac{(2n+1)h + x}{2\sqrt{Dt}} \quad , \tag{6.19}$$

and

$$\frac{M_t}{M_\infty} = 2\left(\frac{Dt}{h^2}\right)^{1/2} \left[\pi^{-1/2} + 2 \sum_{n=1}^{\infty} (-1)^n ierfc \frac{nh}{\sqrt{Dt}} \right] \quad . \tag{6.20}$$

It has been shown in comparative studies of water absorption theories (Shen and Springer, 1977) that with single phase diffusion the weight gain due to absorption can be expressed in terms of two parameters, the diffusion coefficient D and the weight gain at saturation M_∞.

For $\frac{Dt}{h^2} > 0.05$, Eq. 6.18 reduces to

$$M = M_\infty \left[1 - \frac{8}{\pi^2} \exp\left(- \frac{Dt}{h^2} \pi^2 \right) \right] \quad . \tag{6.21}$$

For $\frac{Dt}{h^2} < 0.05$, the Eq. 6.18 reduces to

$$M = M_\infty \frac{4}{h} \sqrt{\frac{Dt}{\pi}} \quad . \tag{6.22}$$

These theoretical curves based on Eqs 6.21 and 6.22 are plotted in Fig. 6.5.

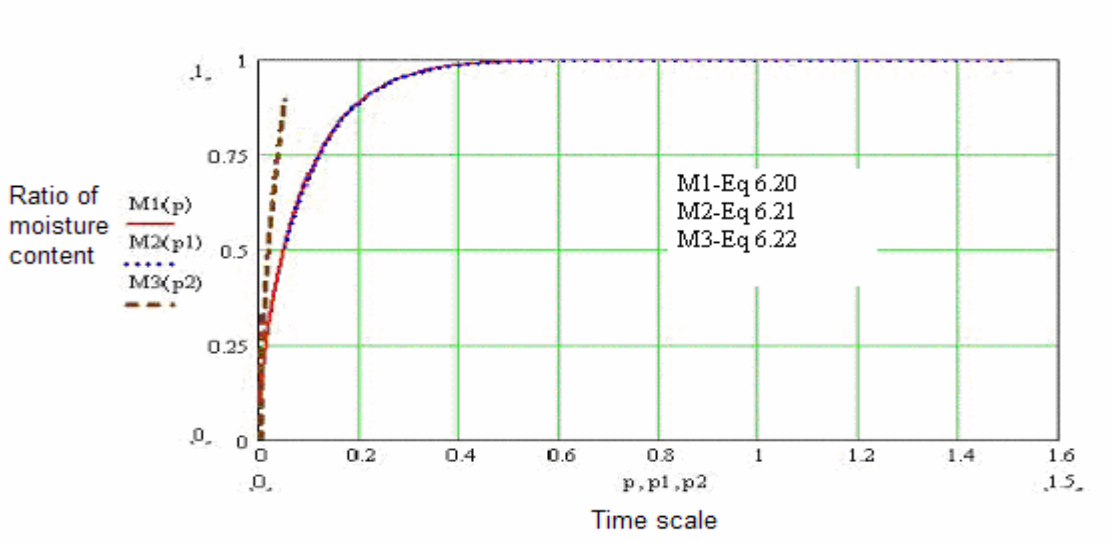

Fig . 6.5. Theoretical curves, single absorption model.

In fig 6.5 the $\frac{Dt}{h^2} = p_i$ and $M1$, $M2$, $M3$ is $\frac{M}{M_\infty}$.

In the two phase model, the water molecule which is polar, is capable of forming hydrogen bonds with the hydroxyl groups. Water molecules can exist in polymeric media in two states: unbound, or bound to the polymer molecule groups. During moisture diffusion in plastic molding compounds, some of the water molecules may form hydrogen bonds with the polymer molecules and become immobilized, while other diffusing water molecules move freely through the voids in the plastic compound. This phenomenon is called dual mode absorption. Considering this model the weight gain M as a function of time t is written in terms of four parameters, the diffusion coefficient D, weight gain at saturation M_∞, the probability α of a molecule of water passing from a combined state to the free phase and the probability β of a molecule of water passing from the free to the combined phase.

For $\alpha << \frac{D\pi^2}{h^2}$ and $\beta << \frac{D\pi^2}{h^2}$

$$M = M_\infty \left[1 - \frac{\beta}{\alpha+\beta}\exp(-\alpha t) - \frac{\alpha}{\alpha+\beta}\frac{8}{\pi^2}\sum_{n=0}^{\infty}\frac{1}{(2n+1)^2}\exp\left(\frac{-Dt}{h^2}\pi^2(2n+1)^2\right)\right] \quad (6.23)$$

For $\frac{Dt}{h^2} > 0.05$ Eq. 6.23 reduces to

$$M = M_\infty \left[1 - \frac{\beta}{\alpha+\beta}\exp(-\alpha t) - \frac{\alpha}{\alpha+\beta}\frac{8}{\pi^2}\exp\left(-\frac{Dt}{h^2}\pi^2\right)\right] \quad . \quad (6.24)$$

For $\frac{Dt}{h^2} < 0.05$ Eq. 6.23 becomes

$$M = M_\infty \frac{\alpha}{\alpha+\beta}\frac{4}{h}\sqrt{\frac{Dt}{\pi}} \quad . \quad (6.25)$$

The two phase model reduces to the single phase case when $\alpha=1$ and $\beta=0$.

The theoretical curves for the two phase based on Eqs 6.24 and 6.25 model are shown in Fig. 6.6.

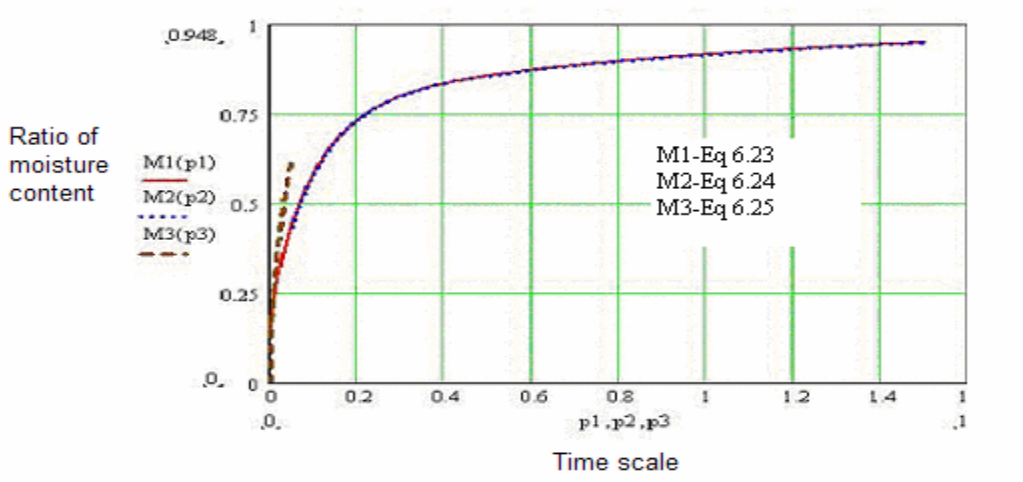

Fig. 6.6. Theoretical curves, two phase absorption model.

The theoretical curves presented here are to compare the two theories that can be used to study the moisture diffusion phenomenon in the plastic package.

In this Thesis, the single phase absorption model has been considered, without any reactions between the water molecule and the epoxy resin.

7. HYBRID METHOD

To understand and analyze the moisture diffusion phenomenon analytical., computational and experimental methods have been used to obtain the final pressure build up in the encapsulant (Roman, 2004; Lim, 1998; Marinis and Carter, 2004). The deformation results are then verified with constitutive equations derived from the theory of bending of plates. A MATLAB generated code is written to analyze the pressure build up in the encapsulant due to the moisture accumulation and the deformation it causes due to warpage.

The diffusion coefficient D is related to the absorbed moisture content per unit time, N, by one-dimensional Fick's diffusion equation, i.e.,

$$N = -D \frac{\partial C}{\partial x} \quad . \quad , \tag{7.1}$$

where C is the moisture concentration and x is the coordinate in the through thickness direction. The diffusion coefficient is generally known as the function of temperature, concentration and stress, but the major parameter is the temperature. Hence D is expressed as (Kitano et al., 1988)

$$D(T) = D_o \exp(-\frac{E_a}{kT_a}) \quad , \tag{7.2}$$

where D_o is a constant, E_a is the activation energy (ev), k is the Boltzmann's constant, and T_a is the absolute ambient temperature (K). Representative values for the mentioned parameters are summarized in Table 7.1

Table 7.1. Values of the parameters used in the diffusion simulation

D_o	E_a	k	T_a
0.472	0.5 ev	8.617×10^{-5} eV/K	298 K

It has been assumed that the moisture flux at the die-encapsulant interface is equal to zero, i.e.,

$$\frac{\partial C(x=0,t)}{\partial x} = 0 \quad . \tag{7.3}$$

At the surface exposed to the ambient, a steady-state moisture concentration is given by the ambient temperature, T_a, the relative humidity, RH, and the encapsulant moisture saturation coefficient as (Fukuzawa et al., 1985)

$$C(x=h,t) = RH \cdot P_{sat} \cdot S_{sol} \quad , \tag{7.4}$$

where the P_{sat} is the saturation vapor pressure at the ambient temperature. The moisture solubility coefficient, S_{sol}, depends on the temperature, T_m, of the molding compound:

$$S_{sol} = S_o \cdot 10^{-4} \exp\left(\frac{E_a}{kT_m}\right) \quad , \tag{7.5}$$

where S_o is a constant, T_m is the mold compound temperature (K).

The values of the parameters have been summarized in Table 7.2 (Kitano, 1988).

Table 7.2. Values used for calculating solubility.

S_{sol}	T_m
4.96×10^{-4}	448 K

Using the ideal gas equation, deformation values from the experiment and the accumulated moisture the pressure build up at a particular deformation can be calculated (Tay and Lin, 1985; Deshpande and Pryputniewicz, 2004b).

The accumulated moisture can be calculated as

$$m = A\int_0^t D\left(\frac{\partial C}{\partial x}\right)dt \quad , \tag{7.6}$$

where A is the area of the encapsulant and D is the moisture diffusion coefficient. With this known quantity of the accumulated moisture ingressed into the package the pressure can be calculated by the Ideal gas equation (Tong and Hun, 2002)

$$pV = mRT_a \quad , \tag{7.7}$$

where p is the pressure, V is the colume, m is the mass of moisture, R is the universal gas constant, and T_a is the temperature. The volume can be empirically calculated to be

$$V = \delta A \ . \tag{7.8}$$

7.1. Finite difference method

The finite difference numerical method was used to solve the diffusion equation (Constantinides and Mostoufi, 1999). The one-dimensional diffusion equation is non-homogenous form of the parabolic differential equations. The Crank-Nicolson method was used. This method is semi-implicit numeric method. It has been popularly used for solving heat transfer problems. Here it has been implemented for the Fick's second law

of diffusion with Dirichlet, Neumann, or Cauchy boundary conditions (Kharab and Guenther, 2002).

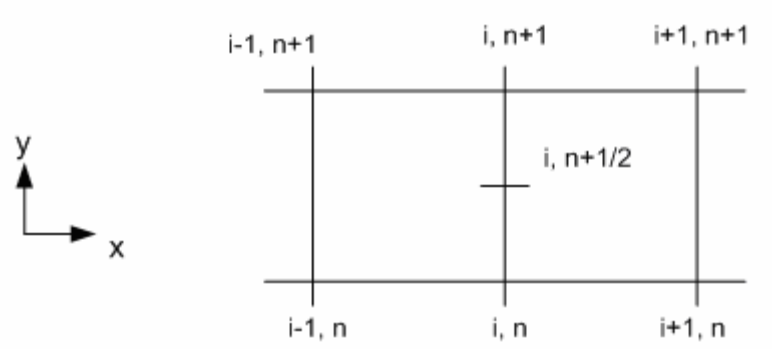

Fig. 7.1. Finite difference grid for derivation of implicit formulas.

Utilizing the grid of Fig. 7.1, in which half the point in the *t*-direction (*i*, *n*+1/2) is shown. Instead of expressing $\partial C/\partial t$ in terms of forward difference around (*i, n*), the partial derivative is expressed in terms of central difference around the half point (Kharab and Guenther, 2002).

$$\frac{\partial C}{\partial t}\Big|_{i,n+1/2} = \frac{1}{\Delta t}\left(C_{i,n+1} - C_{i,n}\right) \quad . \tag{7.9}$$

The second order partial derivative is expressed at the half point as a weighted average of the central differences at points (*i, n+1*) and (*i, n*):

$$\frac{\partial^2 C}{\partial x^2}\Big|_{i,n+1/2} = \theta\frac{\partial^2 C}{\partial x^2}\Big|_{i,n+1} + (1-\theta)\frac{\partial^2 C}{\partial x^2}\Big|_{i,n} \tag{7.10}$$

$$= \theta\left[\frac{1}{\Delta x^2}\left(C_{i+1,n+1} - 2C_{i,n+1} + C_{i-1,n+1}\right)\right]$$

$$= (1-\theta)\left[\frac{1}{\Delta x^2}\left(C_{i+1,n} - 2C_{i,n} + C_{i-1,n}\right)\right] \quad ,$$

where θ is in the range $0 \le \theta \le 1$. A combination of Eqs 7.9 and 7.10 results in the variable-weighted implicit approximation of the parabolic partial differential equation, i.e.,

$$D\theta\left[\frac{1}{\Delta x^2}\left(C_{i+1,n+1} - 2C_{i,n+1} + C_{i-1,n+1}\right)\right] - \frac{1}{\Delta t}C_{i,n+1} \tag{7.11}$$

$$= -D(1-\theta)\left[\frac{1}{\Delta x^2}\left(C_{i+1,n} - 2C_{i,n} + C_{i-1,n}\right)\right] - \frac{1}{\Delta t}C_{i,n} \quad .$$

Equation 7.11 is implicit because the left hand side involves more than one value at the (n+1) position of the difference grid.

Finally, when θ=1/2, Eq. 7.11 yields the Crank Nicolson semi-implicit representation.

$$-\left(\frac{D\Delta t}{\Delta x^2}\right)C_{i-1,n+1} + 2\left(1 + \frac{D\Delta t}{\Delta x^2}\right)C_{i,n+1} - \left(\frac{D\Delta t}{\Delta x^2}\right)C_{i+1,n+1} \tag{7.12}$$

$$= \left(\frac{D\Delta t}{\Delta x^2}\right)C_{i-1,n} + 2\left(1 - \frac{D\Delta t}{\Delta x^2}\right)C_{i,n} + \left(\frac{D\Delta t}{\Delta x^2}\right)C_{i+1,n} \quad .$$

When written for the entire difference grid, implicit formulas generate sets of simultaneous linear algebraic equations whose matrix of coefficients is usually a tridiagonal matrix. This type of problem may be solved using the Gauss elimination procedure, or more efficiently using the Thomas algorithm, which is a variation of Gauss elimination.

Implicit formulas of the type described above have been found unconditionally stable. It can be generalized that most explicit finite difference approximations are conditionally stable, whereas most implicit approximations are unconditionally stable.

8. EXPERIMENTAL SETUP

8.1. Optoelectronic holography methodology

Optical methods can provide noninvasive and full-field of view information about components subjected to realistic loading and boundary conditions. In addition they provide a wide range of measuring possibilities. Optoelectronic holography (OEH) techniques have been successfully applied to nondestructive testing (NDT) of objects (Pryputniewicz, 1995). Advantages of the OEH methodology over various other optical techniques are:

1) noninvasive,
2) full-field of view information,
3) requires much less mechanical stability that that required in conventional holography,
4) possible to perform static and dynamic investigations,
5) possible to measure the shape and deformations of a component using multiple-wavelength optical contouring techniques with minimum modifications to the experimental setup,
6) can be used for on-site investigations in order to study and diagnose problems in industrial environment.

8.2. OEH system

Figure 8.1 depicts the schematic of the OEH system used in the experiment to measure deformations, in this Thesis, due to warpage of the plastic encapsulant. In this configuration, the coherent light source is a laser with an operational wavelength of 530 nm, 3 mW output power. The output of the laser is directed towards a beam splitter. The beam splitter splits the light into reference beam and the object beam. The reference beam is directed to a lens and through an optical fiber towards a CCD camera. The object beam is directed towards the package, by a mirror and a lens. Reflected object beam carrying the deformation information of the warped package, is imaged by means of an objective. The object beam is then directed via a beam splitter to the CCD camera. The measurement of irradiances produced by mutual interference of the object and the reference beams are made electronically by the camera. Processing of this interferometric information and display of the quantitative results are carried out concomitantly with measurement of irradiation (Pryputniewicz, 2003c).

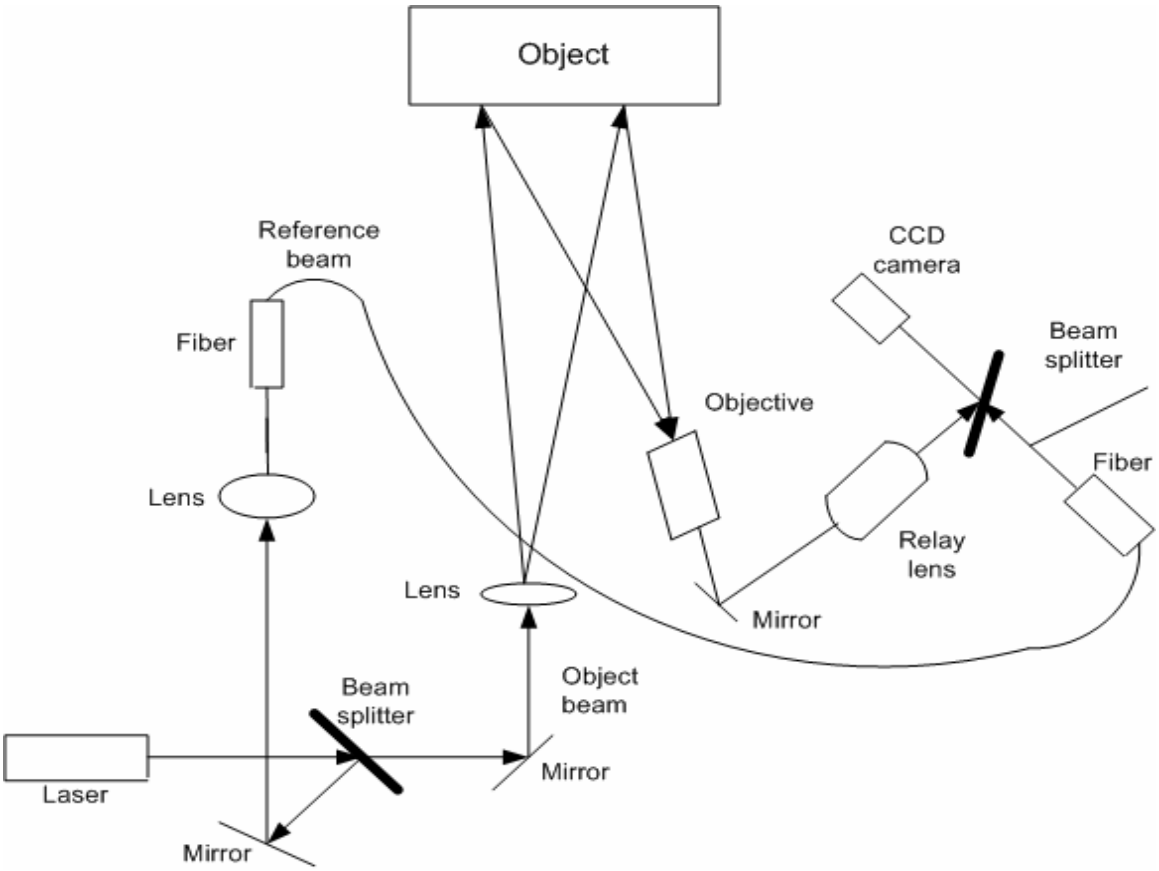

Fig. 8.1. OEH setup used in this Thesis.

8.3. Data acquisition and processing

In OEH the process is carried out by recording sequential frames of images of the object corresponding to the two states of stress. Typically, four sequential frames are recorded, with a finite phase step-imposed on the reference beam between each frame, for every single exposure image of the object.

One OEH approach used to perform the static, dynamic, and shape measurement investigations of objects consists of acquiring and processing two sets, *I(u,v)* and *I'(u,v)* of phase-stepped speckle intensity patterns, recorded before and after, respectively, event

effects of which are to be measured. The first set of phase-stepped speckle intensity patterns is described by

$$I_n(u,v) = I_B(u,v) + I_M(u,v)\cos\left[\Delta\phi(u,v) + \theta_n\right] \quad , \tag{8.1}$$

where

$$I_B(u,v) = I_o(u,v) + I_r(u,v) \tag{8.2}$$

is the background irradiance, and

$$I_M(u,v) = 2\left[I_o(u,v)\cdot I_r(u,v)\right]^{1/2} \tag{8.3}$$

is the modulation irradiance. In Eqs 8.1 to 8.3, $I_o(u,v)$ and $I_r(u,v)$ are the object and reference beams irradiances, respectively, while.

$$\Delta\phi(u,v) = \phi_o(u,v) - \phi_r(u,v) \quad , \tag{8.4}$$

is the phase difference between the object and reference beams, with $\phi_o(u,v)$ representing a random phase due to light scattering from the object of interest and $\phi_r(u,v)$ representing a uniform phase from a smooth reference beam wavefront, θ_n is the applied n-th phase step, value of which is obtained during the caliberation procedures applied according to the specific phase stepping algorithm that is implemented, and (u,v) represents Cartesian coordinates of the image space.

The second set of phase-stepped speckle intensity patterns is described by

$$I_n'(u,v) = I_B(u,v) + I_M(u,v)\cos\left[\Delta\phi(u,v) + \Delta\Omega(u,v) + \theta_n\right] \quad . \tag{8.5}$$

In Eq. 8.5, $\Delta\Omega(u,v)$ is the change in the optical phase that occurred between acquisition of the two sets of phase-stepped speckle intensity patterns, value of which relates to the shape, or to the changes in states of deformation, of the object of interest. With the OEH,

two sets of phase-stepped speckle intensity patterns are processed in the display and data modes. In the display mode, secondary interference patterns, $Q_D(u,v)$, are generated and displayed at video rates and are modulated by a cosinusoidal function of the form

$$Q_D(u,v) = 4I_M(u,v)\cos[\Delta\gamma(u,v)/2] = \{[I_1(u,v) - I_3(u,v) + I'_1(u,v) - I_3'(u,v)]^2 + I_2(u,v) - I_4(u,v) + I_2'(u,v) - I_4'(u,v)]^2\}^{1/2}, \quad (8.6)$$

which represents an 8-bit resolution video image obtained after application of four phase steps: $\theta_n = 0, \pi/2, \pi,$ and $3\pi/2$. The display mode is used for adjusting, in real time, the experimental parameters for accurate OEH investigations, such parameters include

1) beam ratio r = avg$[I_r(u,v)]/I$avg$[I_o(u,v)]$, which is important to characterize and set in order to obtain appropriate fringe visibility and also to avoid optical saturation of the CCD array detector of the CCD camera;
2) phase step θ_n, which is obtained by calibration and used in order to acquire accurate phase-stepped speckle intensity patterns, $I_n(u,v)$, based on which further processing is conducted.

The data mode is used for quantitative investigations, which involve the determination of $\Delta\Omega(u,v)$, related to the shape, or to the changes in states of deformation, of objects of interest (Furlong and Pryputniewicz, 2001; Pryputniewicz, 1995). The values of $\Delta\Omega(u,v)$ are determined using double-float point arithmetic as

$$\Delta\Omega(u,v) = \tan^{-1}\left[\frac{I_4 - I_3}{I_1 - I_2}\right], \quad (8.7)$$

where (u,v) arguments have been omitted for simplification. Equation 8.7 corresponds to the implementation of the 4-phase step algorithm with $\theta_n = 0, \pi/2, \pi, 3\pi/2$. Application

of such algorithm minimizes errors in determination of $\Delta\,\Omega(u,v)$ due to possible phase stepping miscalibration.

The three packages tested for deformation due to moisture accumulation are shown in Fig 8.2.

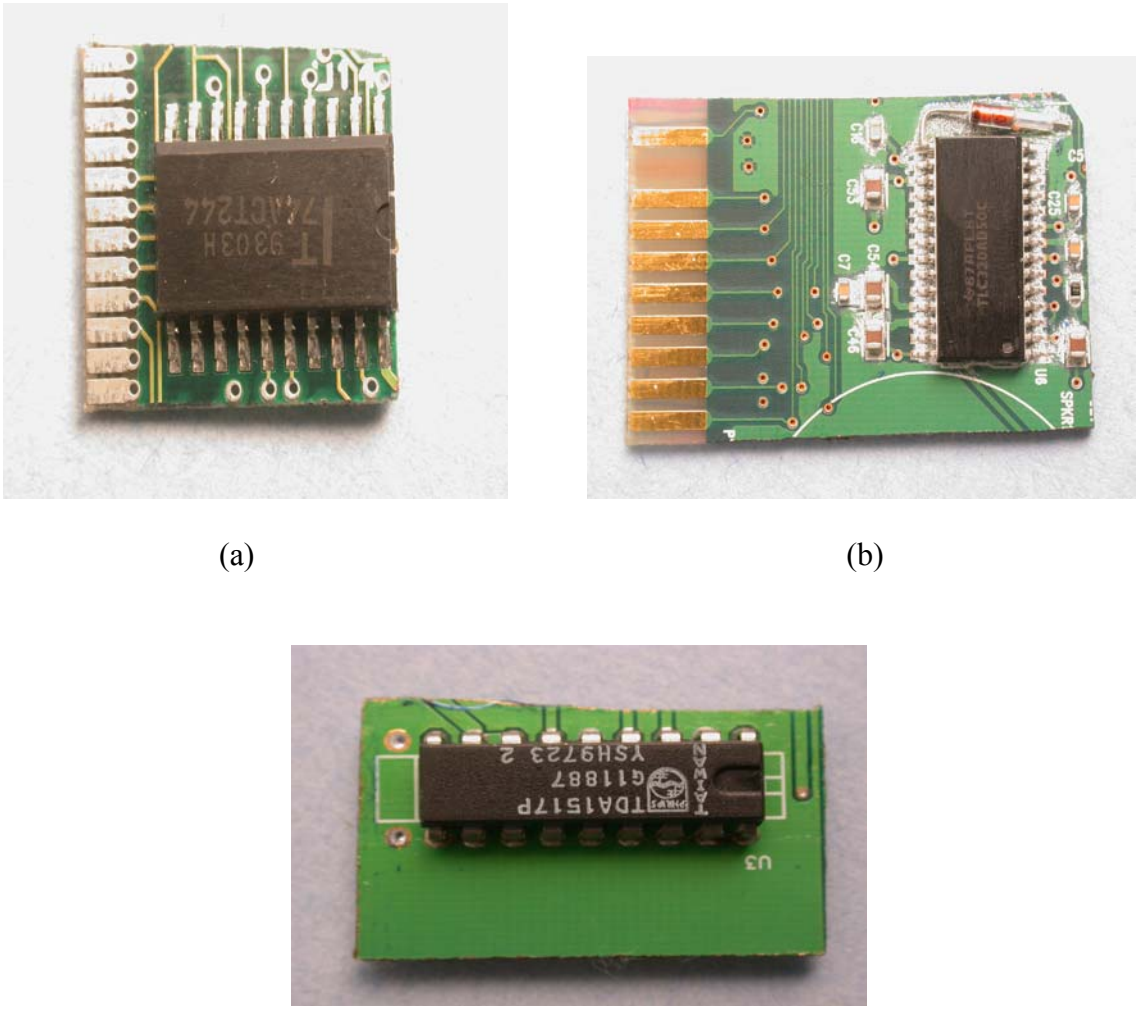

(a) (b)

(c)

Fig. 8.2. Packages tested in this Thesis: (a) package 1: Fairchild 74ACT244, (b) package 2: Texas instruments TLC320AD50C, (c) package 3: Philips TDA1517P.

1) Package 1: is a Fairchild 74ACT244. It is an Octal Buffer/Line Driver packaged in 20 lead, Small Outline Integrated Circuit (SOIC). The physical parameters considered for the experiment are shown in Fig. 8.3,

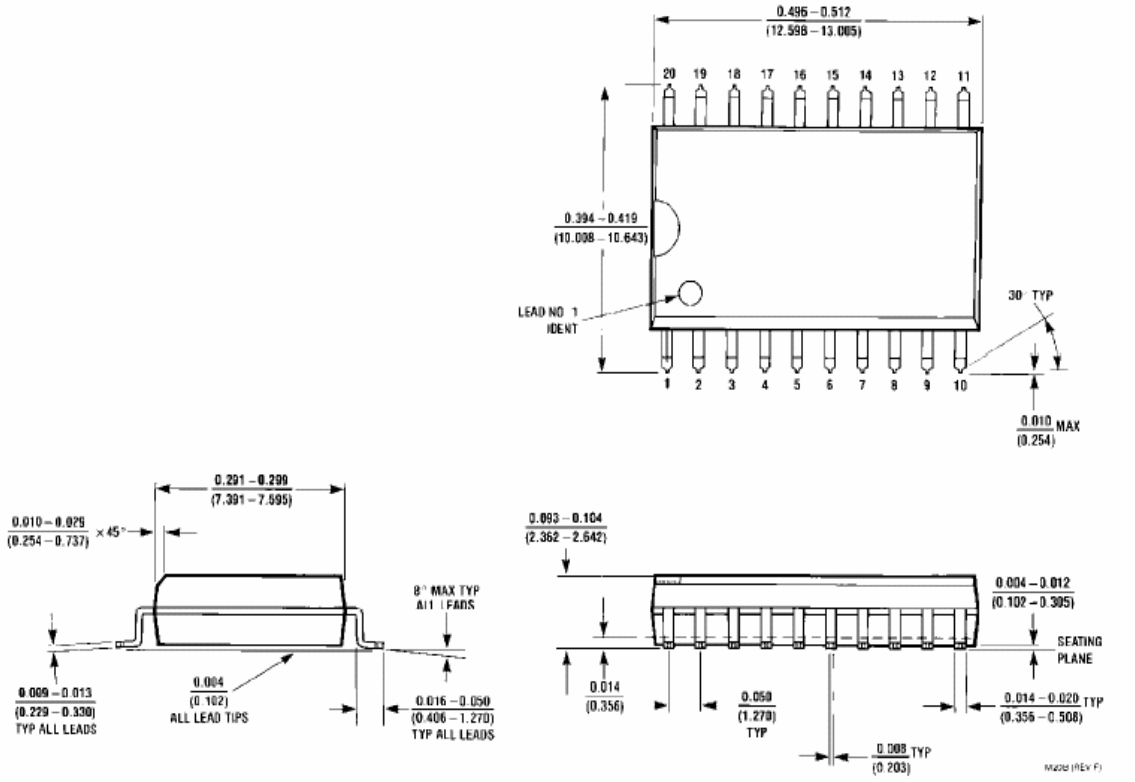

Fig. 8.3. Physical dimensions (Fairchild Semiconductors).

2) Package 2: is a Texas Instruments TLC320AD50C. It is a single channel codec w/master-slave function. The package type is Plastic Small Outline Package (PSOP). The physical parameters used for the experiment are shown in Fig. 8.4.

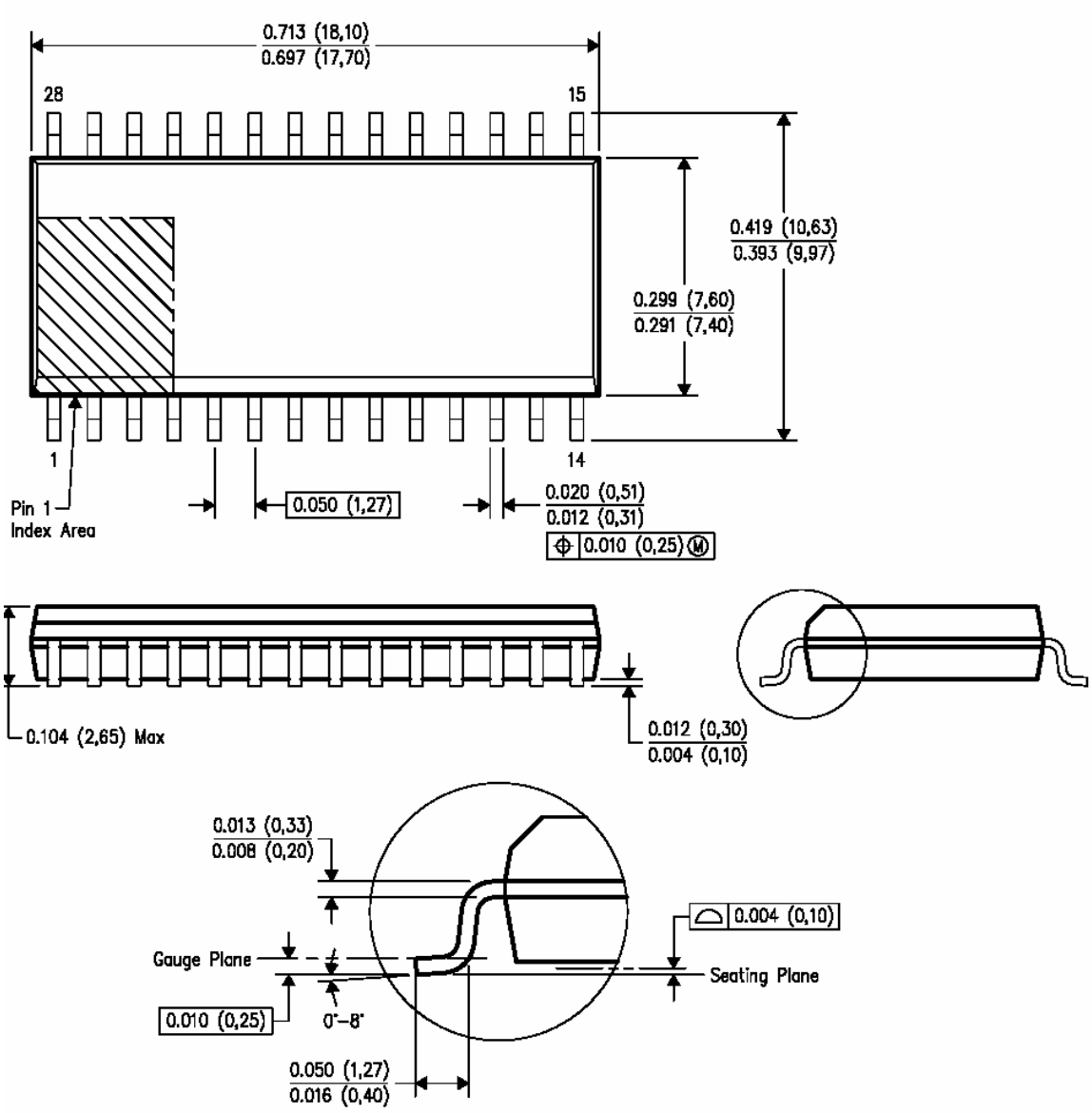

Fig. 8.4. Physical dimensions (Texas Instruments).

3) Package 3: is a Philips TDA1517P. It is an integrated class-B dual o/p amplifier. The package type is Plastic Dual-In-Line Package (PDIP). The physical parameters of the package are shown in Fig. 8.5.

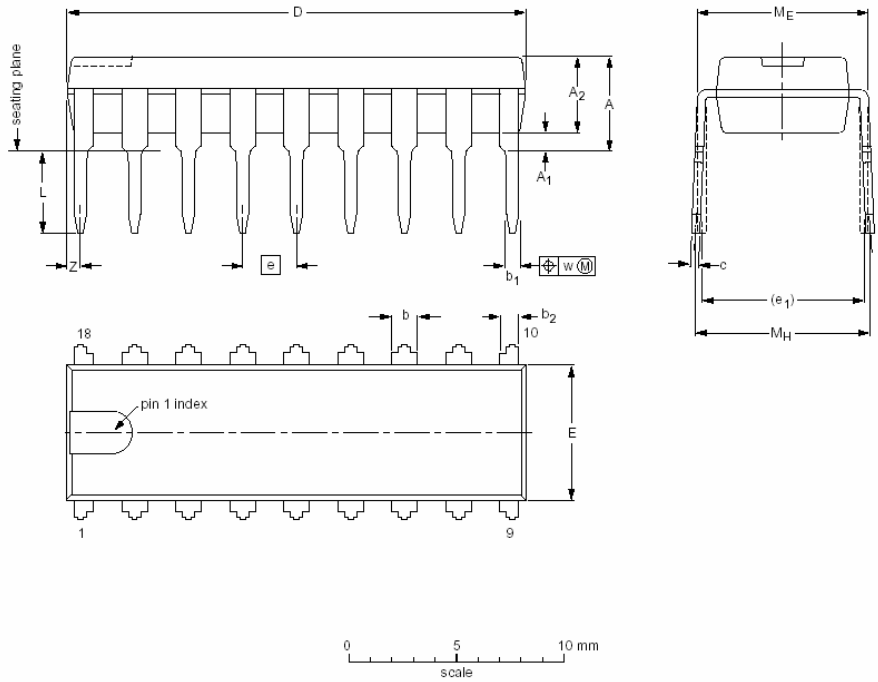

DIMENSIONS (inch dimensions are derived from the original mm dimensions)

UNIT	A max.	A_1 min.	A_2 max.	b	b_1	b_2	c	D (1)	E (1)	e	e_1	L	M_E	M_H	w	Z (1) max.
mm	4.7	0.51	3.7	1.40 1.14	0.67 0.50	1.05 0.75	0.47 0.38	21.85 21.35	6.5 6.2	2.54	7.62	3.9 3.1	8.32 8.02	8.7 7.7	0.25	1
inches	0.19	0.02	0.15	0.06 0.04	0.03 0.02	0.04 0.03	0.02 0.01	0.87 0.84	0.26 0.24	0.1	0.3	0.15 0.12	0.33 0.32	0.34 0.30	0.01	0.04

Fig. 8.5. Physical dimensions (Philips).

Table 8.1 is the summary of the physical parameters of the three packages used in this Thesis.

Table 8.1. Summary of the physical parameters of the packages.

	Package type	Number of leads	Length (mm)	Width (mm)	Thickness (mm)	Area (mm^2)
Package 1	SOIC	20	12.6	10.008	1.006	126.101
Package 2	PSOP	28	18.10	7.50	1.000	135.75
Package 3	DIP	18	21.8	6.48	1.610	141.264

The sample was held in a vice, under boundary and loading conditions as shown in Fig 8.6.

The boundary conditions of the package depend on the way it is clamped. In this Thesis to estimate the warpage behavior under normal operating conditions the package is kept attached to the circuit board. This method of clamping prevents stresses to be build up at the package. The circuit board is then clamped to the fixture. The clamping stresses are different for all the three packages as the hand clamping pressure varies. To obtain results without this effect on the package, the clamped fixture with the package was kept aside for almost half a day and then mounted in the chamber. To prevent any mounting disturbances on the package initial exposures were taken, until no fringe was observed. At this time a reference was taken and the OEH experiment was performed based on the double exposure method.

Fig. 8.6. Vice showing the placement of the package.

To determine the deformation of the plastic package it is important to expose it to a moist environment. Such experiments usually take long term continuous exposure of the package to the humid environment in an environmental chamber. Due to time constraints the chamber was fixed at a temperature of 20°C and 90% RH. The experiment has been used to study deformations of the plastic package over a period of time, without changing the humidity and temperature. The samples were subjected to

humid conditions in the chamber, one by one, Fig 8.7. The controllable humidity range was 20% to 98% ± 2% relative humidity as limited by a ±2 °C dew point temperature as specified in the chamber manual.

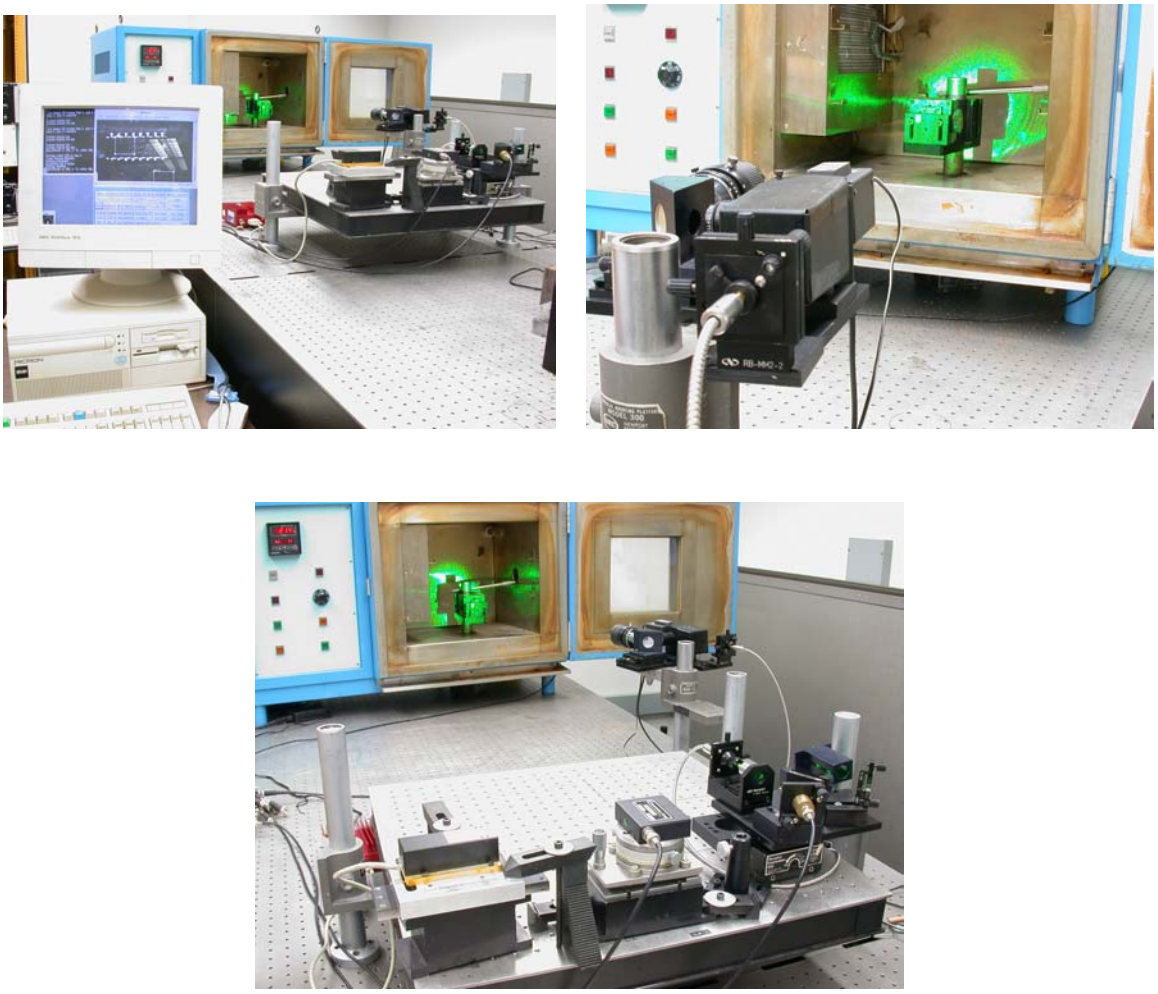

Fig. 8.7. OEH experimental setup.

9. PLATE THEORY

Constitutive equations, based on the bending theory of thin plates are presented for the assessment of the deformation due to warpage of the plastic encapsulant (Suhir, 1995). The theory was assumed and found to be applicable after the displacemenr of the packages observed from the experimental studies. The encapsulant over the die is displaced by the pressure of the moisture accumulation, the displacement and the pressure can be related by the plate theory (Lim et al., 1998; Nakazawa et al., 1996). Theoretically the warpage phenomenon and the stresses and strains developed due to it can be solved by the generalization of the viscoelasticity law, which corresponds to the three-dimensional form of Hooke's law (Flugge, 1975). But it is mathematically difficult to solve for a membrane or a plate case. It is well established for a beam structure (Flugge, 1975).

The ideal-gas equation, Eq. 7.7, for the relation between the pressure build up by the moisture at a particular temperature and accumulated moisture content, and the plate theory for the relation between that pressure built up and package deformation are assumed for further understanding of the warpage phenomenon for small times(Tay and Lin, 1985; Lim et al., 1998) . It has been studied that a uniformly loaded rectangular plate clamped around its support contour can be a suitable analytical model for the evaluation of the maximum stress in the plastic encapsulant (Fukuzawa, 1985). In the analysis that follows a comprehensive analytical model is derived based on the Kirchoff's theory of bending plates (Suhir, 1991). The Kirchoff's theory has been applied assuming the packages to be thin i.e. not less than 1/50 thickness to length ratio, Table 9.1. A

partial differential equation (PDE) formulation is described which can be used to further developed to calculate the von-Mises stress in the molding compound to be used as a suitable failure criterion (Suhir, 1995). Calculation of the von-Mises stresses with the information of deformations and bending stresses is a structural criterion (Suhir, 1995). This reflects the cumulative role of various geometrical and material factors affecting the strength of the package. The results of experimental investigations, valuable as they might be, inevitable reflect the combined effect of variety of factors. Therefore, theoretical and analytical modeling can be helpful for understanding, predicting and optimizing the mechanical behavior of a plastic package (Shoraka, 1986).

The plate in bending is a plane structure, Fig. 9.1. It is loaded laterally to its surface. Depending on the thickness-to-length ratio several theories of plate have been developed, Table 9.1.

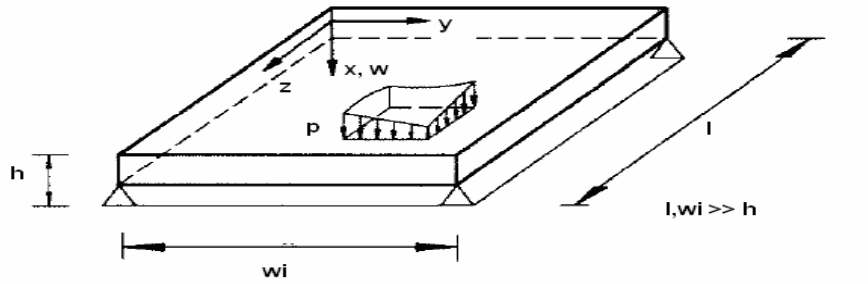

Fig. 9.1. Plate in bending.

Table 9.1. Plate theories.

	moderately thick	thin	very thin
h/L, h/w	1/5 to 1/10	1/5 to 1/50	<1/50
	With transverse shear deformation	Without transverse shear deformation, mostly used for practical applications	Geometrically non-linear, with membrane deformation
Theory	Reissner, Mindlin	Kirchhoff	von Karman
Related beam theory	Timoshenko	Euler Bernoulli	Theory of second order

The displacements of very thin plates are usually so large that a geometrically non-linear theory, von-Karman theory becomes necessary which is able to consider the membrane action (Suhir, 1995). On the other hand, the shear deformation of moderately thick plates has to be considered, Reissner Mindlin theory (Bletzinger, 2000). Most of the practical applications deal with thin plates. Within the valid range of linear behavior a pure bending theory will be good enough and shear deformation can be neglected, Kirchhoff theory (Timoshenko, 1940; Tee, 2002). With the experimental results obtained the Kirchoff's theory has been considered applicable to the deformation due to warpage for a plastic encapsulant (Suhir, 1995; Bletzinger, 2000).

The principal load carrying behavior can be compared with that of a beam grid which is resistant to bending and torsion. The related deformations are curvatures κ_x, κ_y, and the twist $\kappa_{yz,}$, Fig. 9.2.

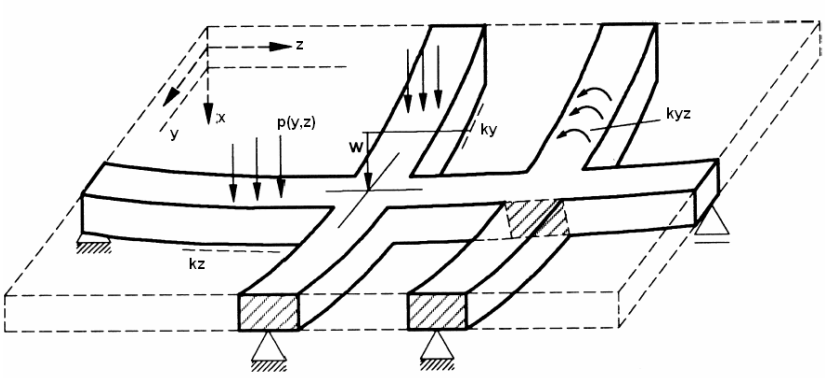

Fig. 9.2. Load carrying behavior of plates in bending.

9.1. Differential equation based on the Kirchhoff theory

The plate is described by its mid-surface in the idealized system. The statical and geometrical equations are given for an infinitesimal element (Reddy, 1999; Suhir, 1995).

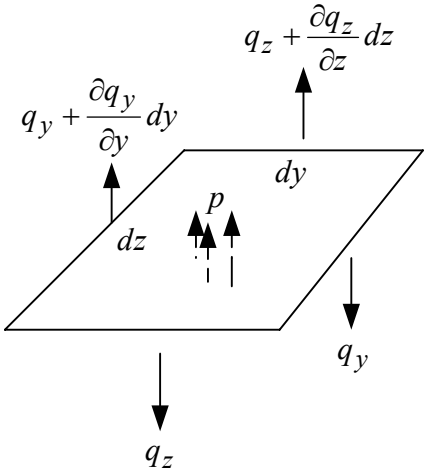

Fig. 9.3. Shear forces at an infinitesimal element of a package.

$$\sum V = 0: \quad -q_y dy + \left(q_y + \frac{\partial q_y}{\partial y} dy \right) dz - q_z dy + \left(q_z + \frac{\partial q_z}{\partial z} dz \right) dy + p dy dz = 0 \quad ,$$

$$\frac{\partial q_y}{\partial y} + \frac{\partial q_z}{\partial z} + p = 0 \quad . \tag{9.1}$$

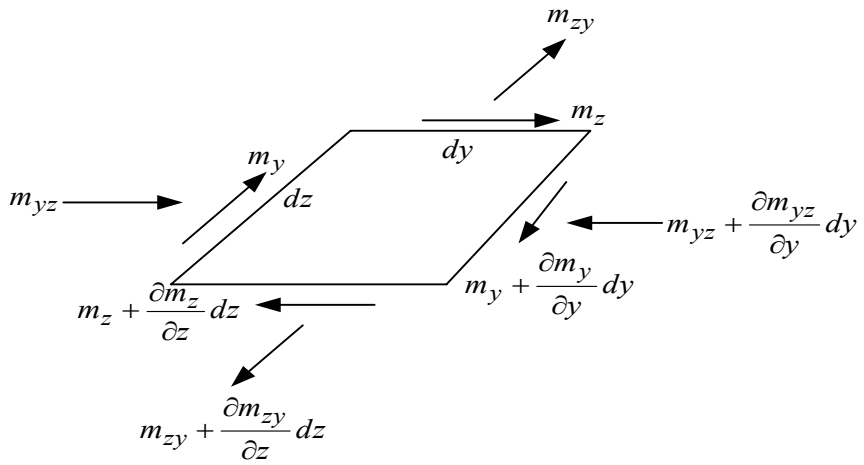

Fig. 9.4. Moments at an infinitesimal element of the package.

$$\sum M_z = 0: \quad -m_y dy + \left(m_y + \frac{\partial m_y}{\partial y} dy \right) dz + m_{zy} dy - \left(m_{zy} + \frac{\partial m_{zy}}{\partial z} dz \right) dy - q_y dz dy = 0 \quad ,$$

$$\sum M_y = \frac{\partial m_y}{\partial y} + \frac{\partial m_{zy}}{\partial z} - q_y = 0 \tag{9.3}$$

$$\frac{\partial m_z}{\partial z} + \frac{\partial m_{yz}}{y} - q_z = 0$$

Statical equations under equilibrium are (Bletzinger, 2000):

$$\sum V: \quad \frac{\partial q_y}{\partial y} + \frac{\partial q_z}{\partial z} + p = 0 \quad . \tag{9.4}$$

$$\sum M_z: \quad \frac{\partial m_y}{\partial y} + \frac{\partial m_{zy}}{\partial z} - q_y = 0 \quad . \tag{9.5}$$

$$\sum M_y: \quad \frac{\partial m_z}{\partial z} + \frac{\partial m_{yz}}{\partial y} - q_z = 0 \quad . \tag{9.6}$$

Equations 9.7 to 9.9 are the curvatures which pertain to the geometrical parameters, during the twisting of the plate, Fig. 9.5 (Bletzinger, 2000).

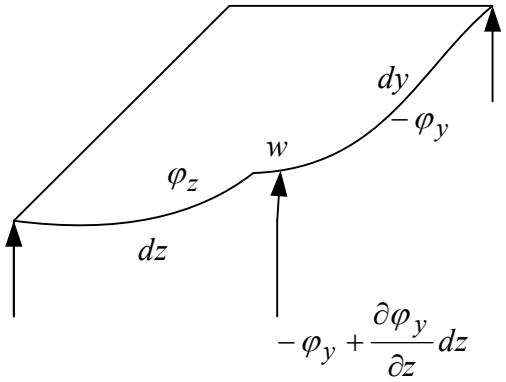

Fig. 9.5. Twisting of the plate (Bletzinger, 2000).

$$\kappa_y = \frac{\partial \varphi_y}{\partial y} = -\frac{\partial^2 w}{\partial y^2} \quad . \tag{9.7}$$

$$\kappa_z = \frac{\partial \varphi_z}{\partial z} = -\frac{\partial^2 w}{\partial z^2} \quad . \tag{9.8}$$

$$\kappa_{yz} = \frac{\partial \varphi_y}{\partial z} = -\frac{\partial^2 w}{\partial y \partial z} \quad . \tag{9.9}$$

Equations 9.10 to 9.12 are related to the material parameters (Bletzinger, 2000)

$$m_y = -K\left(\frac{\partial^2 w}{\partial y^2} + \nu \frac{\partial^2 w}{\partial z^2}\right) \quad , \tag{9.10}$$

$$m_z = -K\left(\frac{\partial^2 w}{\partial z^2} + \nu \frac{\partial^2 w}{\partial y^2}\right) \quad , \tag{9.11}$$

$$m_{yz} + m_{zy} = -2K(1-\nu)\frac{\partial^2 w}{\partial y \partial z} \quad . \tag{9.12}$$

With elimination of shear forces from the equilibrium conditions given by Eq 9.1, (Bletzinger, 2000)

$$\frac{\partial^2 m_y}{\partial y^2} + \frac{\partial^2 (m_{yz} + m_{zy})}{\partial y \partial z} + \frac{\partial^2 m_z}{\partial z^2} = -p \quad . \tag{9.13}$$

With elimination of moments given by Eq. 9.2.

$$\frac{\partial^4 w}{\partial y^4} + 2\frac{\partial^4 w}{\partial y^2 \partial z^2} + \frac{\partial^4 w}{\partial z^4} = \frac{p}{K} \quad . \tag{9.14}$$

With the solution *w* obtained from the Eq. 9.14, the stress resultants can be calculated (Suhir, 1995; Bletzinger, 2000). This information can then be used to calculate the failure criterion and hence assess the reliability (Suhir, 1995). The solution of Eq. 9.14 is solved here by exact solutions. By means of series expansion and the partial differential equation *w* can be obtained from differential equations. This single series expansion is used which satisfies the Navier conditions $w=0$, $\Delta w=0$ of two opposite edges. In this case the package has been considered to be a plate which is simply supported at two edges. The support conditions of the remaining edges can be chosen arbitrarily and in this case it is observed that the edges move out of plane.

The solution is derived assuming that the load distribution and deformation are constant in *z*-direction. The differential equation hence reduces to:

$$\frac{d^4 w(y)}{dy^4} = \frac{p(y)}{K} \quad , \tag{9.15}$$

where K is the plate stiffness

$$K = \frac{Eh^3}{12(1-v^2)} \quad , \tag{9.16}$$

where E is the modulus of elasticity, v is the Poisson's ratio.

Deformation w is expanded by Fourier Series.

$$w(y) = \sum_n w_n \sin(\alpha_n y) \quad , \tag{9.17}$$

Which implies the Navier conditions *(w=0 and w''=0)* at both edges (Bletzinger, 2000)

Inserting deformations into the differential equation 9.17:

$$\sum_n \alpha_n{}^4 w_n \sin(\alpha_n y) = \frac{1}{K} \sum p \sin(\alpha_n y) \quad . \tag{9.18}$$

Comparison of coefficients in Eq 9.18 yields

$$w_n = \frac{p}{\alpha_n{}^4 K} \quad , \tag{9.19}$$

and the general solution becomes

$$w(y) = \frac{a^4}{K\pi^4} \sum_n \frac{p}{n^4} \sin(\alpha_n y) \quad . \quad \alpha_n = \frac{n\pi}{a} \text{ , } n = 1,2,3... \tag{9.20}$$

Back substitution in Eqs 9.10, 9.11 gives the stress resultants

$$m_y = -K\frac{d^2w}{dy^2} \quad ,$$
$$m_z = vm_y \quad , \tag{9.21}$$
$$q_y = -K\frac{d^3w}{dy^3} \quad .$$

The load that causes the deformation of the encapsulant has been assumed to be as hydrostatic load (Suhir, 1995), Fig 9.6.

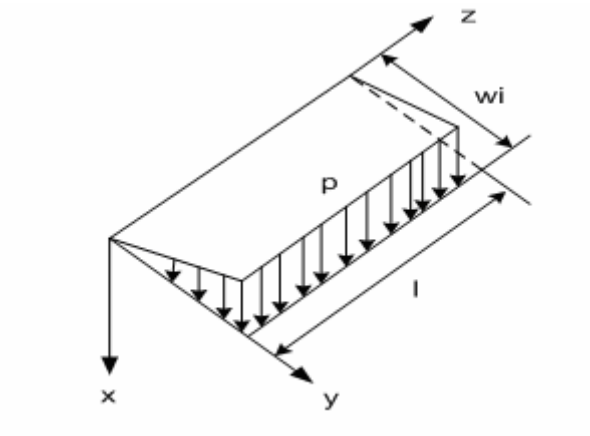

Fig. 9.6. Loading nature of the plate.

The hydrostatic loading can be given as (Reddy, 1999)

$$p(z,y) = p\frac{y}{wi} \quad . \tag{9.22}$$

Hence the deformation *w* with exact solution can be given as

$$w(z,y) = 0.013021\frac{p(z,y)wi^4}{K} \quad . \tag{9.23}$$

10. REPRESENTATIVE RESULTS AND DISCUSSION

10.1. Representative results for package 1

In this Section representative results from the experiments are presented. All packages were kept in the chamber at 20°C, 90% RH, at a saturation pressure of about 2.33 x 10^{-3} Pa. The loading conditions have been explained in chapter 8, Fig. 8.6. The due to warpage behavior due to moisture accumulation for package 1 is shown in Fig. 10.1.

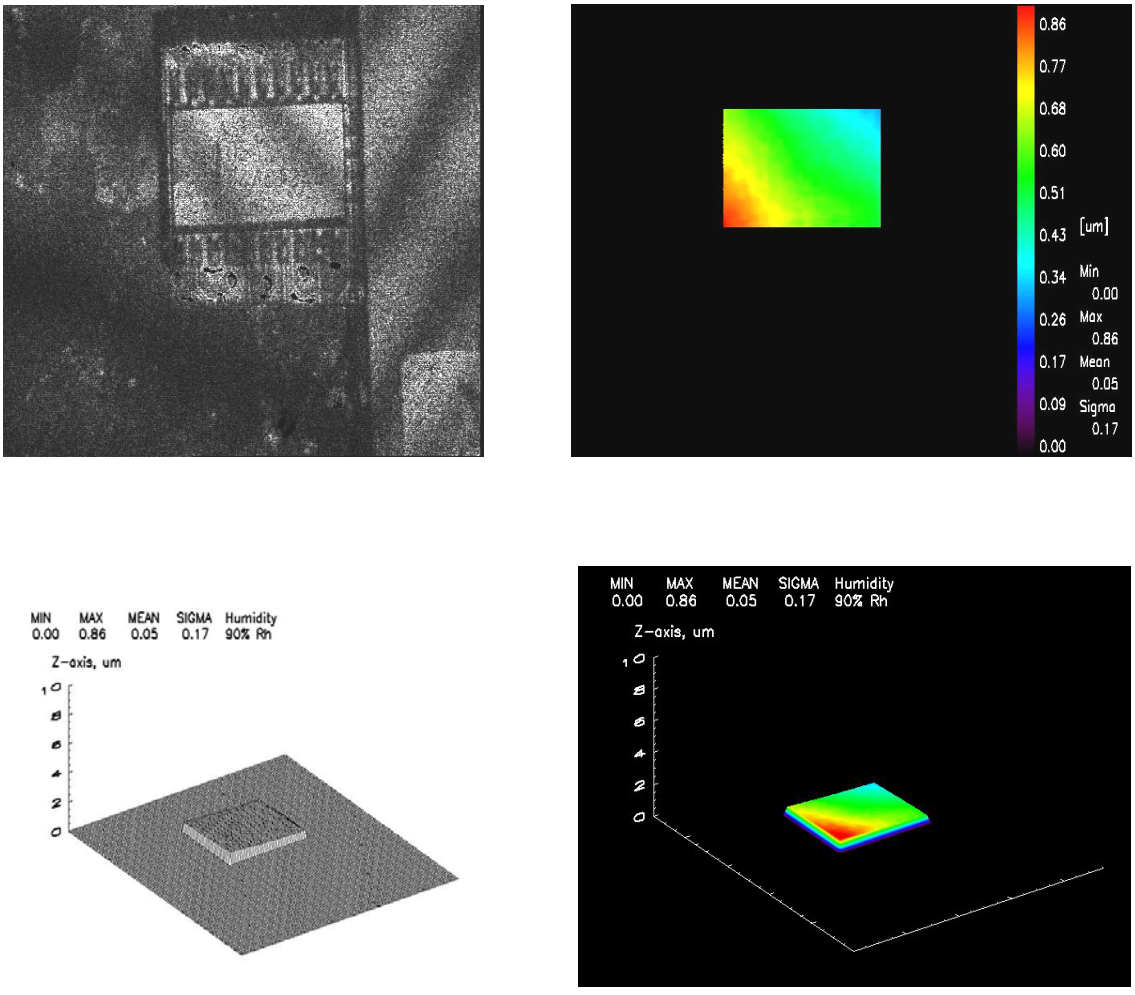

Fig. 10.1. Quantitative results for package one after three days.

Fig 10.1. shows the results for sample 1 after 3 days. The results obtained from the current OEH setup and data analysis gives a rigid body translation of the package. The maximum rigid body displacement obtained is 0.86 µm.

Fig 10.2 shows the quantitative results for sample 1 after 6 days. The maximum rigid body displacement was observed to be 1.17 µm.

The third exposure has not been included as it resulted into a very minimal contrast and hence proper quantitative results that could not be analyzed.

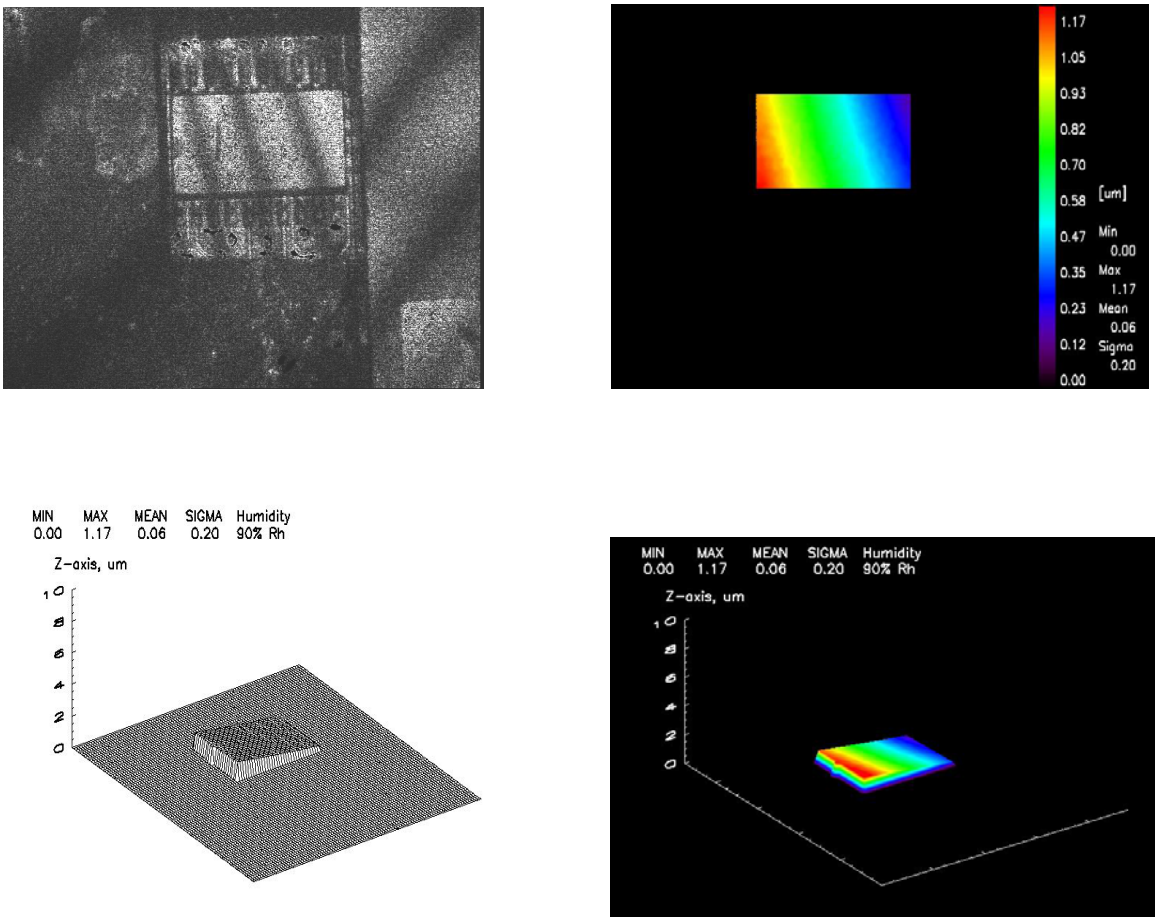

Fig 10.2. Quantitative results for package one after six days.

10.2. Representative results for package 2

Package 2 was also kept in the chamber under same environmental conditions as used for package 1. The mounting of the sample was also not changed.

Fig 10.3 shows the quantitative results for sample 2 after 3 days. The maximum displacement observed was 2.13 μm.

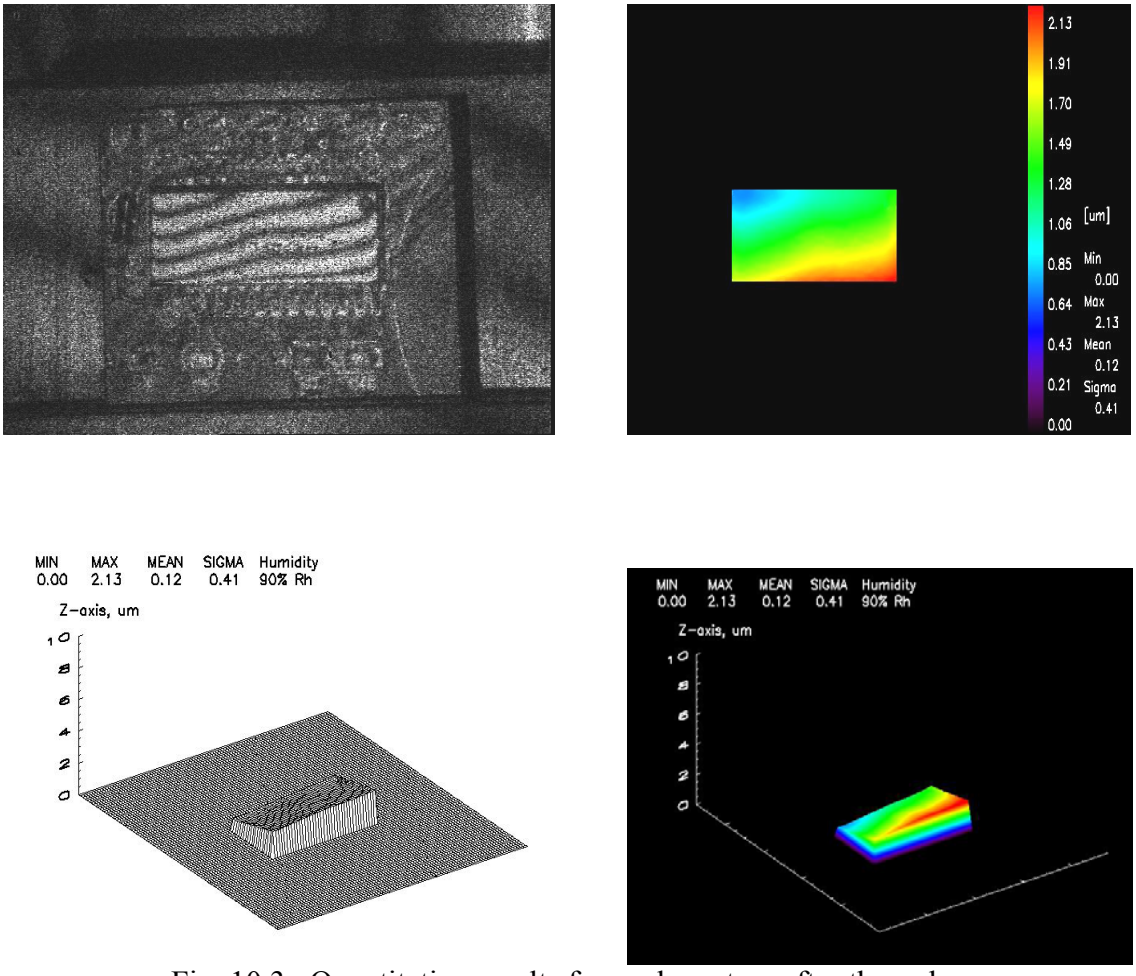

Fig. 10.3. Quantitative results for package two after three days.

Figure 10.4 shows the quantitative results for package 2 after 6 days. The maximum displacement observed is 2.64 μm.

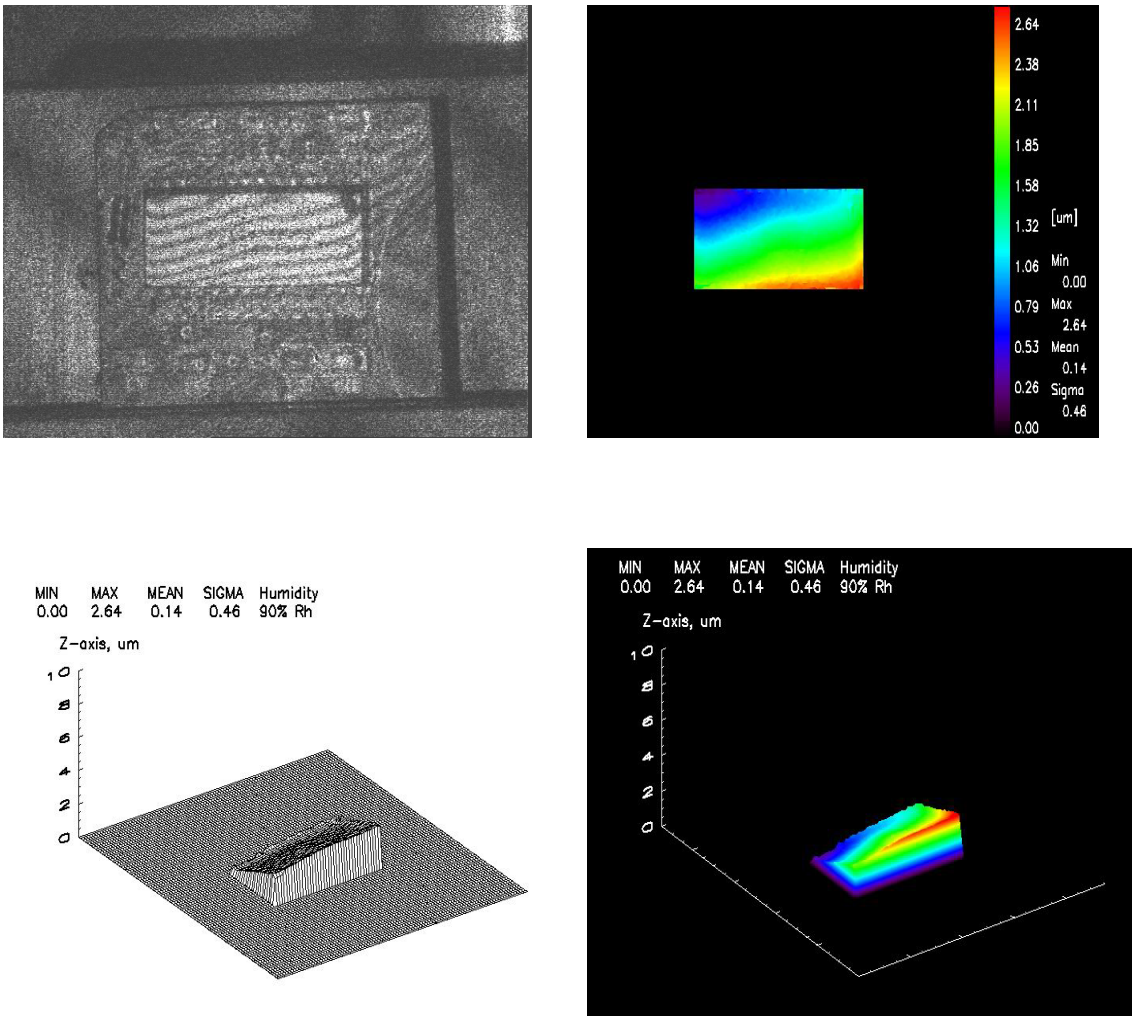

Fig. 10.4. Quantitative results for package two after six days.

Figure 10.5 shows the quantitative results for package 2 after 10 days. It is observed that maximum displacement obtained is 3.43 μm.

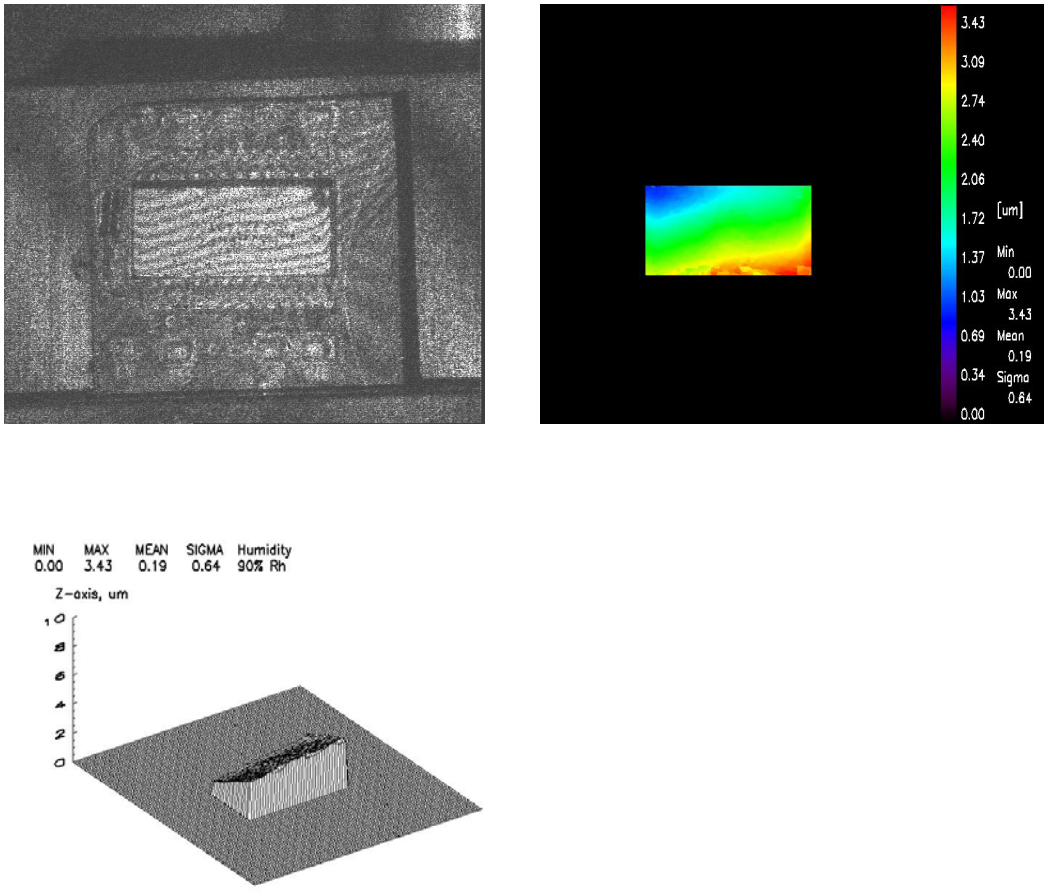

Fig. 10.5. Quantitative results for package two after ten days.

10.3. Representative results for package 3

Fig. 10.6 shows the quantitative results for package 3 after 3 days. The maximum displacement after 3 days is observed to be 0.84 μm.

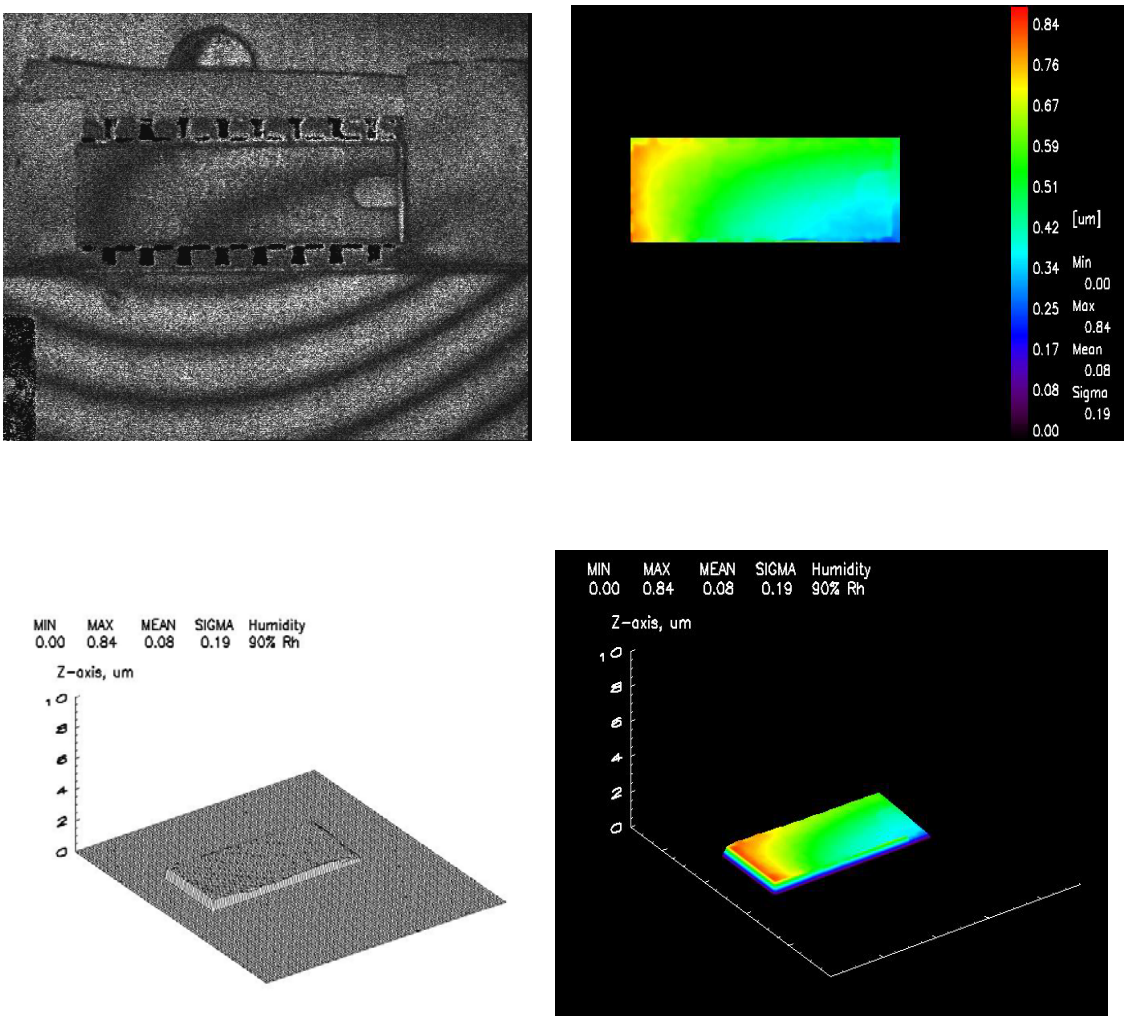

Fig. 10. 6. Quantitative results for package three after three days.

Fig 10.7. shows the quantitative results for sample 3 after 6 days. The maximum displacement observed is 1.11 μm.

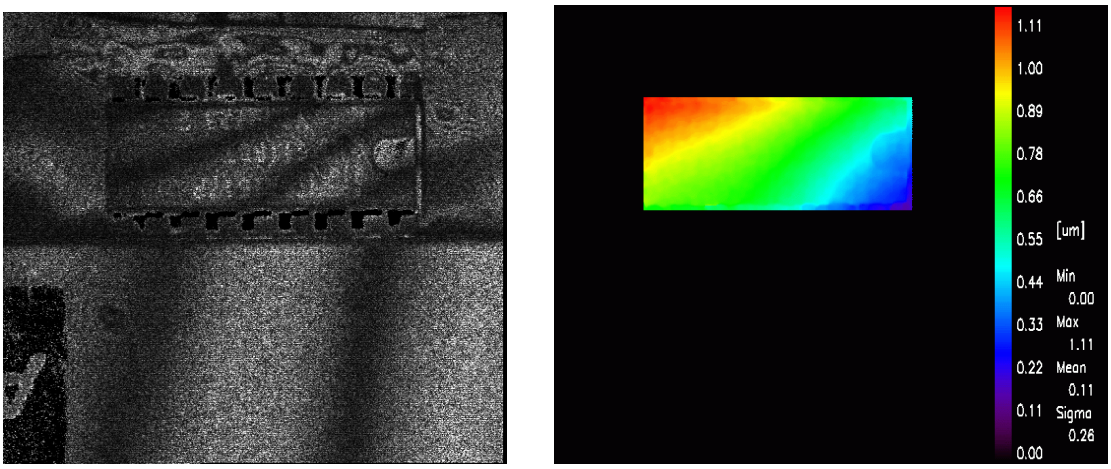

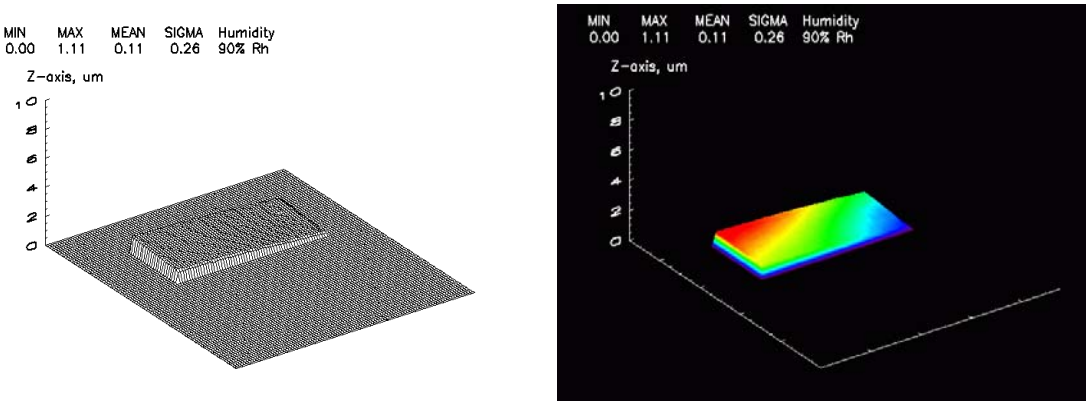

Fig. 10.7. Quantitative results for package three after six days.

Fig. 10.8 shows the quantitative results for sample 3 after 10 days. The maximum displacement obtained is 1.33 μm.

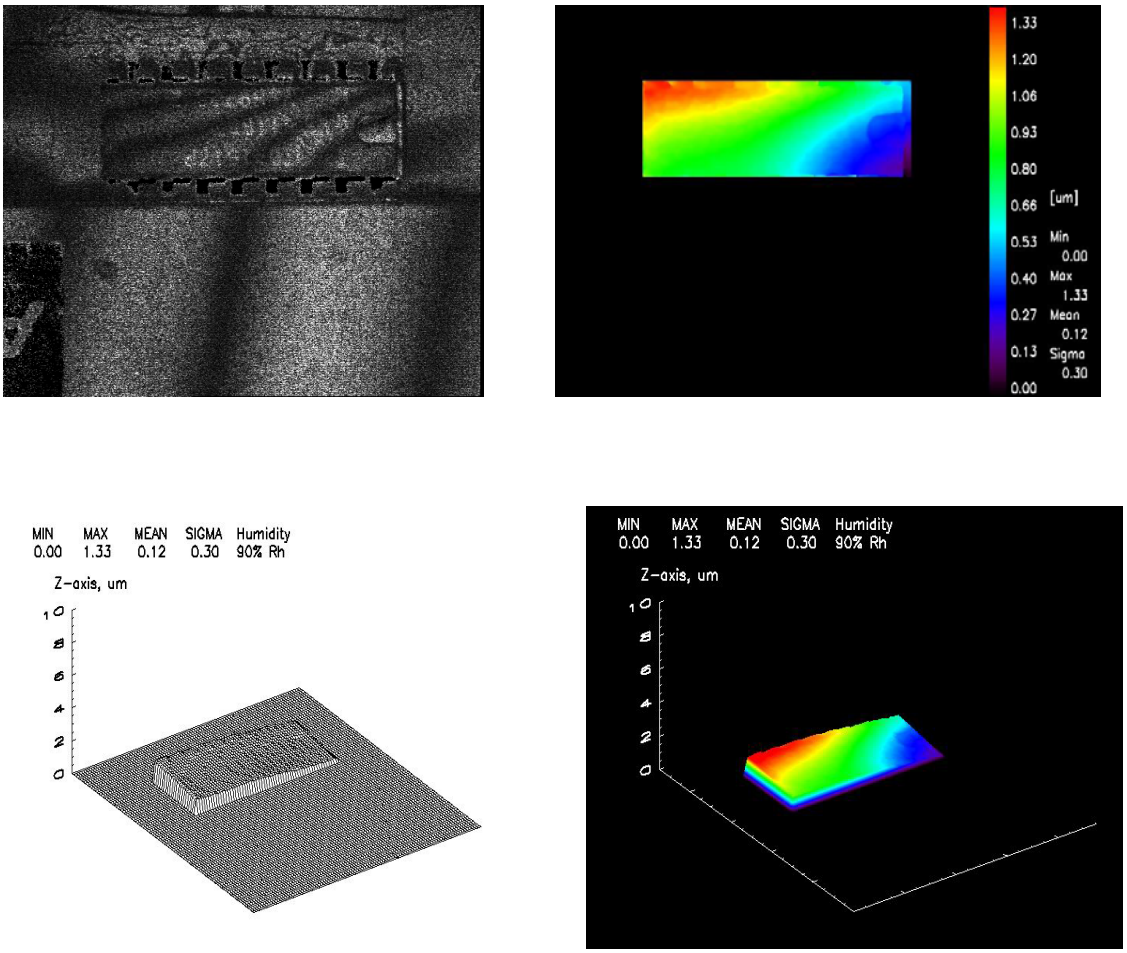

Fig. 10.8. Quantitative results for package three after ten days.

The experimental results are summarized in Table 10.1.

Table 10.1. Summary of deformation obtained for each sample over 10 days.

	Displacement after 3 days (μm)	Displacement after 6 days (μm)	Displacemenr after 10 days (μm)
Package 1	0.86	1.17	-
Package 2	2.13	2.64	3.43
Package 3	0.84	1.11	1.33

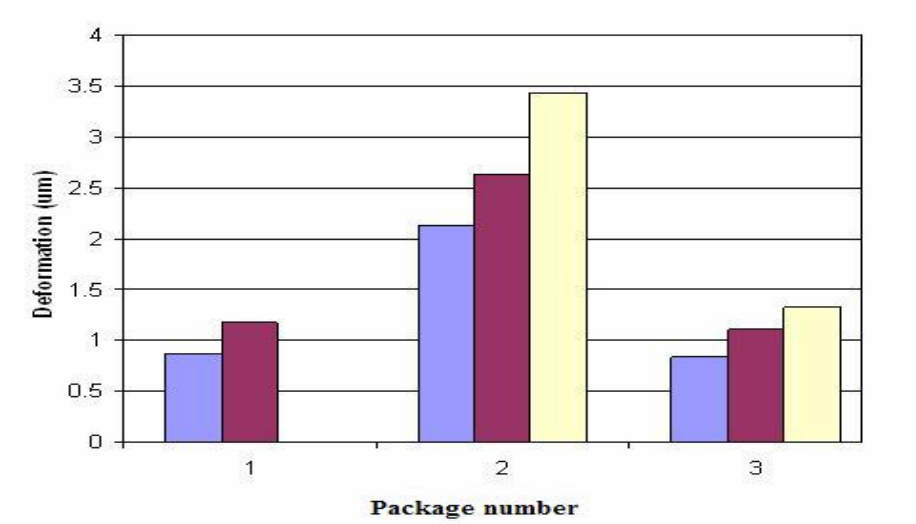

Fig. 10.9. Graphical representations of the variation of the rigid body translations.

It is observed from the results obtained from the experiments that the displacement occurring due to a rigid body motion of the package due to warpage depends upon the physical dimensions of the packages. The displacement increases non linearly as a function of time for each of the package. For package 1 it is observed that the displacement after 3 days is 0.86 μm as compared to package 2 which shows a displacement of about 2.13 μm. The displacement observed for package 3 is approximately equal to that for sample 1. The displacement of package 2 is more that that of package 1 and 3 because it is less thick and it is also observed that the number of leads are more than the other packages. The displacement of package 3 is lesser than package 1. It is observed from the physical dimensions of the package 3, that the lead frame thickness is around 0.24 mm whereas the lead frame thickness of package 1 is 0.114 mm.

It is also observed that as the area of the package increases the translation also increases. The lead frame and number of leads on to the package also affect the

displacement. Plastic leadframe interface is a mechanical joint (Tummala, 1989). Water penetrates by capillary migration along leads (Pecht et al.,1995). The ability to retard water penetration along the metal/plastic interface is a function of plastic shrinkage around the leads. Generally more the plastic coverage, the greater will be the compressive forces. Hence the area of the metal lead and lead frames should be less or equal to the plastic encapsulant (Tummala, 1989). It is proposed to study in future the influence of deformed encapsulant on the lead coplanarity.

It is also observed that the rectangular shaped packages 2 and 3 were far more prone to warpage than the approximately square shaped package 1. This fact has been established by experimental studies in previous studies (Kong et al.,2003).

The results obtained show a rigid body translation from which the deformation results can be obtained using IDL software by fitting a plane such that the rigid body tilt can be subtracted out such that only the out of plane deformations are obtained. Another way of getting the rigid body translations and general deformations or a combination of both can be obtained by measuring the three-dimensional displacement vector field of the surface points.

Some other experimental methodologies that can be used to study the hygroscopic phenomenon of warpage and swelling include spectroscopic methods. Many works have suggested that water molecules in a polymeric material can be present as free molecules in the voids (Ardebili et al., 2003). The Moire interferometry methods can be used to measure the in-plane and out of plane deformations results.

10.4. Finite difference method results

This Section presents the results of the moisture concentration profiles through the thickness of the package. The code was developed in MATLAB 6.5 and a user interface, Fig. 10.10 was created so that it can be used for various encapsulant material properties. The interface also makes it possible to enter variable values of the environmental conditions and material parameters.

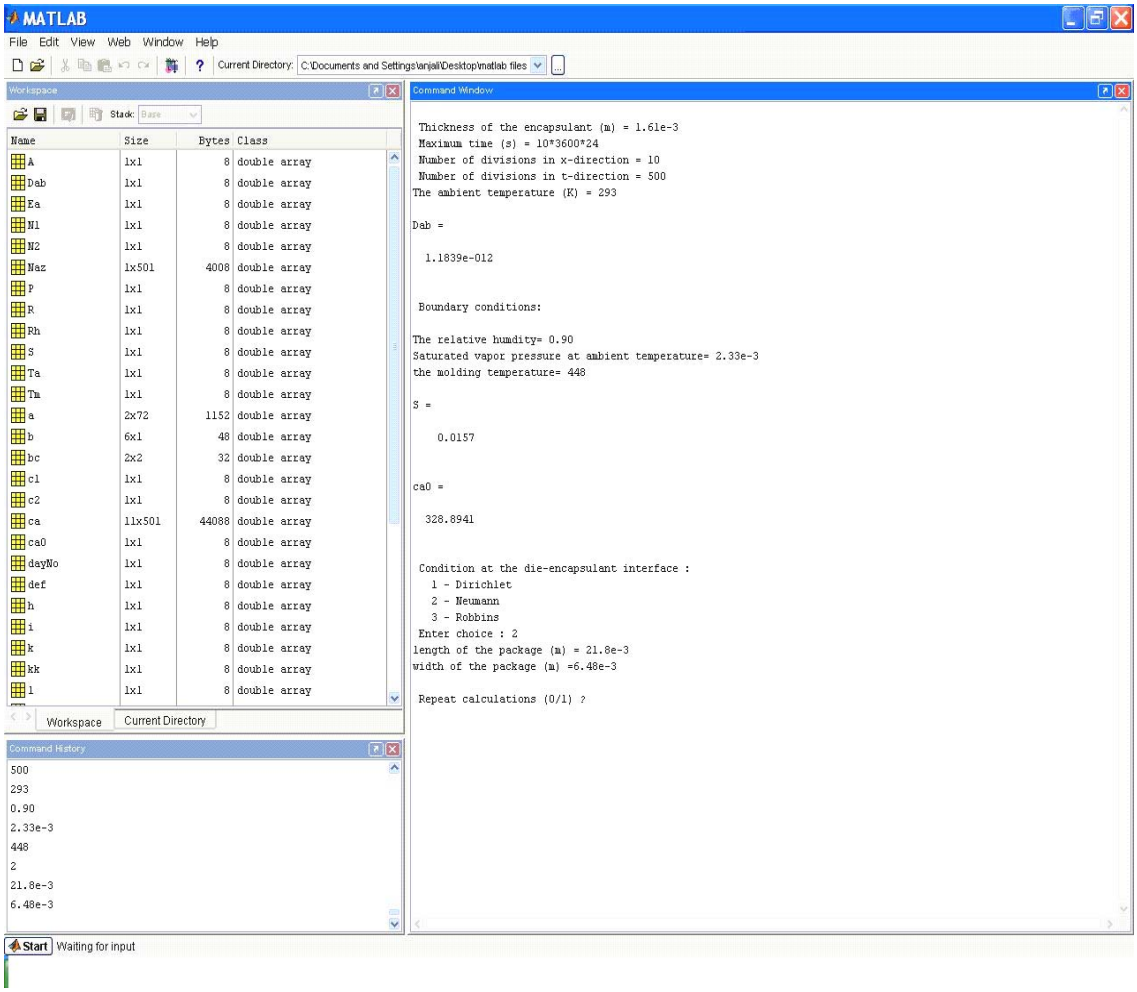

Fig. 10.10. User interface for the Matlab code.

The code is listed in Appendix A.

10.4.1 Representative computational results

This section represents the computational results for the three packages. The graphs presented here are:

1) the concentration profile as a function of thickness and time Figs 10.11(a), 10.12(a), 10.13(a),
2) the flux over a period of 10 days Figs 10.11(b), 10.12(b), 10.13(b),
3) the moisture content in grams Figs 10.11(c), 10.12(c), 10.13(c),

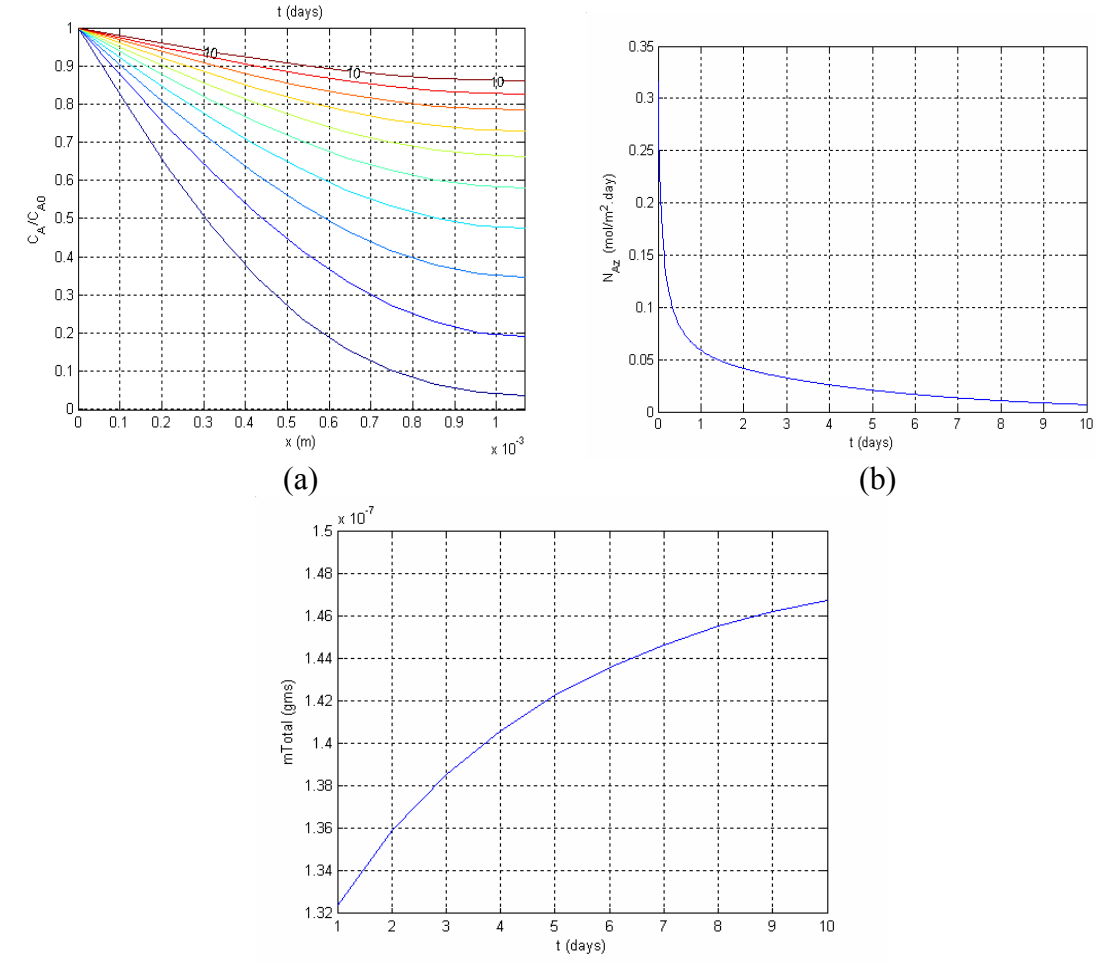

Fig. 10.11. Computational simulation for package 1: (a) concentration profile (b) flux as a function of time (c) accumulated moisture at the interface.

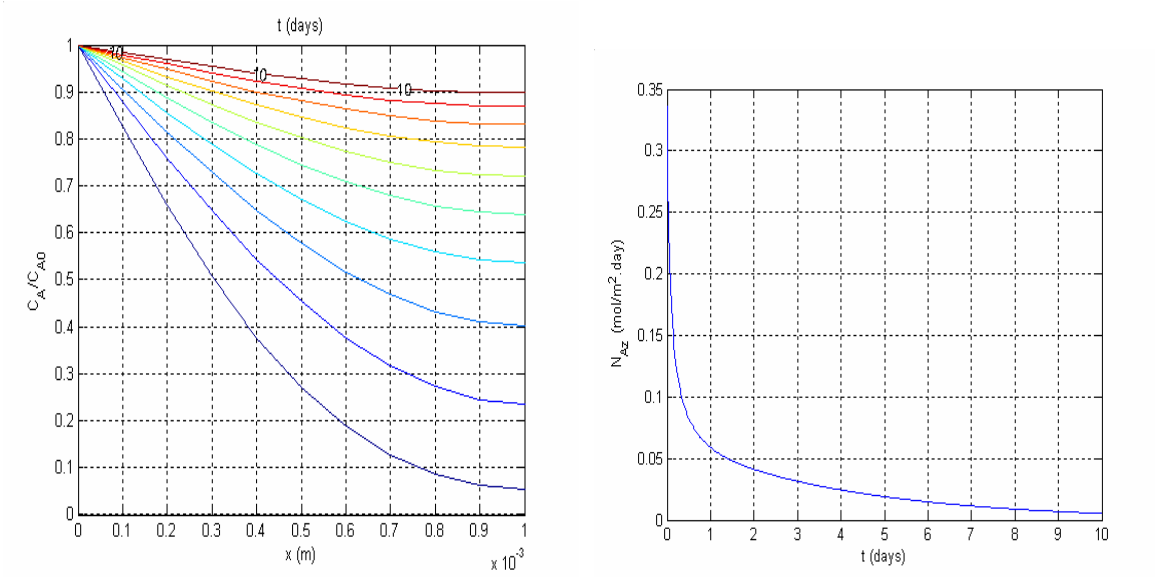

(a) (b)

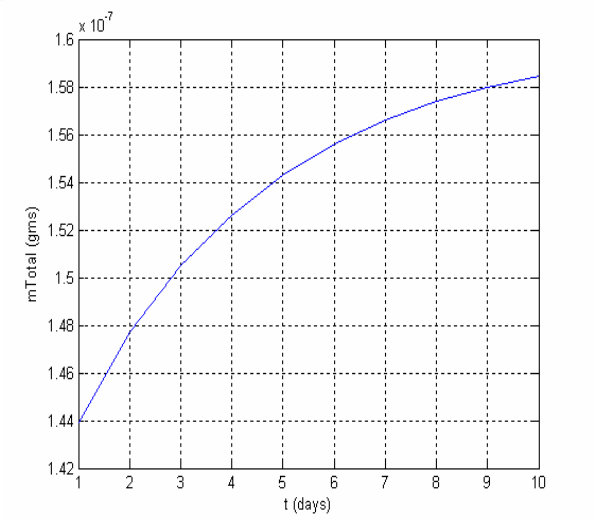

(c)

Fig. 10.12. Computational simulation for package 2: (a) concentration profile (b) flux as a function of time c) accumulated moisture at the interface.

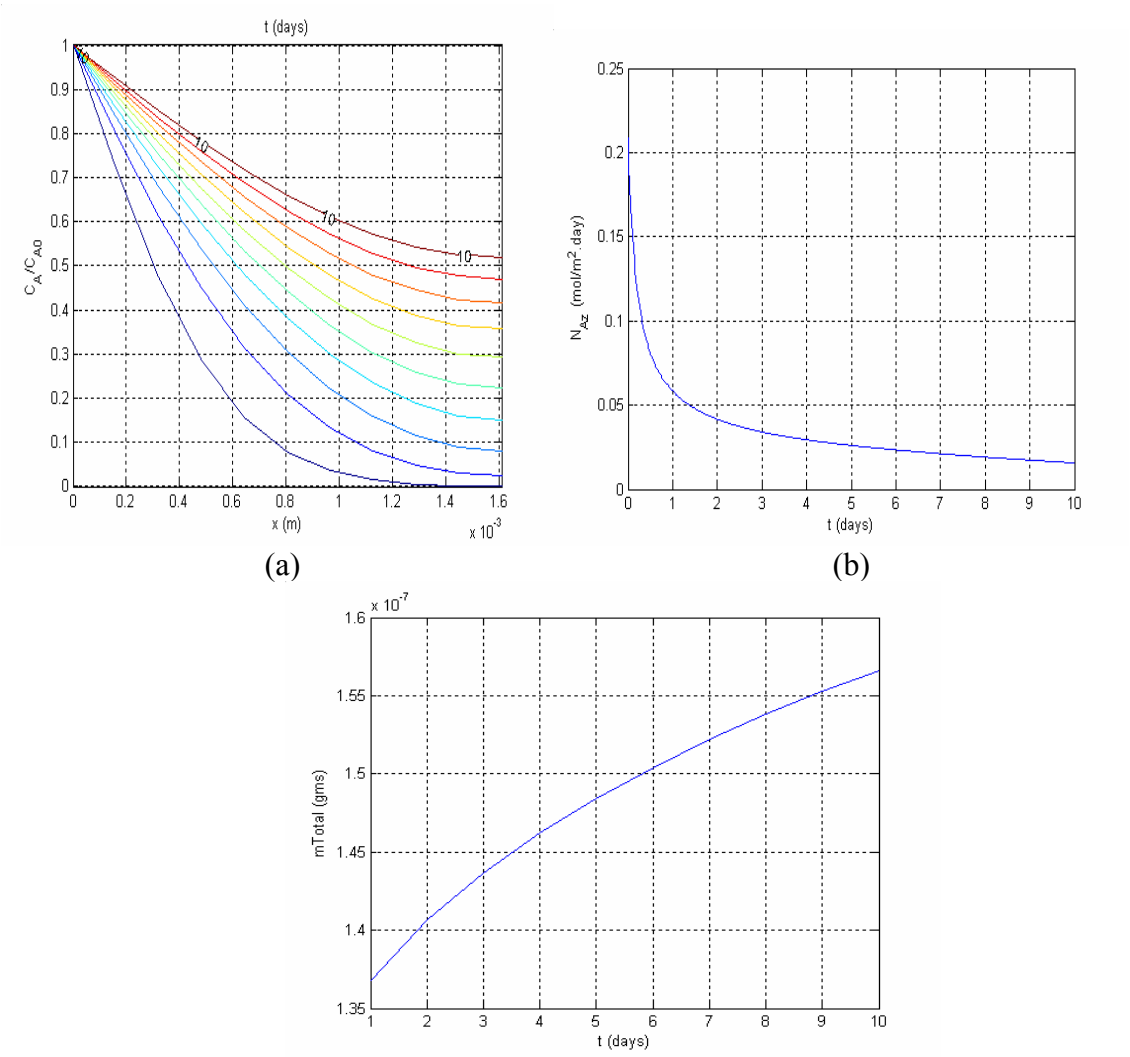

Fig. 10.13. Computational simulation for package 3: (a) concentration profile (b) flux as a function of time (c) accumulated moisture at the interface.

The results presented in Figs 10.11 to 10.13 show moisture diffusion simulation through the package. This helps in understanding the phenomenon of moisture diffusion through various encapsulants. Due to lack of literature regarding various plastic package, the modulus of elasticity and the Poisson's ratio have been kept constant for all simulations. The code developed can be used for different material properties for

simulating the moisture diffusion through the various other encapsulants. The results obtained from the moisture diffusion simulation are summarized in Table 10.3.

Table 10.2. Summary of results obtained from moisture diffusion simulation.

	Concentration			Flux (mol/m^2.day)			Moisture accumulated (x 10^{-7} gm)		
	3 days	6 days	10 days	3 days	6 days	10 days	3 days	6 days	10 days
Package 1	0.35	0.67	0.86	0.03	0.025	0.01	1.441	1.512	1.575
Package 2	0.4	0.71	0.9	0.03	0.025	0.01	1.505	1.559	1.584
Package 3	0.09	0.39	0.52	0.032	0.026	0.02	1.383	1.438	1.465

It is observed that the concentration profile for package 3 is not very steep. The concentration which is denoted in fraction is less for the third package, about 0.52 after 10 days as compared to the concentration of the other two packages. Package 1 and package 2 have approximately same thickness, hence not much difference is seen in the concentration profiles. This can be attributed to the larger thickness of the encapsulant for package 3, which adds on to the bulk of material through which the moisture diffuses. The moisture accumulated is highest in package 2 after 10 days with 1.584 x 10^{-7}gm. Package 1 has the lowest moisture accumulation after 10 days with 1.465 x 10^{-7}gm. The flux profiles are almost same for all the three packages because the material and environment conditions are taken to be similar for all the three packages. Fig. 10.14 is the graphical representation of the variation of moisture content in the encapsulants.

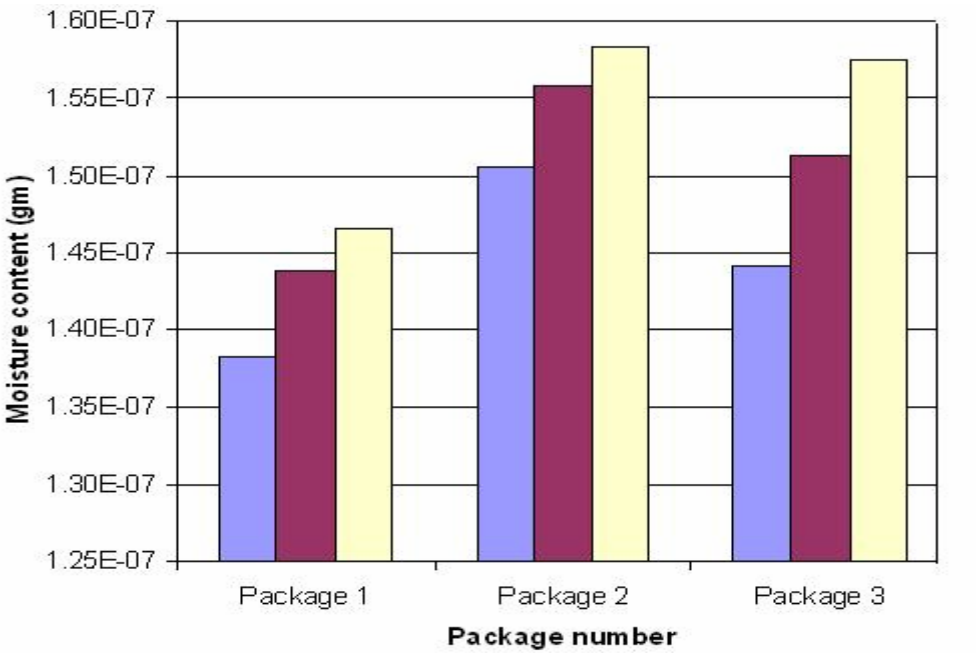

Fig. 10.14. Graphical representation of the variation of moisture content based on Matlab simulations.

The results of total mass of moisture the package are correlated to the theoretical curves discussed in Section 6.3. It is observed that the region for small times is a very small portion of the non-linear curve obtained with the matlab simulations results, as marked by the red rectangle in Fig 10.15.

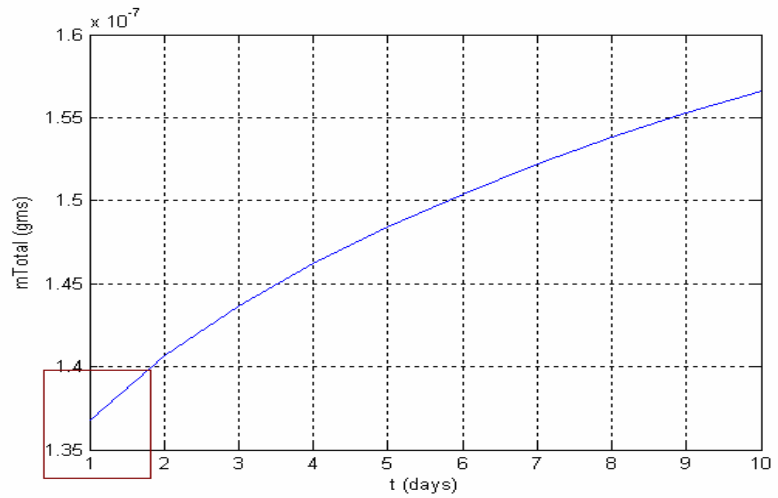

Fig. 10.15. Comparison of the analytical curve and matlab generated curve.

It can be established from this that the moisture diffusion equations should be theoretically solved for longer time.

The results of the moisture accumulated in the package and the displacement results obtained from the experimental part can be used to calculate the build up of water vapor pressures at about 235°C, which is a typical solder reflow temperature. With this information the hygroscopic stresses can be calculated to further analyze the failure criterion by von-Mises (Suhir, 1995).

10.5. Calculation of pressure and deformation

Using the ideal gas equation and the results obtained from the experimental and computational analysis the pressure developed in the encapsulant was calculated. By applying the theory of plates the deflection developed due to the pressure was calculated and verified with the experimental results. This section presents the deflection obtained due to the pressure build up after 6 days. The calculation sheet is attached in Appendix B.

Figure 10.16 shows the deformation function for package 1 after 6 days. The maximum deformation obtained is 1.886×10^{-7} m. The experimental results show a deformation of 1.17×10^{-6} m. There is a difference of one order of magnitude.

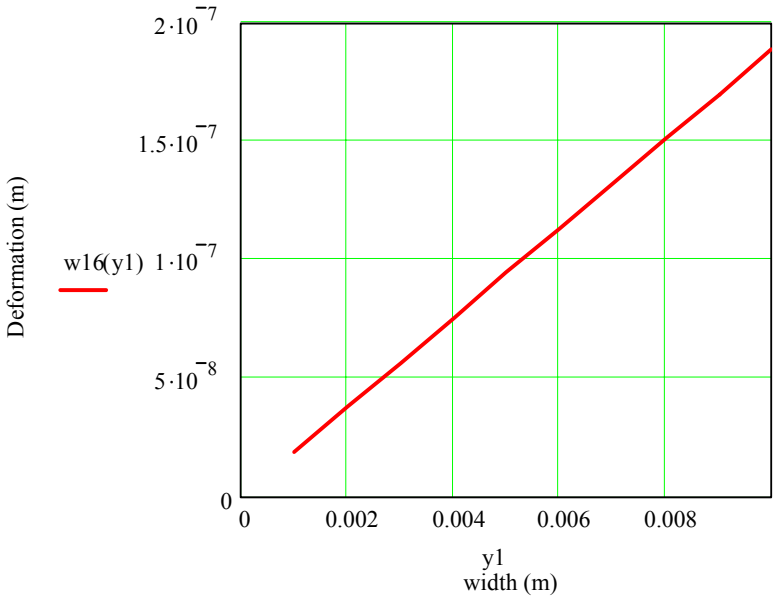

Fig. 10.16. Deformation of package 1 after 6 days.

Figure 10.17. shows the deformation function of package 2 after 6 days. The maximum deformation obtained is 2.221 x 10^{-7} m. The experimental results show a deformation of about 2.64 x 10^{-6} m.

Figure 10.18 shows the deformation function for package 3 after 6 days. The maximum deformation obtained is 5.091 x 10^{-7} m.

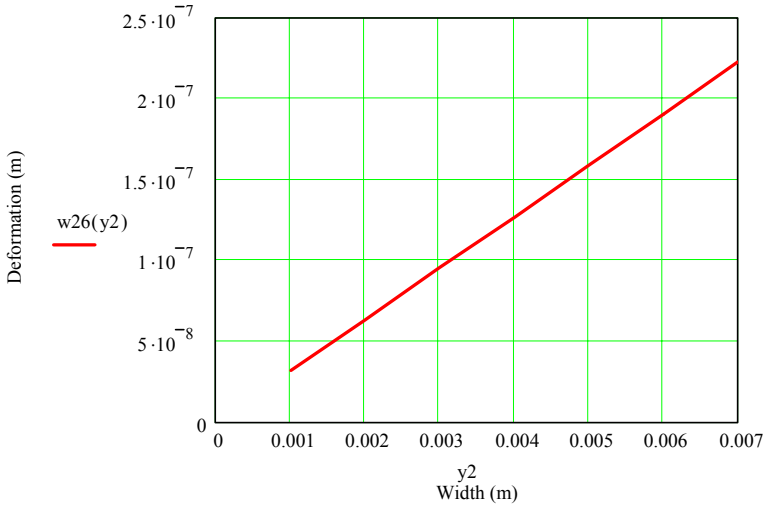

Fig. 10.17. Deformation of package 2 after 6 days.

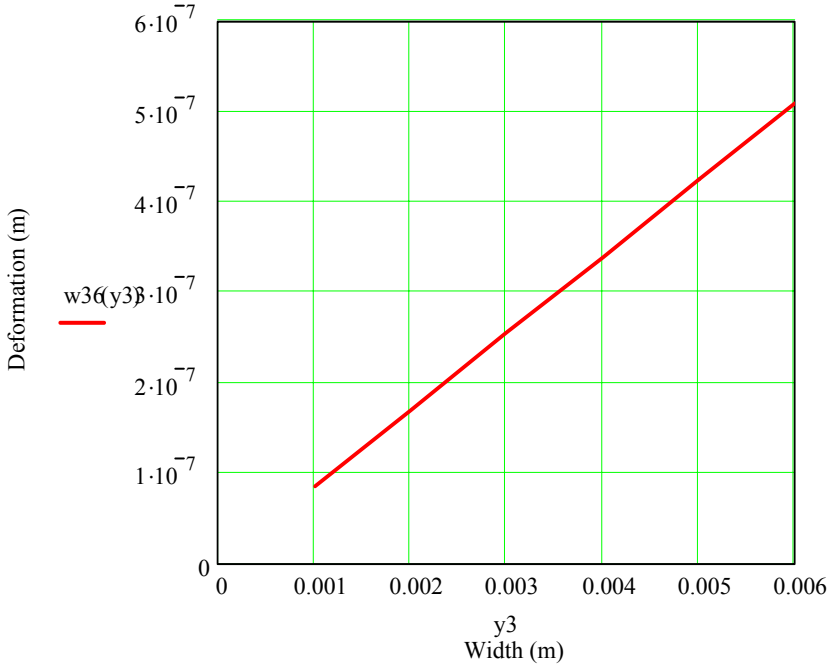

Fig. 10.18. Deformation of package 3 after 6 days

Figure 10.19 shows the comparison of deformations for all three packages.

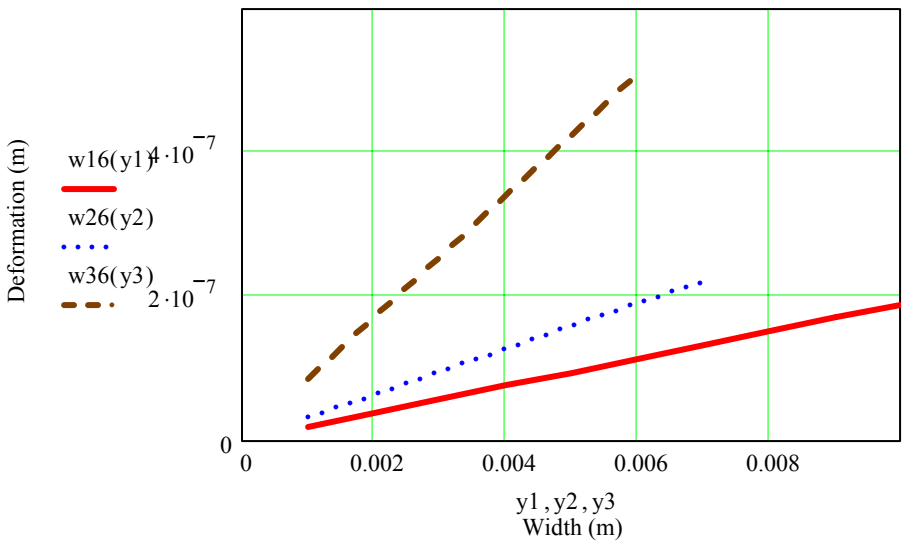

Fig. 10.19. Comparison of deformations after 6 days obtained analytically.

The discrepancy in the difference between the two results of deformation was studied. The deformation function used as analytical theory needs to take the varying concentration at the top and bottom surface. The analytical expression has been developed with curvatures due to varying concentration. This has been formulated into the flow chart, Fig 10.20, to obtain a new set of differential equation for moisture absorption loading. Another reason for this difference maybe considering the moisture diffusion as non-fickian diffusion and developing the diffusion equations accordingly. The plausible cause for this is the time dependent, viscoelastic response of polymers (Weitsman, 1990).

The major portion of deformation of the encapsulant is due to varying concentration in the through thickness direction. It is assumed that the concentration distribution is linear through the thickness. In this Thesis half model, till the mid plane

has been considered. This also accords with the bending behavior of plates where it is assumed that the change in concentration at the mid surface vanishes, because this will cause pure membrane stresses.

The definition of curvature due to concentration expansion can be given as (Bletzinger, 2000):

$$\kappa_C = \beta \frac{\Delta C}{t} \tag{10.1}$$

where κ_c is the curvature, β is the coefficient of hygroscopic swelling, t is the time and ΔC is the change in concentration.

The differential equation for deformation w, Eq 9.14 becomes (Bletzinger, 2000)

$$\Delta\Delta w = -(1+\nu)\left(\frac{\partial^2 \kappa_C}{\partial z^2} + \frac{\partial^2 \kappa_C}{\partial y}\right) = -(1+\nu)\Delta\kappa_C \tag{10.2}$$

The partial differential equation formulation for deformation and stress resultants can be summarized with the flow chart given in Fig 10.20.

With this formulation the experimental results can be verified. The information of the deformation due to moisture accumulation helps in further understanding of the stress resultants in the encapsulant that can be used for reliability assessment of the package.

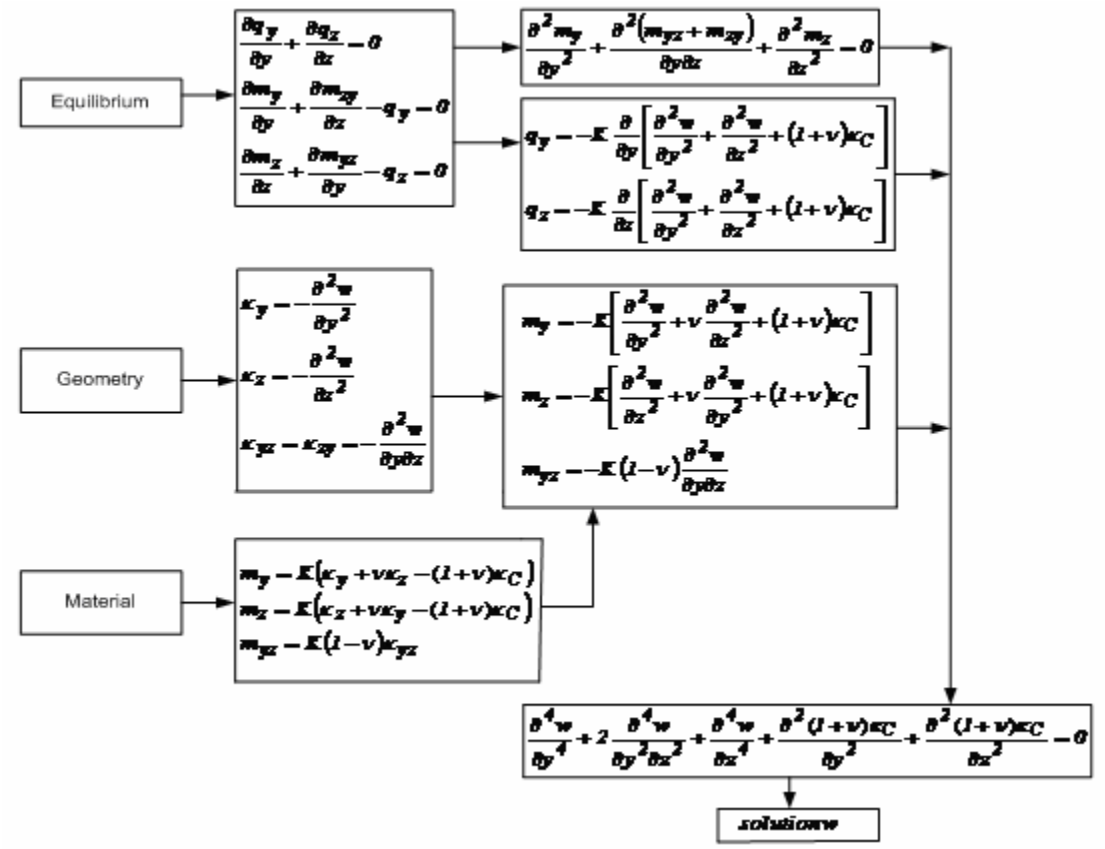

Fig. 10.20. Flowchart for the formulation of PDE considering concentrations.

The hybrid method developed in this Thesis is summarized in Table 10.3. The table gives the values of parameters obtained with the matlab simulation and the experimental results with the verification of the displacements due to rigid body translations.

Table 10.3. Summary of computational and experimental results.

	Concentration	Moisture accumulated (x 10^{-7} gm)	Experimental results (μm)	Pressure (MPa)	Analytical results (μm)
Package 1	0.67	1.512	1.17	0.23	0.1886
Package 2	0.71	1.559	2.64	0.53	0.221
Package 3	0.39	1.438	1.11	0.26	0.5091

10.6. Concept of the package model for MEMS

The plastic package for MEMS will have a different configuration and fabrication process than those used in the IC industry. For MEMS die a head space will be required to provide movement of the mechanical structure. To protect the device at the wafer level, an extra fabrication process is involved. The fragile MEMS structure can be covered with a second wafer which has appropriate cavities etched into it (Baert, 2004). A concept is being developed to apply a microcap at the wafer level and then proceed to standard packaging (Gilleo, 2001). The cap essentially produces a micro-hermetic package. The present caps are of silicon wafer. Cavities between the top lid and the MEMS wafer allow the device structures to move freely (Persson, 2002). After this wafer bonding, the device can be packaged for electrical connections and environmental isolation in standard plastic encapsulation process similar to those used in fabrication of integrated circuits (ICs). Plastic encapsulant has the inherent property of moisture absorption. But with suitable selection of material and characterization techniques like OEH a reliable package can be modeled. The results obtained from OEH type non destructive testing, the estimate of deformation of the encapsulant can be made and hence the cavity space determined. Based on the results obtained in this Thesis a package model has been suggested, Fig 10.21 (Deshpande and Pryputniewicz, 2004a). .

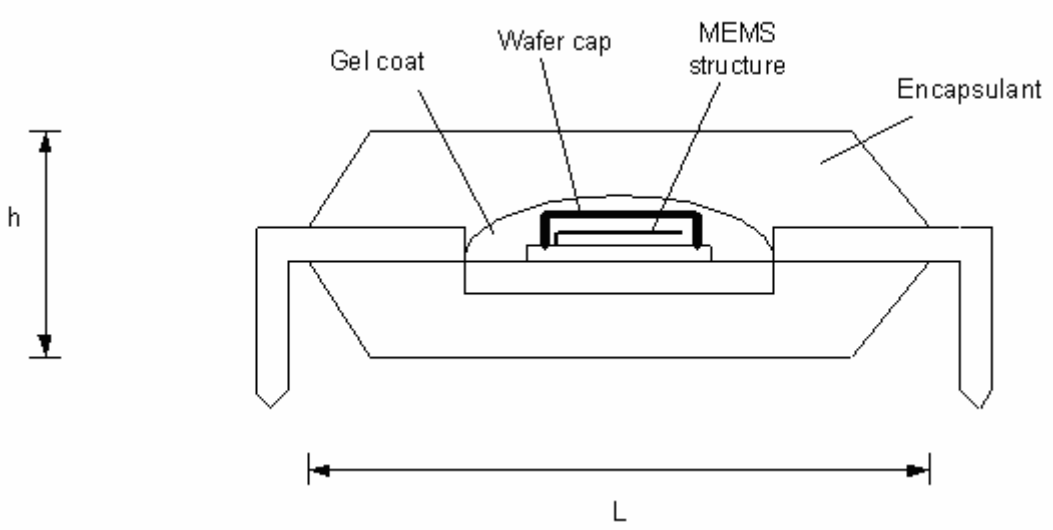

Fig. 10.21. Suggested package model.

It is observed that for the configuration of package 3, the deformation due to warpage is less as compared to the deformation of package 1 and package 2. Also the moisture accumulation rate is lower. Hence the optimum design parameters for the plastic encapsulated package are:

L = 21.8 mm,

h = 3.7 mm,

wi = 6.5 mm,

Lead frame thickness = 0.5 mm,

Wafer cap thickness = 0.5 mm.

11. CONCLUSIONS AND FUTURE WORK

Integrated circuit packaging and their testing is well advanced because of the maturity of the IC industry, their wide applications, and availability of industrial infrastructure. The study of the packaging methods for MEMS shows that this is not true for MEMS with respect to packaging and testing. A standardized MEMS device packaging is difficult to adopt due to the wide applications of the MEMS.

The movement of the mechanical element also makes this problem difficult. In this Thesis the functions of MEMS packages have been studied. The most important function that distinguishes MEMS packaging from the standard IC packaging are that they are in direct contact with the environmental physical and chemical parameters, which can eventually degrade the reliability of the package. Other functions include mechanical support, electrical connections and thermal considerations. MEMS packaging transcend three major tasks assembly, packaging, and testing. It is found that this costs about 50 % to 90 % of the cost of the finished product. The reason behind the high cost of MEMS packaging was studied. Packaging of MEMS is application specific and hence desired process steps vary significantly from application to application. Some other issues are problems in dicing, die handling, residual stresses, moisture penetration, etc.

The various types of packages and packaging methods were studied. The state of art packaging methods include, single chip packaging, wafer level packaging and multi chip modules. MEMS devices today are available in hermetically sealed packages. It was found that hermetic packages may cost up to ten times more than a plastic-package

because of the rigorous testing and screening required for low production volume hermetic parts. Hermetic packages usually have a higher material cost and are fabricated with more labor intensive manual processes. Also hermetically sealed packages require that the active signal lines travel through the seal region to make electrical connection to the device.

This Thesis investigates new prospects in plastic packaging by building on the principles of from the already established plastic encapsulated microcircuits. This can be a good cost saving option with added advantages of size and weight. The plastic encapsulation process methodology has been presented. However, molded plastic packages are not hermetic unlike metal and ceramic. The porous nature of the plastic encapsulant allows moisture to penetrate through the package.

An analytical model was developed to understand the moisture diffusion phenomenon. The moisture accumulation was found to be dependent on the thickness of the encapsulant and the time over which the moisture diffuses through the package. A characterization technique using OEH methodolgy was developed to measure deformations due to warpage caused by moisture accumulation. The OEH methodology is non-invasive and full-field-of-view information is obtained. The experimental results show that the deformation increases linearly with time. For package 1 the maximum deformation after a period of 6 days is 1.17 μm. For package 2 the maximum deformation after a period of 6 days was observed as 2.64 μm. Package 3 has a deformation of about 1.11 μm after 6 days. It is concluded that the deformation of the encapsulant is dependent on the geometrical parameters of the package. Comparing

packages 2 and 3, it is noted that the greater is the thickness, the lower is the deformation. Also the area of the package through which moisture ingress occurs makes a notable difference. Package 1 and package 2 have similar thicknesses but there is a huge difference of deformations. Package 2 has a larger area than the package 1.

The diffusion analysis was done with the help of finite difference methods, using the Crank-Nicolson semi implicit formula. Graphs corresponding to concentration profiles, the flux profile and the moisture accumulation over 10 days have been presented. The moisture content is highest, 1.584×10^{-7} gm in package 2 after 10 days.

Constitutive equations based on the theory of bending of plates were derived to understand and verify the deformation function due to warpage for encapsulants.

With results obtained from the hybrid methodology of experimental and computational processes, a concept for the package for MEMS has been presented.

Future work includes analyzing the discrepancy between the experimental and analytical results by solving the PDE derived for the deformation function taking into account the moisture concentration difference in the thickness direction. It is propsed to develop a finite element methodology which incorporates both structural and hygroscopic modeling to understand the propensity of the warpage and swelling due to the moisture accumulation in the encapsulant. The actual deformation results need to be extrapolated from subtracting the rigid body translation by the method of fitting a plane. Extending the characterization technique of OEH to measure in-plane strains, for obtaining the value of hygroscopic swelling β will also be required. Finally, it is necessary to monitor the moisture ingress in real-time for complete information of the reliability of the plastic

encapsulation. This can be done by applying the principle of dew point sensor, which can be positioned at the wafer level.

12. REFERENCES

Amkor Technology, 2003, "Packaging the micro- machine", website: http://www.amkor.com, visited: 7 May 2003.

H. Ardebilli, C. Hillman, and M. A. E Natishan, 2002 "A comparison of the theory of moisture diffusion in plastic encapsulated microelectronics with moisture sensor chip and weight gain measurements," *IEEE-Components and Packaging Technologies*, 25:132-139.

H. Ardebili and E. H. Wong, 2003, "Hygroscopic swelling and sorption characteristics of epoxy molding compounds used in electronic packaging," *IEEE-CPT*, 26:206-214.

K. Baert, P. D Moor, H. Tilmans, J. John, A. Witvrouw, C. Van Hoof and E. Beyne**,** 2004 **"**Trends in wafer-level packaging of MEMS", *Advanced packaging*.

H. Baltes, O. Brand, A. Heirlemann, D. Lange, and C. Hagleitner, 2002, "CMOS MEMS-present and future", *Proc. Symp. on MEMS 2002*, Las Vegas, NV, pp. 459-466.

D. Banks, 2002, "Introduction to microengineering," http://www.dbanks.demon.co.uk/ueng/liga.html, visited: January 2002.

I. K Bletzinger, 2000, *Theory of plates*, website:http://www.statik.bauwesen.tu-muenchen.de/, visited Aug 2004.

P. Bonniau and A. R. Bunsell, 1981, "A comparative study of water absorption theories applied to glass epoxy composites," *J. Composite Materials*, 15:272-293.

A. Bossche, C.V.B. Cotofana, and J. R. Mollinger, 1998, "MEMS packaging: state of the art and future trends," *SPIE Conf. on Smart Electronics and MEMS*, San Diego, CA. pp. 166-173.

L. Camporesi, 2003, "An overview of the applications of microelectromechanical devices," http://www.dig.bris.ac.uk/teaching/o_a_hf/lcamp.htm, visited: June, 2003.

H. K. Charles, 1989, "*Electrical connection*," Electronic materials handbook-1, ASM-International, OH.

J. Crank, 1975, *The mathematics of diffusion,* Claredon Press, Oxford, United Kingdom.

A. Constantinides and N. Mostoufi, 1999, *Numerical methods for chemical engineers with MATLAB applications*, Upper Saddle River, N.J.

J. R. Dale and R. C. Oldfield, 1977, "Mechanical stresses likely to be encountered in the manufacture and use of plastically encapsulated devices," *Microelectronics and Reliability*, 16:255-258.

P. W. Davies, 1989, "*Wafer level physical test methods*," Electronic materials handbook-1, ASM-International, OH.

A. W. Deshpande and R. J. Pryputniewicz, 2004a,"Moisture diffusiona characterization of a plastic encapsulated package," *IMAPS-New England Chapter*, Boxboro, MA.

A. W. Deshpande and R. J. Pryputniewicz, 2004b, "Characterization of a plastic encapsulated package for MEMS using OEH," 15th UACEM Symposium on MEMS and Nanotechnology, Springfield, MA.

P. V. Dressendorfer, D. A. Peterson, and C. A. Reber, 2000, "MEMS Packaging-Current Issues and Approaches", *Internat. Conf. and Exhibition on High Density Interconnect and Systems Packaging*, Denver, CO, pp. 208-213.

Electronic materials handbook, 1989, Vol. 1, ASM International, Materials Park, OH.

Fairchild semiconductors, 2004, http://www.fairchildsemi.com, visited: April 2004.

Z. Feng, H .Zhang, W. Zhang, B. Su, K. C. Gupta, V. M. Bright, Y. C. Lee, 2000, "MEMS based variable capacitor for millimeter-wave applications," *IEEE Solid state sensor and actuator and micro-system workshop*, Hilton Head Island, SC.

W. Flugge, 1975, *Viscoelasticity*, Springer-Verlag, NY

I. Fukuzawa, S. Ishiguro, and S. Nanbu, 1985, "Moisture resistance degradation of plastic LSI's by reflow soldering", *Proc. IRPS*, pp. 192-197.

C. Furlong, R. J. Pryputniewicz, 2001, "Sensitivity, accuracy, and precision issues in quantitative optical metrology characterizations," *Proc. Internat. Congress on Experimental and Applied Mechanics for Emerging Technologies*, Portland, OR, pp. 631-634.

R. D. Gerke, 2003, "MEMS packaging," Ch. 8, NASA documents, website: http://parts.jpl.nasa.gov/ docs/JPL%20PUB%2099-1H.pdf, visited: 8 April 2003.

T. Gessner, M. Wiemer, and J. Fromel, 2004, "MEMS-Packaging", website: http://www.zfm.tu-chemnitz.de/tu/pdf/annual_report_2002/special_report_15.pdf, visited: April 2004.

K. Gilleo, 2001, "Overview of new packages, materials and processes," Internat. Symp. on Advanced Packaging Materials, pp.1-5.

K. Gilleo, 2002, *Area array packaging handbook*, McGraw-Hill, New York, NY.

G. R. Grzelak, 2000, "*Testing*," The electronics packaging handbook, CRC Press LLC, Morgan Hill, CA.

D. F. Guillou, 2003, "*Packaging MEMS*," http://www.sensorsmag.com/articles/1203 /20/main.shtml, visited: Dec 2003.

C. A. Harper, 1969, *Handbook of electronic packaging*, McGraw-Hill, New York, NY.

R. J. Holmes, 2000, *Handbook of thick film technology*, EPL, UK.

C. T Hsieh, J. M. Ting, C. Yang, and C. K. Chung, 2002, "The introduction of MEMS packaging technology," *Internat, Symp. on Electronics materials and packaging- IEEE*.

T. R. Hsu, 2002, *MEMS and microsystem design and manufacturing*, McGraw-Hill, New York, NY.

B. C. Johnson,1989, "Overview of chip-level packaging," *Electronics material handbook*, ASM International, OH.

A. Kharab, and R. B. Guenther, 2002, *An introduction to numerical methods-A Matlab approach*, Chapman and Hall/CRC, New York, NY.

N. Kitano, A. Nishimura, S. Kawai, and K. Nishi, 1998, "Analysis of package cracking during reflow soldering process*," Proc. 26th IRPS*, pp. 90-95.

J. W. Y. Kong, J.K. Kim, and M. F. Yuen, 2003, "warpage in plastic packages: effects of process, conditions, geometry and materials," IEEE Trans. on Electronic Packaging Manufacturing, 26:245-252.

Kyocera, 2004 website: http://www.kyocera.com, visited: Jan 2004.

Lattice Semiconductor Corporation, 2004, website: http://www.gtmkorea.co.kr/data/support/PKG_MACH.PDF, visited: 1 February 2004.

J. Lawson, 2003, "LTCC-based packaging enables 3D functionality", *Wireless system design*, website: http://www.wsdmag.com/Articles/ArticleID/6599/6599.html, visited: 29 May, 2004.

J. H. Lim, K.W. Lee, S. S. Park, and Y. Y. Earmme, 1998, "Vapor pressure analysis of popcorn cracking in plastic IC packages by fracture mechanics," *IEEE-CPMT*, pp. 36-42.

S. Liu, 2002, "MEMS packaging and testing," *Proc. of the EU forum on nanosized technology*, Beijing, China, pp. 153-168.

Kyocera, 2004, Microelectronic packages, fiber optic components and ultra high vacuum products, website: http://www.kyocera.de/kyocera_n/english/microelectronics/applicationexamples.html, visited: January 2004.

M. Madou, 1997, *Fundamentals of microfabrication: The Science of Miniaturization*, CRC Press, Irvine, CA.

N. Maluf, 2000, *An introduction to micromechanical systems engineering*, Boston: Artech House.

T. F. Marinis and D. J. Carter, 2004, "Packaging of MEMS and NEMS- based instruments," *Short Course*: *Proc. of the 15th Internat. Invitational UACEM Symposium*, Springfield, MA.

Micromachines: MEMS overview, 2004 http://www.sandia.gov/mstc/technologies/micromachines/tech-info/overview/, visited: June 2004.

A. R. Mirza, 2000, "*Wafer level packaging technology for MEMS*," IEEE-ITHERM, Las Vegas, NV.

K. L. Mittal, 1976, "Adhesion measurement of thin films," *Electrocomponent Sci. Technolog*., 3:21-42.

F. K. Moghadam, 1983 "Development of adhesive die attach technology in cerdip packages material issues." *Proc. ISHM*, 27:149-157.

B. A. Moore, K. A. Berry and P. Speicher, 1989, "*Package–level physical test methods*," Electronics material handbook-1, ASM-International, OH.

T. Nakazawa, Y. Inoue, K. Sawada, and T. Sudo, 1996, "A novel structure ro realize crack free plastic package during reflow soldering process-development of chip side support CSS package," *IEEE-CPMT*, pp: 61- 68.

National Semiconductors, 2003, website: http://www.national.com, visited: March 2003.

C. B. O'Neal, A. P. Malshe, S. B. Singh, and W. D. Brown, 1999, "Challenges in the packaging of MEMS," *Internat. Symp. on Advanced packaging materials*, pp:41-47.

D. R Olsen and H.M Berg, 1997, "Properties of die bond alloys relating to thermal fatigue." *IEEE-Components, Hybrids, and Manufacturing Technology*, 2: 257-263.

D. W. Palmer, 1989, "*Component and board level physical test methods*," Electronics materials handbook-1, ASM-International, OH.

M. G. Pecht, R. Agarwal, D. Quearry, 1993, "Plastic packaged microcircuits: quality, reliability, and cost issues," *IEEE-transactions on reliability*, 42:513-517.

M. G. Pecht, L. T. Nguyen, and E. B. Hakim, 1995, *Plastic encapsulated microelectronics*, Wiley, New York, NY.

M. G. Pecht, R. Agarwal, P. McCluskkey, T. Dishongh, S. Javadpour, R. Mahajan, 1999, *Electronic packaging materials*, CRC Press, NY

K. Persson, A. H. Backe, K. Boustedt, 2002, "Fundamental requirements on MEMS packaging and reliability," *8th Internat. Symp. on Advanced Packaging Materials-IEEE*.

K. A. Peterson and W. R. Conley, 2004, "Pre-release plastic packaging of MEMS and IMEMS devices," *MicroPatent/ Sandia Corporation*, website: http://search.globalspec.com/engineering-search/patents/abstract/14544489399/Pre-release_plastic_packaging_of_MEMS_and_IMEMS_devices_, visited: Dec 2004.

Philips, 2004, http://semiconductorsphilips.com, visited: April 2004.

R. J. Pryputniewicz, 1995, "Quantitative determination of displacements and strains from holograms," Ch. 3 in *Holographic interferometry*, Vol. 68 of Springer Series in Sciences, Springer-Verlag, Berlin, pp. 33-72.

R. J. Pryputniewicz, 2002, *MEMS SUMMiT™-V Technology*, Worcester Polytechnic Institute, Worcester, MA.

R. J. Pryputniewicz, 2003a, MEMS/Nanotechnology, Worcester Polytechnic Institute, Worcester, MA.

R. J. Pryputniewicz, 2003b, *MEMS packaging*, Worcester Polytechnic Institute, Worcester, MA.

R. J. Pryputniewicz, T. F. Marinis, J. W. Soucy, P. Hefti, A. R. Klempner, and C. Furlong, 2003c, "Novel noninvasive methodology for characterization of packaging for MEMS inertial sensors," *Proc. 35th Internat. Symp. on Microelectronics*, Boston, MA, 392-397.

R. J. Pryputniewicz, E. Shepherd, J. J. Allen, and C. Furlong, 2003d, "University-National Laboratory alliance for MEMS education." *Proc. 4th Internat. Symp. on MEMS and Nanotechnology (4th – ISMAN)*, Charlotte, NC, pp. 364-371, 2003.

R. Ramesham and R. Ghaffarian, 2000, "Challenges in interconnection and packaging of microelectromechanical systems (MEMS)", *50th Proc. ECTC-IEEE*, pp. 666-675.

V. Rao, 2002, "MEMS Technology," website: http://www.ewh.ieee.org/r6/phoenix/phoenixcpmt/meetings/sep2002slides.pdf, visited: Dec 2003.

J. N. Reddy, 1999, *Theory and analysis of elastic plates*, Taylor and Francis, PA.

J. W. Roman, 2004, "Pre-molded liquid crystal polymer MEMS packaging and the quest for lower cost," *Proc. of the 15th Internat. Invitational UACEM Symposium*, Springfield, MA.

S. Roy, W. Xu, S.J. Park, and K.M. Liechti , 2002,"Anomalous Moisture Diffusion in Viscoelastic Polymers: Modeling and Testing", *Journal of Applied Mechanics,* 67: 391-396.

SemiconFarEast: Semiconductor manufacturing, 2004, website:http://www.semiconfareast.com/index.html, visited: June, 2004.

S. Senturia and R. L. Smith, 1988, "Microsensor packaging and system packaging", *Sensors and Actuators*, 15:221-234.

SensorMag, 2003, "Packaging MEMS: New Manufacturing Methodology Substantially Reduces Smart MEMS Costs", website: http://www.sensorsmag.com/articles/1203/20/main.shtml, visited: December 2003.

C. H. Shen and G. S. Springer, 1977, "Moisture absorption and desorption of composite materials," *J. Composite Materials*, 10:2-6.

E. Shepherd, 2002, "Micromachines-SUMMiT-V technology", http://www.sandia.gov/mstc/technologies/micromachines/tech-info/technologies/summit5.html, visited: Nov, 2002.

F. Shoraka, 1986, "Package and molding compound mechanics," *6th Annual Int. Electronic Packaging Conf. Proc*, pp. 309-314.

N. Sinnadurai, 1985, "Advances in microelectronics packaging and interconnection technologies toward a new hybrid microelectronics," *Microelectronics Journal*, 16, 5.

E. Suhir, 1991, *Structural analysis in microelectronic and fiber optic systems*, Van-Nostrand reinhold, NY.

E. Suhir, 1995, "Predicted failure criterion (von-Mises stress) for moisture sensitive plastic packages," *IEEE*, pp:266-284.

R. R. Swafford, H. Joseph, and V. Vaganov, 1997, "Implementing MEMS Technology in Today's Medical Electronics," *Medical Electronics Manufacturing Fall 1997,* website: http://www.devicelink.com/mem/archive/97/10/002.html, visted: September, 2004.

Z. H. Tao and Z. Bin, 2002, "Microelectromechanical system technology and its application," *Electronic Components and Materials*, 21:28-30.

A. Tay and T. Lin, 1996, "Moisture diffusion and heat transfer in plastic IC packages", *IEEE-CPMT*, 19:186-193.

T. Y. Tee and H. S. Ng, 2002, "Whole field vapor pressure modeling of QFN during reflow with coupled hygro-mechanical and thermo-mechanical stresses," *IEEE-ECTC*, pp:1552-1558.

Texas Instruments, 2004, http://www.ti.com, visited: April 2004.

S. Timoshenko, 1940, *Theory of plates and shells*, McGraw-Hill, New York, NY.

W. Trimmer, 1997, *Micromechanics and MEMS*, IEEE press, New York, NY.

Y. T. Tong, and S. N. Hun, 2002, "Whole field vapor pressure modeling of QFN during reflow with coupled hygromechanical and thermomechanical stresses," *Proc. 52nd IEEE-ECTC*, pp. 28-31.

R. Tummala, 1989, *Microelectronics packaging handbook,* Van Nostrand Reinhold, New York, NY.

R. Tummala, 2001, *Fundamentals of microsystem packaging*, McGraw-Hill, New York, NY.

J. H. Ulvensoen and G. L. Karlsen, 1999, "Packaging for volume production of MEMS-a great challenge", *36th IMAPS Nordic Conference*, Helsinki, pp. 142-149.

Wabash MPI, 2004, website: http://www.wabashmpi.com/tm.asp, visited: July 2004.

E. H. Wong, R. Rajoo, S. W. Koh, and T. B. Lim, 2002, "The mechanics and impact of hygroscopic swelling of polymeric materials in electronic packaging," *Trans. of the ASME*, 124: 122-126.

Y. Weitsman, 1990, “A continuum diffusion model for viscoelastic materials,” *J. Physical Chemistry*, 94:961-968.

S. Wu, 1982, *Polymer interface and adhesion*, Marcel Dekker, New York, NY.

APPENDIX A: Matlab code

```
clear
redo = 1;
clc

while redo
  disp(' ')
  h = input(' Thickness of the encapsulant (m) = ');
  tmax = input(' Maximum time (s) = ');
  p = input(' Number of divisions in x-direction = ');
  q = input(' Number of divisions in t-direction = ');
  % to calculate the diffusion coefficient as a function of temperature
c1=0.472; %constant
% Activation energy in ev
Ea=0.5;
% Boltzmann constant in ev/K
k=8.617e-5;
Ta=input('The ambient temperature (K) = ');
%diffusion coefficient
Dab=c1*(10e-4)*exp(-Ea/((k)*Ta))

  disp(' ')

  disp(' Boundary conditions:')
  disp(' ')
% to calculate the concentration at the surface exposed to the ambient.
Rh=input('The relative humdity= ');
% The saturated vapor pressure in MPa
P=input('Saturated vapor pressure at ambient temperature= ');
% solubility dependent on molding temperature
c2=4.96e-4;
Ea=0.40;
k=8.617e-5;
% Molding tempertaure in K
Tm=input('the molding temperature= ');
S=c2*(10e-4)*exp(Ea/((k)*Tm))
ca0=Rh*P*S*10e+6

  bc(1,1) = 1;
  bc(1,2) = ca0;
  disp(' ')
  disp(' Condition at the die-encapsulant interface :')
```

```
  disp('   1 - Dirichlet')
  disp('   2 - Neumann')
  disp('   3 - Robbins')
  bc(2,1) = input(' Enter choice : ');

  u0 = [ca0; zeros(p,1)];

    [z,t,ca] = parabolic1D(p,q,h/p,tmax/q,Dab,u0,bc);

  % Calculating the flux of A
  Naz = -Dab*diff(ca(1:2,:))/diff(z(1:2));
%%Calculating the accumulated moisture at the interface
%Calculate the area of the encapsulant
l=input ('length of the package (m) = ');
w=input ('width of the package (m) =');
A=l*w;

for i=1:10

dayNo=i;

N1=1+50*(dayNo-1); N2=50*dayNo;
m_N1_N2(i)=A*trapz(Naz(N1:N2))*1;
if i>1
   mTotal(i)=m_N1_N2(i)+mTotal(i-1);
else
   mTotal(i)=m_N1_N2(i);
end
end

% R=8.3144;
% def=1.88e-6;
% pr=(mTotal*18*R*Ta)/(def*A)

  % Plotting concentration profile
  tt=[]; % Making time matrix from time vector
  for kk = 1 : p+1
    tt = [tt; t];
  end
  zz = [];         % Making height matrix from height vector
  for kk = 1 : q+1
    zz = [zz z'];
  end
```

```
  figure(1)
  [a,b]=contour(zz,ca/ca0,tt/3600/24,[0:1:tmax/3600/24]);


clabel(a,b,[10:10:tmax/3600/24])
  xlabel('x (m)')
  ylabel('C_A/C_A_0')
  title('t (days)')
  grid on
  % Plotting the unsteady-state flux
  figure(2)
  plot(t/3600/24,Naz*3600*24)
  xlabel('t (days)')
  ylabel(' N_{Az} (mol/m^2.day)')
  grid on
  figure(3)
  plot(mTotal)
  xlabel('t (days)')
  ylabel('mTotal (gms)')
  grid on
%    figure(4)
%   plot(pr)

%    figure(4)
%    plot(m,pr)
%    figure(5)
%    plot(t/3600/24,pr*3600*24)
%    xlabel('t (days)')
%    ylabel(' pr (mol/m^2.day)')
%    grid on

  disp(' ')
  redo = input(' Repeat calculations (0/1) ? ');
  clc
end
```

Appendix B. MathCAD sheet: calculations for deformations

FOR PACKAGE 1 after 3 days

Calculating the pressure developed in the encapsulant with the ideal gas equation

$n13 := \frac{1.39 \cdot 10^{-7}}{18}$ The number of moles have been obtained from the Matlab results (Appendix A). It has been divided by 18 to convert the gms into moles.

$R := 8.314$ J / mol / K

$Ta := 293$ K The temperature was kept constant due to experimental constraints.

$\delta 13 := 0.84 \cdot 10^{-6}$ m The value of the deformation was obtained from the experimental OEH results.

$wi1 := 10.008 \cdot 10^{-3}$ m Width of the encapsulant

$l1 := 12.6 \cdot 10^{-3}$ m Length of the encapsulant

$A1 := l1 \cdot wi1$ m ^2

$Pr13 := \frac{n13 \cdot R \cdot Ta}{\delta 13 \cdot A1}$ Pa $Pr13 = 1.776 \times 10^{5}$

It is observed in the experimental results that the deformation pattern is due to a nature of hydrostatic loads. Hence, the value if the pressure load will be calculated as

$y := 1 \cdot 10^{-3}, 2 \cdot 10^{-3} .. wi1$

$Ph13(y) := \frac{Pr13 \cdot y \cdot A1}{wi1}$ Pa Hydrostatic loading

Calculating the deformation to verify the experimental results

$E := 1.1 \cdot 10^{9}$ Pa

$h1 := 1.0065 \cdot 10^{-3}$ m

$v := 0.3$

$K1 := \frac{E \cdot h1^{3}}{12 \cdot (1 - v^{2})}$ Pa.m^3

$w13(y) := 0.013021 \cdot \frac{Ph13(y) \cdot wi1^{4}}{K1}$ m

The deformation function for package 1 after 3 days is shown in Fig. B.1.

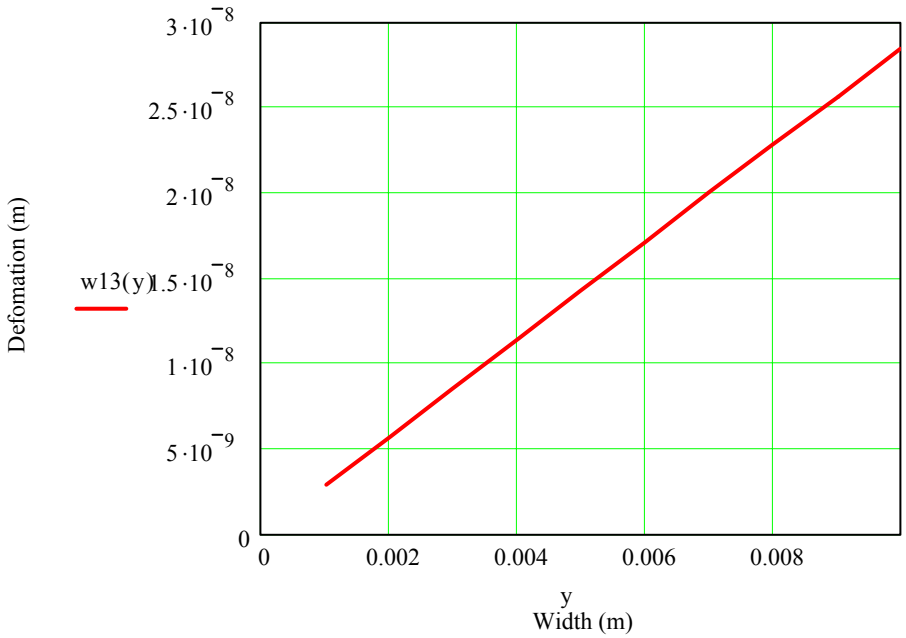

Fig. B.1. Deformation of package 1 after 3 days

FOR PACKAGE 1 after 6 days

Calculating the pressure developed in the encapsulant with the ideal gas equation

$n16 := \frac{1.44 \cdot 10^{-7}}{18}$ The number of moles have been obtained from the Matlab results (Appendix A). It has been divided by 18 to convert the gms into moles.

$R := 8.314$ J / mol / K

$Ta := 293$ K The temperature was kept constant due to experimental constraints.

$\delta 16 := 0.33 \cdot 10^{-6}$ m The value of the deformation was obtained from the experimental OEH results.

$wi1 := 10.008 \cdot 10^{-3}$ m Width of the encapsulant

$l1 := 12.6 \cdot 10^{-3}$ m Length of the encapsulant

$A1 := l1 \cdot wi1$

$Pr16 := \frac{n16 \cdot R \cdot Ta}{\delta 16 \cdot A1}$ Pa

It is observed in the experimental results that the deformation pattern is due to a nature of hydrostatic loads. Hence the value if the pressure load will be calculated as

$y1 := 1 \cdot 10^{-3}, 2 \cdot 10^{-3} .. wi1$

$Ph16(y) := \frac{Pr16 \cdot y \cdot A1}{wi1}$ Pa Hydrostatic loading

Calculating the deformation to verify the experimental results

$E := 1.1 \cdot 10^{9}$ Pa

$h := 1.0065\,10^{-3}$ m

$v := 0.3$

$K1 := \frac{E \cdot h1^{3}}{12 \cdot \left(1 - v^{2}\right)}$ Pa m^3

$w16(y1) := 0.013021 \frac{Ph16(y1) \cdot l1^{4}}{K1}$ m

The deformation function for package 1 after 6 days is shown in Fig. B.2.

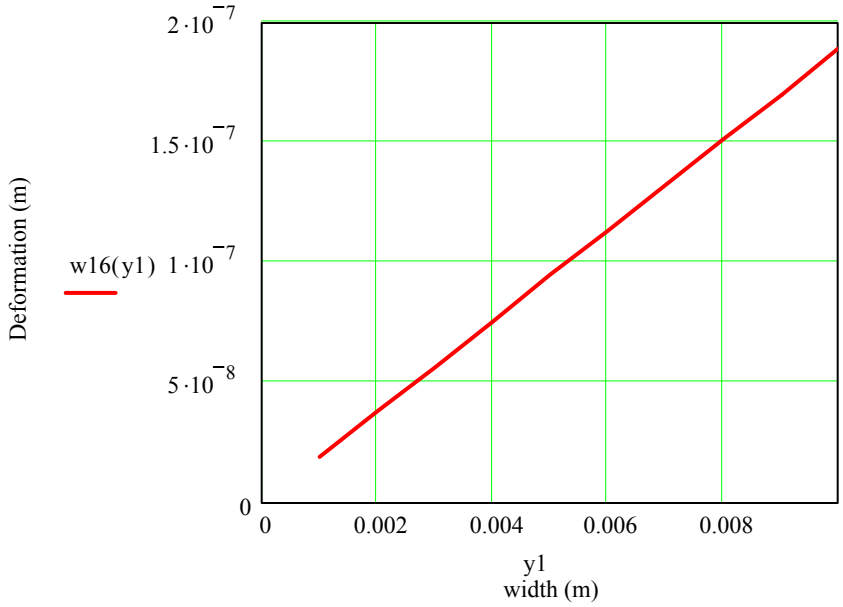

Fig. B.2. Deformation of package 1 after 6 days.

FOR PACKAGE 2 after 3 days

Calculating the pressure developed in the encapsulant with the ideal gas equation

$n23 := \frac{1.52 \cdot 10^{-7}}{18}$ The number of moles have been obtained from the Matlab results (Appendix A). It has been divided by 18 to convert the gms into moles.

$R := 8.314$ J / mol / K

$Ta := 293$ K The temperature was kept constant due to experimental constraints.

$\delta 23 := 2.13 \cdot 10^{-6}$ m The value of the deformation was obtained from the experimental OEH results.

$wi2 := 7.50 \cdot 10^{-3}$ m Width of the encapsulant

$l2 := 18.10 \cdot 10^{-3}$ m Length of the encapsulant

$A2 := l2 \cdot wi2$

$Pr23 := \frac{n23 \cdot R \cdot Ta}{\delta 23 \cdot A2}$ Pa

It is observed in the experimental results that the deformation pattern is due to a nature of hydrostatic loads. Hence the value if the pressure load will be calculated as

$z := 1 \cdot 10^{-3}, 2 \cdot 10^{-3} .. l2$

$Ph23(z) := \frac{Pr23 \cdot z \cdot A2}{l2}$ Pa Hydrostatic loading

Calculating the deformation to verify the experimental results

$E := 1.1 \cdot 10^{9}$ Pa

$h2 := 1.00 \cdot 10^{-3}$ m

$v := 0.3$

$K2 := \frac{E \cdot h2^3}{12 \cdot \left(1 - v^2\right)}$ Pa m^3

$w23(z) := 0.013021 \cdot \frac{Ph23(z) \cdot l2^4}{K2}$ m

The deformation function for package 2 after 3 days is shown in Fig. B.3.

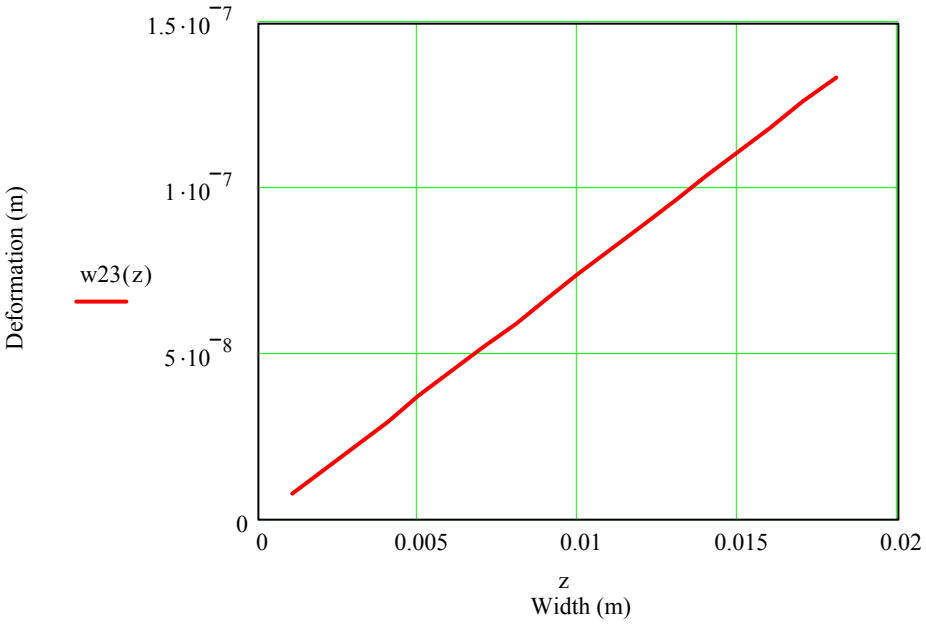

Fig. B.3. Deformation of package 2 after 3 days.

FOR PACKAGE 2 after 6 days

Calculating the pressure developed in the encapsulant with the ideal gas equation

$n26 := \frac{1.56 \cdot 10^{-7}}{18}$ The number of moles have been obtained from the Matlab results (Appendix A). It has been divided by 18 to convert the gms into moles.

$R := 8.314$ J / mol / K

$Ta := 293$ K The temperature was kept constant due to experimental constraints.

$\delta 26 := 0.51 \cdot 10^{-6}$ m The value of the deformation was obtained from the experimental OEH results.

$wi2 := 7.50 \cdot 10^{-3}$ m Width of the encapsulant

$l2 := 18.10 \cdot 10^{-3}$ m Length of the encapsulant

$A2 := l2 \cdot wi$

$Pr26 := \frac{n26 \cdot R \cdot Ta}{\delta 26 \cdot A2}$ Pa

It is observed in the experimental results that the deformation pattern is due to a nature of hydrostatic loads. Hence the value if the pressure load will be calculated as

$y2 := 1 \cdot 10^{-3}, 2 \cdot 10^{-3} .. wi$

$Ph26(z) := \frac{Pr26 \cdot z \cdot A2}{l2}$ Pa Hydrostatic loading

Calculating the deformation to verify the experimental results

$E := 1.1 \cdot 10^{9}$ Pa

$h2 := 1.00 \cdot 10^{-3}$ m

$v := 0.3$

$K2 := \frac{E \cdot h2^{3}}{12 \cdot \left(1 - v^{2}\right)}$ Pa m^3

$w26(y2) := 0.013021 \frac{Ph26(y2) \cdot l2^{4}}{K2}$ m

The deformation function for package 2 after 6 days is shown in Fig. B.4

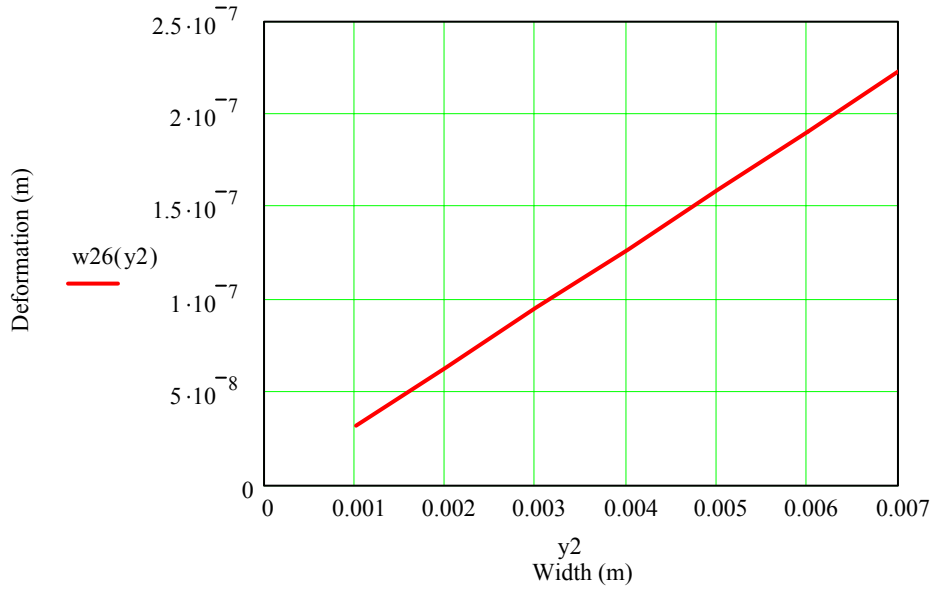

Fig. B.4. Deformation of package 2 after 6 days.

FOR PACKAGE 2 after 10 days

Calculating the pressure developed in the encapsulant with the ideal gas equation

$n210 := \frac{1.59 \cdot 10^{-7}}{18}$ The number of moles have been obtained from the Matlab results (Appendix A. It has been divided by 18 to convert the gms into moles.

$R := 8.314$ J / mol / K

$Ta := 293$ K The temperature was kept constant due to experimental constraints.

$\delta 210 := 0.77 \cdot 10^{-6}$ m The value of the deformation was obtained from the experimental OEH results.

$wi2 := 7.50 \cdot 10^{-3}$ m Width of the encapsulant

$l2 := 18.10 \cdot 10^{-3}$ m Length of the encapsulant

$A2 := l2 \cdot wi2$

$Pr210 := \frac{n210 \cdot R \cdot Ta}{\delta 210 \cdot A2}$ Pa

It is observed in the experimental results that the deformation pattern is due to a nature of hydrostatic loads. Hence the value if the pressure load will be calculated as

$z := 1 \cdot 10^{-3}, 2 \cdot 10^{-3} .. wi2$

$Ph210(z) := \frac{Pr210 \cdot z}{l2}$ Pa Hydrostatic loading

Calculating the deformation to verify the experimental results

$E := 1.1 \cdot 10^{9}$ Pa

$h2 := 1.00 \cdot 10^{-3}$ m

$v := 0.3$

$K2 := \frac{E \cdot h2^3}{12 \cdot (1 - v^2)}$ Pa m^3

$w210(z) := 0.013021 \frac{Ph210(z) \cdot l2^4 \cdot A2}{K2}$ m

The deformation function for package 2 after 10 days is shown in Fig. B.5.

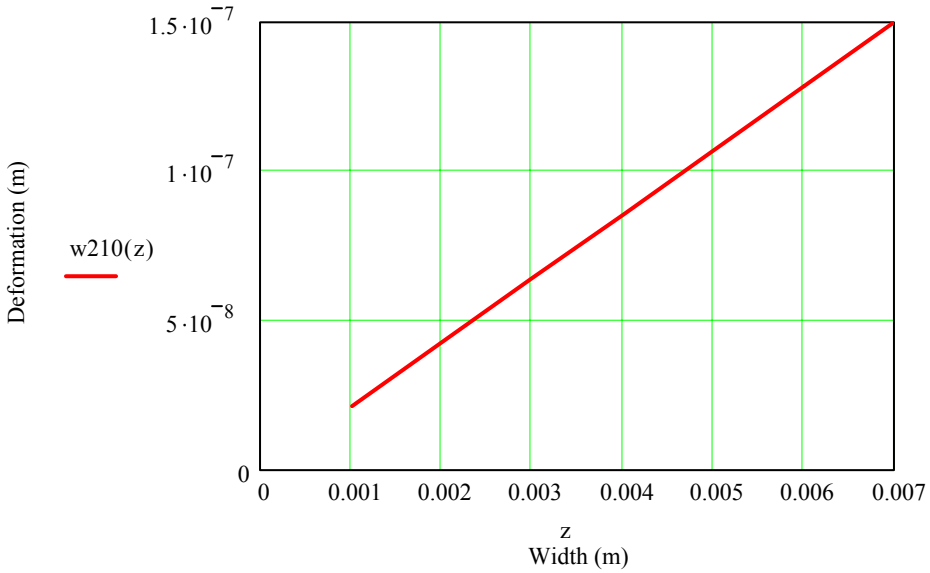

Fig. B.5. Deformation of package 2 after 10 days.

FOR PACKAGE 3 after 3 days

Calculating the pressure developed in the encapsulant with the ideal gas equation

$n33 := \frac{1.45 \cdot 10^{-7}}{18}$ The number of moles have been obtained from the Matlab results (Appendix A). It has been divided by 18 to convert the gms into moles.

$R := 8.314$ J / mol / K

$Ta := 293$ K The temperature was kept constant due to experimental constraints.

$\delta 33 := 0.84 \cdot 10^{-6}$ m The value of the deformation was obtained from the experimental OEH results.

$wi3 := 6.48 \cdot 10^{-3}$ m Width of the encapsulant

$l3 := 21.8 \cdot 10^{-3}$ m Length of the encapsulant

$A3 := l3 \cdot wi3$

$Pr33 := \frac{n33 \cdot R \cdot Ta}{\delta 33 \cdot A3}$ Pa

It is observed in the experimental results that the deformation pattern is due to a nature of hydrostatic loads. Hence the value if the pressure load will be calculated as

$z := 1 \cdot 10^{-3}, 2 \cdot 10^{-3} .. wi3$

$Ph33(z) := \frac{Pr33 \cdot z}{wi3}$ Pa Hydrostatic loading

Calculating the deformation to verify the experimental results

$E := 1.1 \cdot 10^{9}$ Pa

$h3 := 1.61 \cdot 10^{-3}$ m

$v := 0.3$

$K3 := \frac{E \cdot h3^{3}}{12 \cdot \left(1 - v^{2}\right)}$ Pa m^3

$w33(z) := 0.013021 \frac{Ph33(z) \cdot l3^{4} \cdot A3}{K3}$ m

The deformation function for package 3 after 3 days is shown in Fig. B. 6.

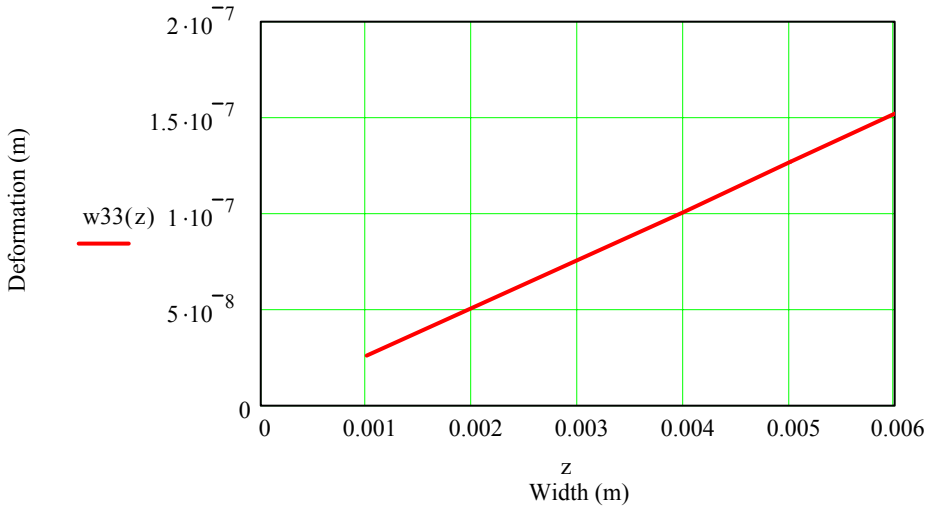

Fig. B.6. Deformation of package 3 after 3 days.

FOR PACKAGE 3 after 6 days

Calculating the pressure developed in the encapsulant with the ideal gas equation

$n36 := \frac{1.51 \cdot 10^{-7}}{18}$ The number of moles have been obtained from the Matlab results (Appendix A). It has been divided by 18 to convert the gms into moles.

$R := 8.314$ J / mol / K

$Ta := 293$ K The temperature was kept constant due to experimental constraints.

$\delta 36 := 0.26 \cdot 10^{-6}$ m The value of the deformation was obtained from the experimental OEH results.

$wi3 := 6.48 \cdot 10^{-3}$ m Width of the encapsulant

$l3 := 21.8 \cdot 10^{-3}$ m Length of the encapsulant

$A3 := l3 \cdot wi3$

$Pr36 := \frac{n36 \cdot R \cdot Ta}{\delta 36 \cdot A3}$ Pa

$Pr36 = 5.564 \times 10^{5}$

It is observed in the experimental results that the deformation pattern is due to a nature of hydrostatic loads. Hence the value if the pressure load will be calculated as

$y3 := 1 \cdot 10^{-3}, 2 \cdot 10^{-3} .. wi3$

$Ph36(z) := \frac{Pr36 \cdot z \cdot A3}{wi3}$ Pa Hydrostatic loading

Calculating the deformation to verify the experimental results

$E := 1.1 \cdot 10^{9}$ Pa

$h3 := 1.61 \cdot 10^{-3}$ m

$v := 0.3$

$K3 := \frac{E \cdot h3^{3}}{12 \cdot (1 - v^{2})}$ Pa m^3

$w36(y3) := 0.013021 \frac{Ph36(y3) \cdot l3^{4}}{K3}$ m

The deformation function for package 3 after 6 days is shown in Fig. B. 7.

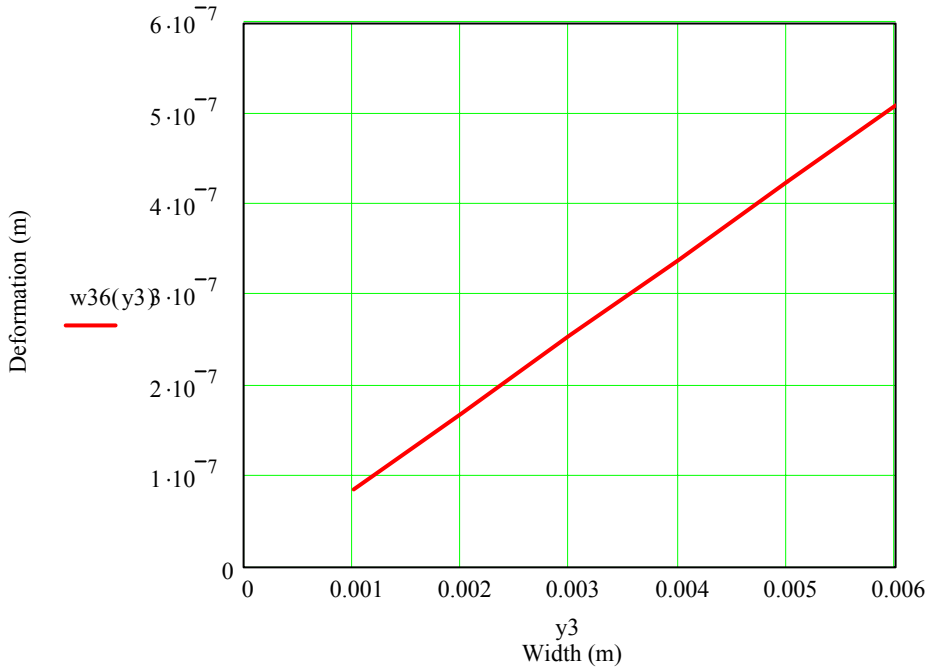

Fig. B.7. Deformation of package 3 after 6 days.

FOR PACKAGE 3 after 10 days

Calculating the pressure developed in the encapsulant with the ideal gas equation

$n310 := \frac{1.58 \cdot 10^{-7}}{18}$ The number of moles have been obtained from the Matlab results (Appendix A). It has been divided by 18 to convert the gms into moles.

$R := 8.314$ J / mol / K

$Ta := 293$ K The temperature was kept constant due to experimental constraints.

$\delta 310 := 0.22 \cdot 10^{-6}$ m The value of the deformation was obtained from the experimental OEH results.

$wi3 := 6.48 \cdot 10^{-3}$ m Width of the encapsulant

$l3 := 21.8 \cdot 10^{-3}$ m Length of the encapsulant

$A3 := l3 \cdot wi3$

$Pr310 := \frac{n310 \cdot R \cdot Ta}{\delta 310 \cdot A3}$ Pa

It is observed in the experimental results that the deformation pattern is due to a nature of hydrostatic loads. Hence the value if the pressure load will be calculated as

$z := 1 \cdot 10^{-3}, 2 \cdot 10^{-3} .. wi3$

$Ph310(z) := \frac{Pr310 \cdot z \cdot A3}{wi3}$ Pa Hydrostatic loading

Calculating the deformation to verify the experimental results

$E := 1.1 \cdot 10^{9}$ Pa

$h3 := 1.61 \cdot 10^{-3}$ m

$v := 0.3$

$K3 := \frac{E \cdot h3^{3}}{12 \cdot \left(1 - v^{2}\right)}$ Pa m^3

$w310(z) := 0.013021 \frac{Ph310(z) \cdot l3^{4}}{K3}$ m

The deformation function for package 3 after 10 days is shown in Fig. B. 8.

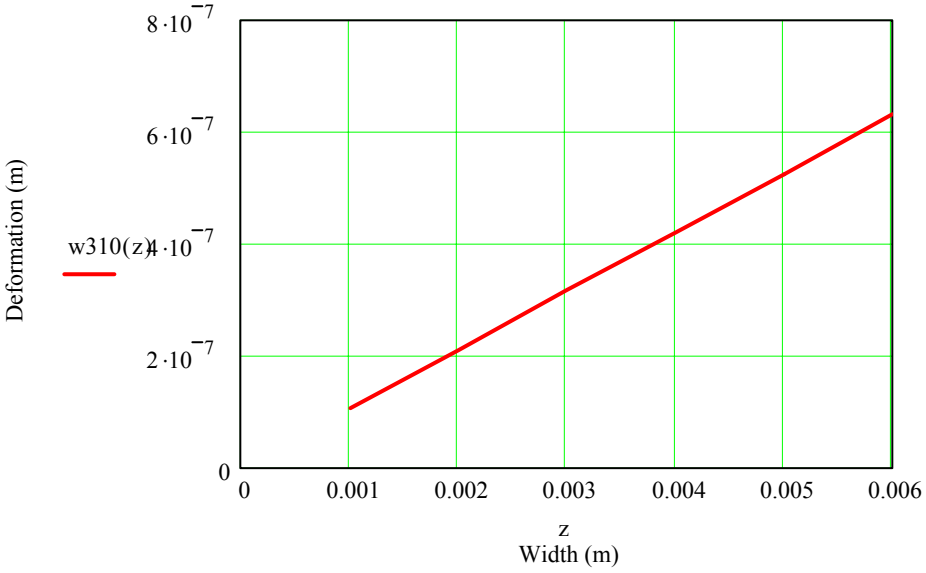

Fig. B. 8. Deformation of package 3 after 10 days.

Comparison of deformation of the packages after 6 days is plotted on the same coordinates, Fig. B. 9.

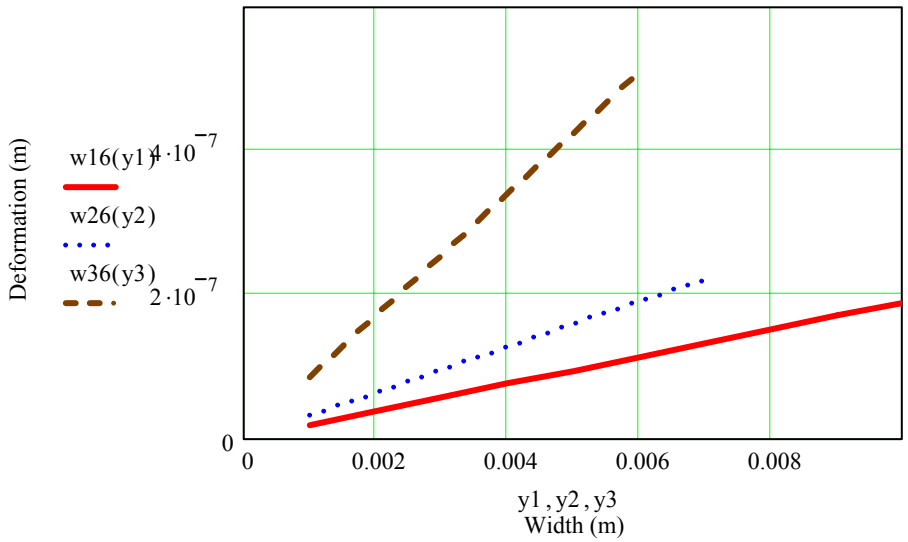

Fig. B. 9. Comparison of the deformations after 6 days.